








EX LIBRIS  
UNIVERSITATIS  
ALBERTENSIS

---

The Bruce Peel  
Special Collections  
Library



Digitized by the Internet Archive  
in 2025 with funding from  
University of Alberta Library

<https://archive.org/details/0162014938367>













**University of Alberta**

**Library Release Form**

**Name of Author:** Kathy Kozlowski

**Title of Thesis:** Molecular Analyses of PITX2 Homeodomain Mutations

**Degree:** Master of Science

**Year this Degree Granted:** 2001

Permission is hereby granted to the University of Alberta Library to reproduce single copies of this thesis and to lend or sell such copies for private, scholarly or scientific research purposes only.

The author reserves all other publication and other rights in association with the copyright in the thesis, and except as herein before provided, neither the thesis nor any substantial portion thereof may be printed or otherwise reproduced in any material form whatever without the author's prior written permission.







**University of Alberta**

**MOLECULAR ANALYSES OF PITX2 HOMEODOMAIN MUTATIONS**

**by**

**Kathy Kozlowski**



A thesis submitted to the Faculty of Graduate Studies and Research in partial fulfillment  
of the requirements for the degree of Master of Science  
in  
Medical Sciences -Ophthalmology

Edmonton, Alberta

Fall, 2001





University of Alberta

Faculty of Graduate Studies and Research

The undersigned certify that they have read, and recommend to the Faculty of Graduate Studies and Research for acceptance, a thesis entitled *Molecular Analyses of PITX2 Homeodomain Mutations* submitted by Kathy Kozlowski in partial fulfillment of the requirements for the degree of Masters of Science in Medical Sciences (Ophthalmology).





## **ABSTRACT:**

This thesis explores the possible genotype-phenotype correlations of PITX2 homeodomain mutations and resultant ocular phenotypes within the spectrum of anterior segment dysgenesis. Missense mutations of the PITX2 homeodomain documented in the literature were characterized by intracellular localization, DNA-binding ability, and transactivation of a reporter gene. Differences in the functional amounts of PITX2 protein resulting from specific *PITX2* mutations were found to correlate with the severity of the resultant anterior segment dysgenesis phenotypes. As well, since the glaucoma associated with anterior segment dysgenesis is not present at birth, the possibility that PITX2 plays a role in the adult eye was also examined by profiling the expression of PITX2 in adult eye tissues. In addition, an attempt was made to identify and examine possible downstream genes of PITX2 in ocular development and glaucoma. The promoter of the *Myocilin* gene, involved in glaucoma, tested positively in transactivation assays as a downstream candidate promoter for transcriptional regulation by PITX2. This thesis will hopefully elucidate the role of PITX2 in the genetic etiology of anterior segment dysgenesis and provide insight into the genetic pathways of ocular development, and simultaneously, that of other systems.





## **ACKNOWLEDGEMENTS:**

It has been a great a honor and a privilege being a member of Dr. Michael Walter's lab. My deepest gratitude to Dr. Walter for giving me a chance to prove myself while offering as much guidance and support as one could ask for. Many thanks also to members of my committee: Drs. Alan Underhill and Susan Andrew, and to Chair of Ophthalmology: Dr. Ian MacDonald. The support and assistance of everyone is greatly appreciated.

The members of the Ocular Genetics lab, past and present, have been wonderful to work with and to learn from. Thank you James, Steve, Doug, Ramsey, Heather, Mike, Alan, Dean, Jody, and Matt. Your friendship will always be remembered. A special thanks to Farideh and Kerry for all that you do for the grad students.

To my parents for all of their support and love. I couldn't have made it without you. It brings immense joy to my heart knowing that I have made you proud.





## TABLE OF CONTENTS:

<b><u>INTRODUCTION:</u></b> .....	<b>Page 1</b>
The Eye as a Model.....	Page 2
Spectrum of Anterior Segment Dysgenesis.....	Page 2
Eye Development.....	Page 15
Mechanisms of Anterior Segment Dysgenesis.....	Page 46
Glaucoma.....	Page 52
Genetic Etiology of AR Malformations.....	Page 56
Allelic Genetic Disorders.....	Page 57
The PITX2 Transcription Factor.....	Page 57
Murine <i>Pitx2</i> Expression.....	Page 62
Pituitary Expression of <i>PITX</i> Transcription Factors.....	Page 65
PITX2 in the Left-Right Pathway.....	Page 65
Ocular Defects of <i>Pitx2</i> Mouse Knock-outs.....	Page 68
Systemic Defects that are Not Seen in Patients.....	Page 68
Project Description.....	Page 71



<b><u>MATERIALS AND METHODS:</u></b> .....	<b>Page 73</b>
I: PITX2 Mutational Analysis.....	Page 74
Patient DNA.....	Page 74
PCR Amplification, Visualization, and Purification of <i>PITX2</i> Exons.....	Page 74
<sup>33</sup> P Sequencing.....	Page 78
LI-COR Sequencing.....	Page 79
II: Functional Analyses of PITX2 Homeodomain Mutants.....	Page 79
<i>PITX2</i> cDNA.....	Page 79
pcDNA4/HisMax Expression Vector.....	Page 85
Cloning of <i>PITX2</i> cDNA into an Expression Vector.....	Page 85
PITX2 Homeodomain Mutants.....	Page 89
Tissue Culture Cells.....	Page 89
Immunofluorescence.....	Page 89
PITX2 Protein Expression.....	Page 90
Deletion of Putative PITX2 NLS.....	Page 91
Western Analysis.....	Page 91
Electrophoretic Mobility Shift Assays (EMSAs).....	Page 92
pGL3 Luciferase Reporter Vectors.....	Page 93
βGal Control Vector.....	Page 94
Transactivation Assays with the CE-3 Element.....	Page 94





III: PITX2 in the Adult Eye.....	Page 95
Eye Tissue cDNA Libraries and Pools.....	Page 95
<i>PITX2</i> and <i>PIT1</i> Expression in the Adult Eye.....	Page 95
<i>MYOC</i> Promoter Constructs.....	Page 96
Transactivation Assays with the <i>Myocilin</i> Promoter.....	Page 96
<i>FOXC1</i> Expression and Transactivation Reporter Constructs.....	Page 97
<b><u>RESULTS:</u></b> .....	<b>Page 98</b>
I: PITX2 Mutational Analysis.....	Page 99
II: Analyses of PITX2 Homeodomain Mutants.....	Page 104
<i>PITX2</i> Expression Constructs.....	Page 104
Intracellular localization.....	Page 104
Deletion of the Putative N-terminal PITX2 Nuclear Localization Signal.....	Page 111
Protein Expression and Western Analysis.....	Page 112
DNA-binding Assays.....	Page 112
Transactivation of the CE-3 Luciferase-Reporter Construct.....	Page 121
III: <i>PITX2</i> Expression and Activity in the Adult Eye.....	Page 126
<i>PITX2</i> is Expressed in the Adult Human Anterior Segment.....	Page 126
Possible Down-stream Targets of PITX2.....	Page 129





Transactivation of the <i>MYOC</i> promoters by wtPITX2.....	Page 132
Increased Transactivation of the <i>MYOC</i> Promoters by Val45Leu.....	Page 132
Transactivation of the <i>MYOC</i> Promoters by FOXC1.....	Page 136
PITX2 and FOXC1 Do Not Interact in Transactivation of the <i>MYOC</i> Promoter.....	Page 136
<b><u>DISCUSSION:</u></b> .....	<b>Page 138</b>
I: PITX2 Mutational Analysis.....	Page 139
Incidence of PITX2 Mutation.....	Page 139
Types of PITX2 Mutations Identified to Date.....	Page 141
Important Residues of the Homeodomain.....	Page 142
II: Characterization of PITX2 Homeodomain Mutations.....	Page 145
Lys50Gln.....	Page 148
Arg52Cys.....	Page 149
Molecular Characterization of the Selected PITX2 Homeodomain Mutations.....	Page 150
IH Mutant (Arg46Trp) .....	Page 150
IGD Mutant (Arg31His) .....	Page 151
AR Mutant 1 (7aa Duplication).....	Page 152
AR Mutant 2 (Leu16Gln) .....	Page 153



AR Mutant 3 (Thr30Pro) .....	Page 154
AR Mutant 4 (Val45Leu) .....	Page 155
AR Mutant 5 (Arg53Pro) .....	Page 161
III: PITX2 in the Adult Eye.....	Page 165
PITX2 Regulation of <i>MYOC</i> .....	Page 166
Conclusions.....	Page 168
Future Directions.....	Page 172

## **APPENDIX A:**

Materials and Methods: Solutions.....	Page 173
---------------------------------------	----------

<b><u>REFERENCES:</u></b> .....	<b>Page 181</b>
---------------------------------	-----------------

<b><u>PERMISSION LETTER:</u></b> .....	<b>Page 197</b>
--	-----------------





## **LIST OF TABLES:**

Table 1. Sequences of the <i>PITX2</i> primers.....	Page 77
Table 2. Sequences of the mutagenesis primers used. ....	Page 86
Table 3. Incidence of PITX2 mutations in patient populations.....	Page 105
Table 4. PITX2 mutations identified to date. ....	Page 140
Table 5. Summary of Results.....	Page 169



## **LIST OF FIGURES:**

1. Basic anatomy of the eye.....	Page 4
2. Anatomy of the anterior chamber.....	Page 6
3. Example of a patient with IGD.....	Page 8
4. Example of a patient with AR malformations.....	Page 10
5. Example of a patient with Peters anomaly.....	Page 13
6. Extraocular features associated with anterior segment dysgenesis.....	Page 16
7. E8.5 mouse embryo demonstrating neural folds.....	Page 18
8. Closure of the neural folds.....	Page 21
9. Demonstration of the optic groove.....	Page 23
10. Demonstration of the optic vesicle.....	Page 25
11. Demonstration of lens placode formation.....	Page 27
12. Invagination of the lens placode.....	Page 29
13. Formation of the lens vesicle.....	Page 32
14. Corneal differentiation at E1.....	Page 34
15. Formation of the iris and cornea.....	Page 36
16. Formation of the ciliary processes.....	Page 38
17. Neural cell migration forms tissues of the anterior chamber.....	Page 40
18. Layers of the cornea and the pupillary membrane.....	Page 42





19. A diagram of anterior chamber formation.....	Page 44
20. Detail of the anterior chamber.....	Page 47
21. A postulated mechanism for anterior segment dysgenesis.....	Page 50
22. Diagrams of open- and closed-angle forms of glaucoma.....	Page 53
23. Genomic structure of PITX2.....	Page 58
24. The paired-bicoid class of transcription factors.....	Page 60
25. The <i>engrailed</i> -DNA complex.....	Page 63
26. Embryonic expression of murine <i>Pitx2</i> .....	Page 66
27. Ocular findings in <i>Pitx2</i> <i>-/-</i> mice.....	Page 69
28. Schematic of the <i>PITX2</i> cDNA with primers indicated.....	Page 75
29. The <i>PITX2</i> -pBS construct.....	Page 80
30. The pcDNA4/HisMax mammalian expression vector.....	Page 82
31. Pedigree of the AR malformation patient found to carry a PITX2 mutation.....	Page 100
32. Sequencing autoradiograph demonstrating the PITX2 mutation found.....	Page 102
33. The <i>PITX2</i> -pcDNA4/HisMax expression construct.....	Page 106
34. Immunofluorescence of the various PITX2 mutants studied.....	Page 108
35. Western blot analysis of the various PITX2 mutant protein extracts.....	Page 113
36. EMSAs with the various PITX2 mutant protein extracts.....	Page 115



37. Transactivation studies with the CE-3 element.....	Page 122
38. PITX2 expression in adult eye tissues.....	Page 127
39. Schematic of the <i>MYOC</i> promoters indicating putative PITX2 and FOXC1 binding sites.....	Page 130
40. Transactivation studies of the <i>MYOC</i> promoters.....	Page 133
41. Schematic indicating the missense mutations of the PITX2 homeodomain with key residues represented.....	Page 143
42. Model of the PITX2 homeodomain mutations.....	Page 146
43. The occurrence of leucine at position 45 in a narrow range of homeodomains.....	Page 157
44. A novel NLS in the C-terminus of the PITX2 homeodomain.....	Page 163





## LIST OF ABBREVIATIONS

μg	micrograms
βgal	βeta-galactosidase
Δ	Deleted
°C	Degrees Celsius
aa	Amino acids
<i>Antp</i>	<i>Antennapedia</i>
APS	Ammonium persulfate
AR	Axenfeld-Rieger
ARA	Axenfeld-Rieger Anomaly
ARA	Axenfeld-Rieger Syndrome
Arg	Arginine
ASD	Anterior Segment Dysgenesis
Asn	Asparagine
bp	base pairs of DNA
BSA	Bovine serum albumin
<i>C. elegans</i>	<i>Caenorhabditis elegans</i>
CIAP	Calf Intestinal Alkaline Phosphatase
C-terminal	Carboxy-terminal
Cys	Cysteine
<i>D. melanogaster</i>	<i>Drosophila melanogaster</i>
DAPI	4',6-diamidino-2-phenylindole dihydrochloride
dH <sub>2</sub> O	distilled water
DMEM	Dulbecco's Modified Eagle Medium
DNA	Deoxyribonucleic acid
ds	Double-stranded
DTT	Dithiothreitol
Dup	duplication
<i>E. coli</i>	<i>Escherichia coli</i>
EDTA	Ethylene-diaminetetra-acetic acid disodium salt
EMSA	Electrophoretic mobility shift assay
<i>en</i>	<i>Engrailed</i>
FBS	Fetal bovine serum
g	grams
Gln	Glutamine
GTB	Glycerol tolerant buffer



HEPES	N-[2-Hydroxyethylene] piperazine-N'-[2-ethanesulfonic acid]
His	Histidine
IGD	Iridogoniodysgenesis
IGDS	Iridogoniodysgenesis Syndrome
IH	Iris Hypoplasia
Ile	Isoleucine
IOP	Intraocular pressure
kb	kilobases
L	Litre
LB	Lactose broth
Leu	Leucine
Lys	Lysine
mLs	millilitres
mm	Millimeter
mM	Millimolar
MOPS	3-[N-Morpholino] propanesulfonic acid
mRNA	Messenger ribonucleic acid
<i>MYOC</i>	<i>Myocilin</i>
ng	nanograms
NLS	Nuclear Localization Signal
nm	nanometers
N-terminal	Amino-terminal
PAGE	Polyacrylamide gel electrophoresis
PBS	Phosphate buffered saline
PBS-T	Phosphate buffered saline with Tween-20
PCR	Polymerase chain reaction
Phe	Phenylalanine
pmol	picomoles
PMSF	Phenylmethylsulfonyl fluoride
PO <sub>4</sub> <sup>-</sup>	Phosphate
POAG	Primary Open Angle Glaucoma
<i>POMC</i>	<i>Pro-opiomelanocortin</i>
Pro	Proline
SDS	Sodium dodecyl sulfate, sodium salt
TBE	Tris-EDTA-Borate Buffer
TEMED	Tetramethylenediamine
Thr	Threonine
TRIS	Tris(hydroxymethyl)aminoethamine
Trp	Tryptophan



Tyr	Tyrosine
UTR	Untranslated region
UV	Ultraviolet
Val	Valine





## **INTRODUCTION:**



### The Eye as a Model

The eye is an excellent system for studying the genetics of development and disease. The processes of ocular tissue differentiation and organization are complex and genetic mutation can result in a wide spectrum of structural and functional abnormalities. As the eye itself is non-essential for life, a great variety of developmental defects (often severe) may be studied. This is in contrast to most major organ systems where loss of function can result in unexplained, or even undetected, pre-natal lethality. Despite being non-essential for life, the importance of sight for sensory input ensures that any loss of function is quickly brought to clinical attention. Structural aberrations that do not affect function are also readily observed due to the remarkable accessibility of the eye, particularly the anterior segment. Ease of detection and non-lethality accounts for the observation that over one quarter of all genetic diseases surveyed in McKusick's Mendelian Inheritance in Man (1985) have ocular findings (cited in Freund et al. 1996), and more than 70 syndromes included in the London Dysmorphology Database include anterior segment malformation (cited in Perveen et al. 2000). The syndromic combination of ocular defects with aberrations of other systems suggests a common genetic defect in related processes of development. Uncovering the genetic basis of ocular disorders such as Axenfeld-Rieger malformations will thereby provide insight into the genetic pathways of ocular development, and simultaneously, that of other systems.

### Spectrum of Anterior Segment Dysgenesis

The great deal of phenotypic overlap existing between autosomal dominant Iris Hypoplasia with glaucoma (IH), Iridogoniodysgenesis (IGD) (OMIM #137600) and Axenfeld-Rieger (AR) malformations (OMIM #180500), suggests a continuous spectrum of anterior segment anomalies (Shields et al. 1985, Chisholm and Chudley 1983,





Alkemade 1969, Reese and Ellsworth 1966). All three disorders are characterized by an association with early-onset glaucoma. To put into perspective the following clinical descriptions, two figures outlining basic anatomy of the eye (Figure 1) and the anterior segment (Figure 2) are provided.

The least severe of these anterior segment defects is IH. Rubel first noted in 1913 a familial hypoplasia of the iris stroma associated with glaucoma with absence of any other ocular malformations (Rubel 1913, as cited by Shields 1989). It is the thinned iris stroma that allows the pupillary sphincter to be visible, as in an example of a patient with IGD with distinct iris hypoplasia (Figure 3). IGD was first reported in 1932 by Berg in a large pedigree with iris hypoplasia and abnormalities in differentiation of iridocorneal angle tissue (goniodysgenesis), especially the trabecular meshwork (Berg 1932, Weatherill and Hart 1969). Sometimes IGD patients demonstrate excess 'woolly' tissue in the angle and anomalous angle vascularity (OMIM # 601631) (Pearce et al. 1983, Pearce et al. 1982).

Axenfeld, in 1920, described a patient with a prominent white line near the limbus at the junction of Descemet's membrane and the trabecular meshwork referred to as Schwalbe's line (Axenfeld 1920, cited in Walter et al. 1996) (Figure 4). Axenfeld also noted a number of delicate fibrillae crossing the anterior chamber from the iris stroma to Schwalbe's line. Rieger, in 1934, subsequently described two patients with the findings observed by Axenfeld, with the addition of iris hypoplasia, pupillary displacement (corectopia), and full thickness tears of the iris resulting in the appearance of extra pupillary openings (polycoria) (Rieger 1934, cited in Walter et al. 1996) (Figure 4). Ocular characteristics of both Axenfeld and Rieger anomalies are often found within one family, sometimes combined within one individual. Shields was the first to refer to them together as Axenfeld-Rieger Syndrome (ARS) (Shields et al. 1985). Axenfeld-Rieger





**Figure 1.**

Basic anatomy of the eye.

(Adapted from Riordan-Eva 1999).

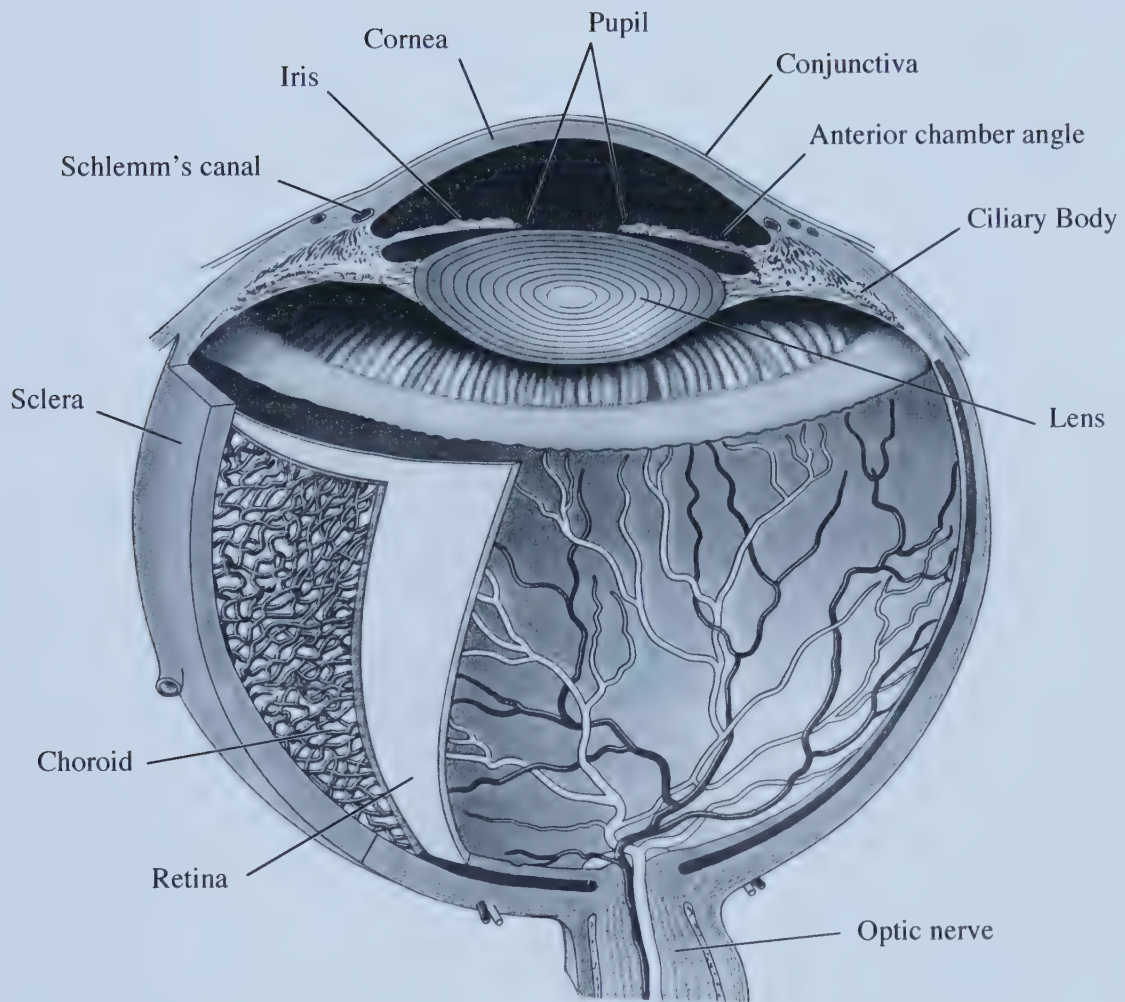








**Figure 2.**

Anatomy of the anterior chamber angle.

(Adapted from Riordan-Eva 1999).

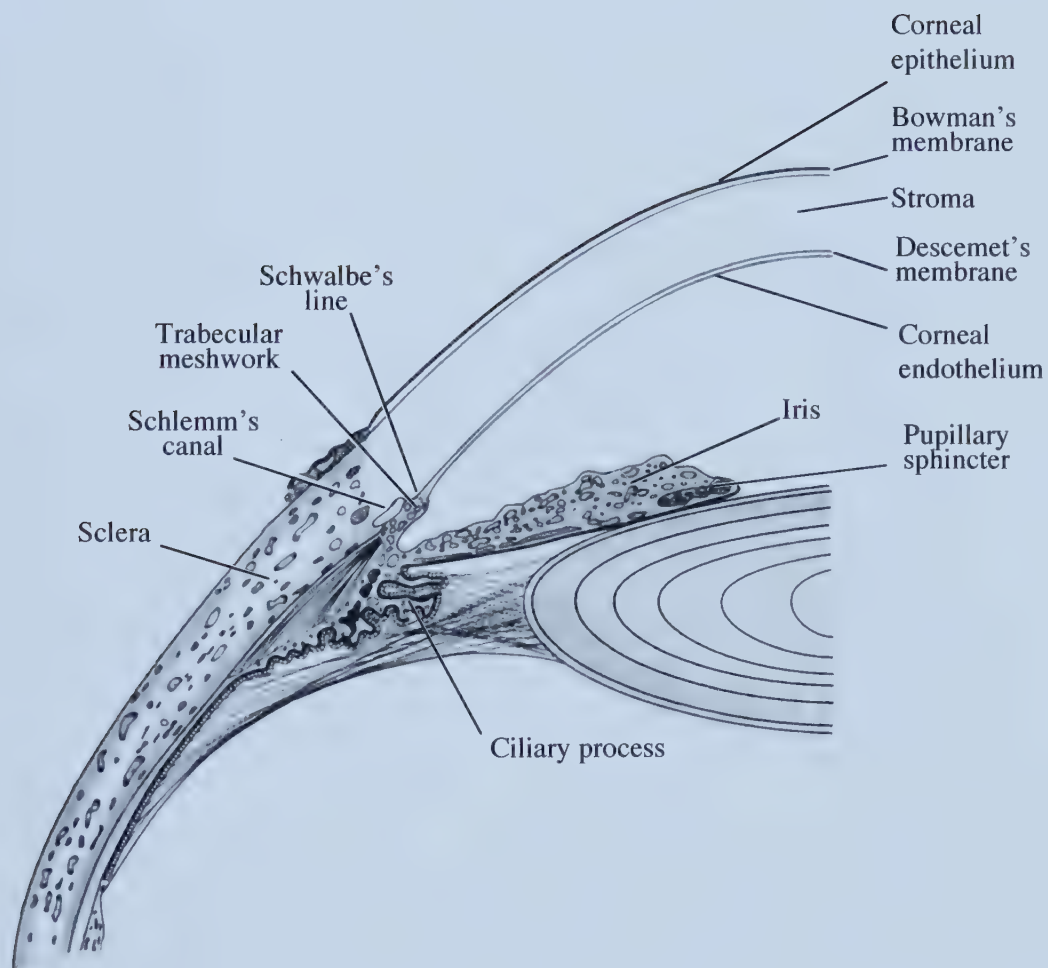






**Figure 3.**

Example of a patient with IGD. Extensive hypoplasia of the iris stroma allows the pupillary sphincter to be visible.

(Photo courtesy of Dr. M. A. Walter).









**Figure 4.**

Example of a patient with AR malformations. A prominent and anteriorly displaced Schwalbe's line is seen on the left. The pupil is displaced nasally and a full-thickness iris hole is visible in the opposite quadrants.

(Photo courtesy of Dr. M. A. Walter).





Anomaly (ARA) has been defined as a separate condition with the presentation of ocular findings alone. However, not all affected individuals of a family diagnosed with ARS have non-ocular features. It is thus difficult to classify a small family with only ocular features as ARA, versus ARS. Since the ocular features of ARA and ARS are clinically identical, the term Axenfeld-Rieger (AR) malformations has been suggested to refer to individuals with Axenfeld-Rieger anterior segment defects (Walter et al. 1996). Many additional ocular abnormalities have been reported in association with AR malformations. These include strabismus, limbal dermoids, cataracts, retinal detachment, macular degeneration, chorioretinal colobomas, choroidal hypoplasia, and hypoplasia of the optic nerve (reviewed in Shields 1989).

Peters anomaly has occasionally been included in this grouping of anterior segment disorders (Waring et al. 1975, Reese and Ellsworth 1966). Peters anomaly consists of a central corneal opacification (leukoma), absence of any endothelium or Descemet's membrane in the central cornea, and a variable degree of attachments between the iris and the central aspect of the posterior cornea (Peters 1906, OMIM #604229) (Figure 5). Peters anomaly can also occur in association with cataracts (OMIM# 603807), or cataracts and microcornea (OMIM #116150). A number of papers report the occurrence of Peters anomaly in association with AR malformations (Perveen et al. 2000, Doward et al. 1999, Phillips et al. 1996, Holmstrom et al. 1991, Awan 1977). A complete loss of Descemet's membrane and endothelium seen in conjunction with AR malformations (Hittner et al. 1982) may be an extension of the central loss and peripheral preservation of Descemet's membrane and endothelium (Nakanishi and Brown 1971) usually associated with Peters anomaly. It is the opinion of this author that the occurrence of this Peters-like feature in conjunction with AR malformations represents a more severe part of the spectrum of anterior segment disorders discussed above, while Peters anomaly







**Figure 5.**

Example of a patient with Peters anomaly. Central corneal opacification is visible. This patient also had attachments between the iris and the central aspect of the posterior cornea.

(From Success in MRCOphth, [www.mrcophth.com](http://www.mrcophth.com)).





itself is not contiguous with the spectrum. Evidence for this idea will be presented in the review of anterior segment dysgenesis mechanisms to follow.

The spectrum of anterior segment dysgenesis of IH, IGD, and AR malformations is associated with non-ocular features of persistent periumbilical skin, and maxillary hypoplasia, dental anomalies (hypodontia, microdontia, anodontia) (Figure 6). In the families to be described herein, systemic involvement is more severe and occurs with a greater percentage in families with AR malformations, and least of all in the family with IH studied. AR malformations are further associated with hypertelorism, hypospadias in males, as well as cardiac, pituitary, gastrointestinal, and limb developmental irregularities (reviewed by Fitch and Kaback 1978).

### Eye Development

To discuss the possible mechanisms of anterior segment dysgenesis, an understanding of the basic embryology of the eye is required. Ocular development involves the neuroectoderm of the forebrain, surface ectoderm of the head and derivative neural crest cells (Johnston et al. 1979), and mesoderm between these layers (Riordan-Eva 1999, Moore 1983). Eye development in humans first becomes evident in the third week following conception when two grooves (optic sulci) appear in the neural folds (Riordan-Eva 1999, Moore 1983) (Figure 7). As the neural folds fuse to form the forebrain and the optic grooves move outwards, optic vesicles are formed (Figures 8, 9, 10) (Riordan-Eva 1999, Moore 1983). As the optic vesicles expand, the connection with the forebrain constricts to form the optic stalk (Figure 11) (Riordan-Eva 1999, Moore 1983). As the optic vesicles grow outward, a lens placode is formed from the thickening of the adjacent surface ectoderm (Figures 11, 12) (Riordan-Eva 1999, Moore 1983). A lens pit is formed as the center of the lens placode invaginates (Riordan-Eva 1999, Moore 1983) (Figure







**Figure 6.**

Examples of patients with AR malformations and IGD (top and bottom, respectively).

Dental anomalies visible include small, misshapen, and missing teeth.

(Photos courtesy of Dr. M. A. Walter)







**Figure 7.**

Two fronto-lateral views of a mouse embryo at 8.5 days post fertilization, comparable to a human embryo at 24 days gestation.

**A.** The entire embryo is shown to put the neural folds in perspective.

**B.** Detailed view of the head region. The optic groove within the neural fold is indicated. The neural folds will shortly begin closing.

(Reproduced with permission from Dr. K. Sulik, University of North Carolina School of Medicine ([http://www.med.unc.edu/embryo\\_images](http://www.med.unc.edu/embryo_images))).

**A**

Neural folds







**B**

Optic groove

Neural folds

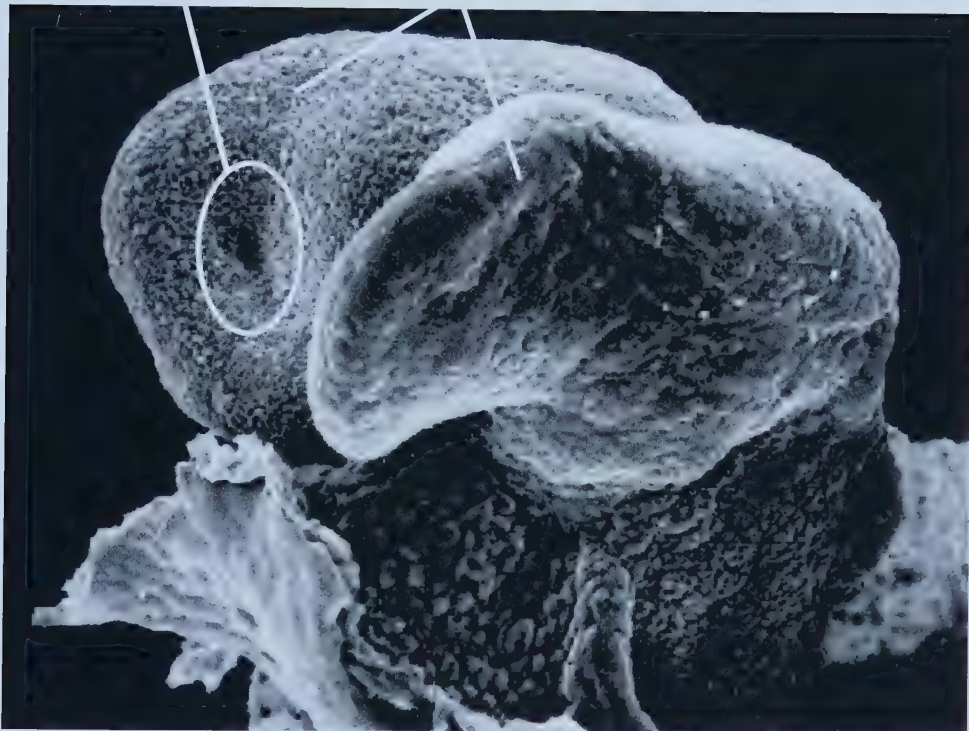






**Figure 8.**

Fronto-lateral view of a mouse embryo at 8.5 days, comparable to a human embryo at 25 days. As the neural folds begin closing, the neuroectoderm of the optic groove (now enclosed by the neural folds) comes into close contact with the surface ectoderm in the area indicated by the oval.

(Reproduced with permission from Dr. K. Sulik, University of North Carolina School of Medicine ([http://www.med.unc.edu/embryo\\_images](http://www.med.unc.edu/embryo_images))).





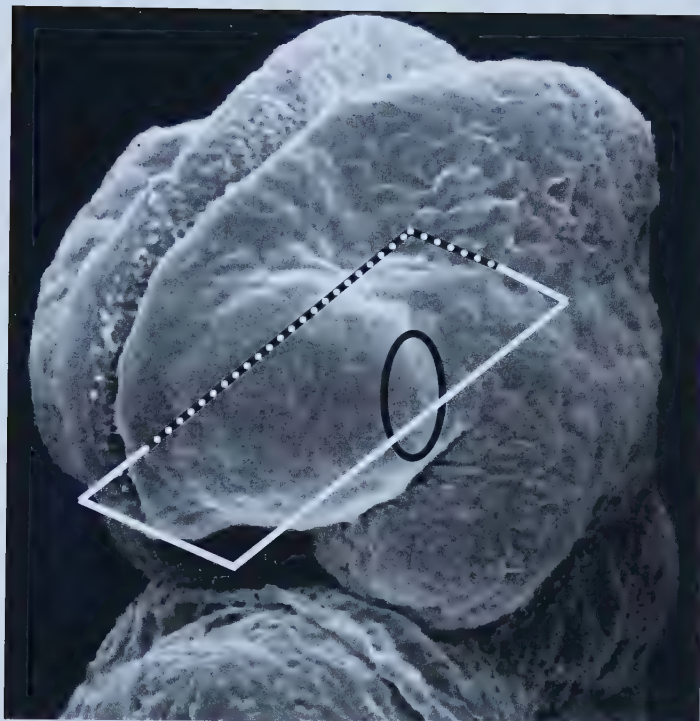




**Figure 9.**

Transverse cut through the fronto-lateral view of a mouse embryo at 8.5 days (indicated by the dotted line) demonstrating how the now enclosed neuroectoderm of the optic groove interacts with the surface ectoderm (in the same area indicated with the oval as in Figure 8).

(Reproduced with permission from Dr. K. Sulik, University of North Carolina School of Medicine ([http://www.med.unc.edu/embryo\\_images](http://www.med.unc.edu/embryo_images))).



Optic groove

Neuroectoderm

Surface ectoderm





**Figure 10.**

A cut (as indicated by the dotted line) through the lateral view of a mouse embryo at 9 days (equivalent to 29 days in human) demonstrating the optic vesicle formed by the enclosed optic groove.

(Reproduced with permission from Dr. K. Sulik, University of North Carolina School of Medicine ([http://www.med.unc.edu/embryo\\_images](http://www.med.unc.edu/embryo_images))).



Hollow  
Optic vesicles







**Figure 11.**

A coronal cut through a mouse embryo at 9 days (equivalent to 28 days human) demonstrating the lens placode being induced by contact between the surface ectoderm and neural ectoderm of the optic vesicle. The optic vesicle closes as indicated by the arrows.

(Reproduced with permission from Dr. K. Sulik, University of North Carolina School of Medicine ([http://www.med.unc.edu/embryo\\_images](http://www.med.unc.edu/embryo_images)))

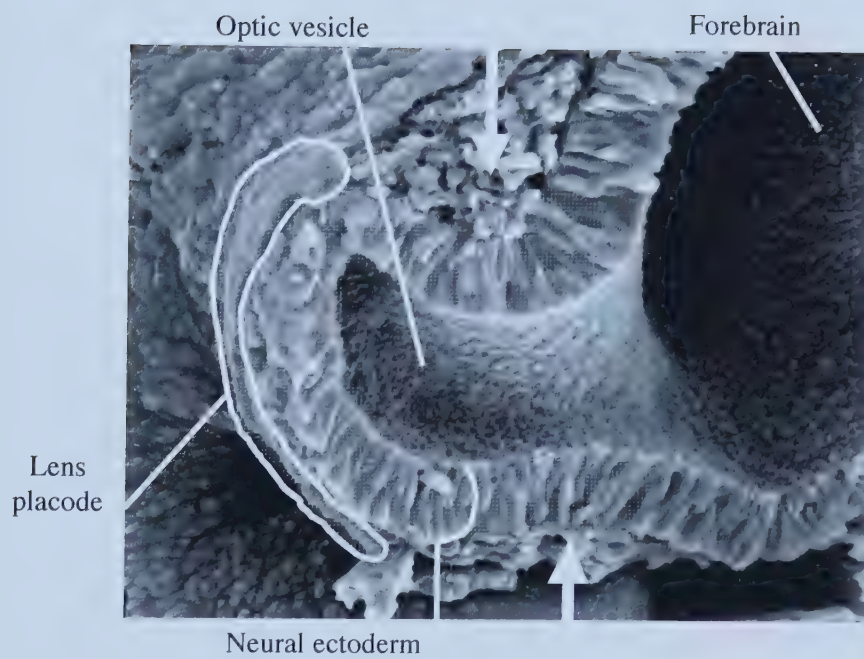


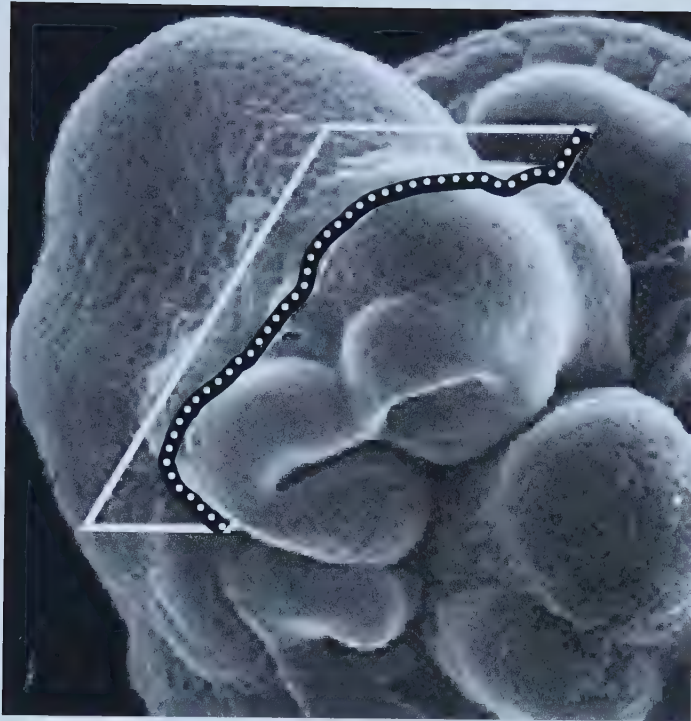




**Figure 12.**

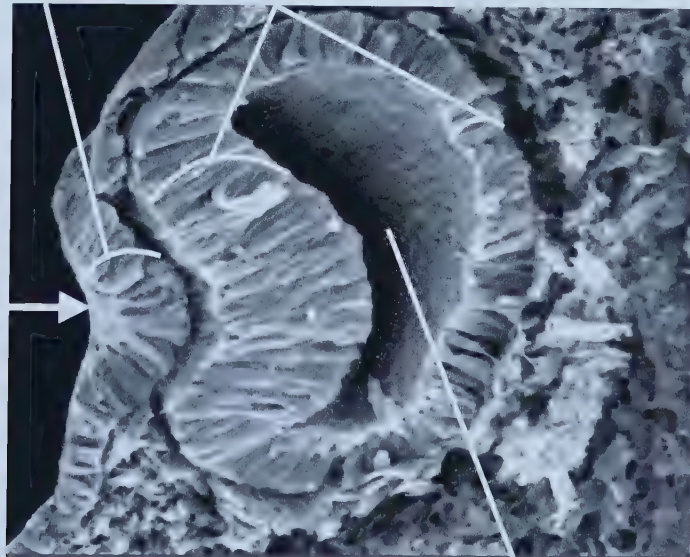
A lateral and coronal cut (as indicated by the dotted line) through a mouse embryo at 9 days (equivalent to 29 days human) demonstrating the invaginating lens placode and adjacent neural ectoderm of the optic vesicle.

(Reproduced with permission from Dr. K. Sulik, University of North Carolina School of Medicine ([http://www.med.unc.edu/embryo\\_images](http://www.med.unc.edu/embryo_images))).



Lens  
placode

Neural  
ectoderm



Optic vesicle



12). Lens vesicles are formed as the edges of the lens pit come together (Figure 13) (Riordan-Eva 1999, Moore 1983). The entire optic vesicle is at the same time further invaginating to form a double-layered optic cup (Figure 13) (Riordan-Eva 1999, Moore 1983). The lens vesicles then separate from the surface ectoderm (Riordan-Eva 1999, Moore 1983) (Figure 14). The outer layer of the optic cup forms the pigment epithelium while the inner layer differentiates into the neural layer of the retina (Riordan-Eva 1999, Moore 1983) (Figure 15). The edges of the optic cup that partially cover the lens form a component of the iris (Figure 15) (Riordan-Eva 1999, Moore 1983). The ciliary body derives from the outer layer of the optic cup (Riordan-Eva 1999, Moore 1983) (Figure 16). The anterior segment of the ocular globe is formed by three stages of neural crest cell invasion into the space between the separated surface ectoderm and the lens vesicle (Riordan-Eva 1999, Shields 1983, Wulle 1972) (Figure 17). The first wave of cells is responsible for formation of the corneal endothelium that subsequently produces Descemet's membrane. The second wave later forms the corneal stroma between the corneal endothelium and epithelium. The third wave insinuates itself between the primordia of the cornea and the lens and will form the iris stroma and pupillary membrane (Figure 18). As a continuous layer of endothelium creates a closed cavity to form the anterior chamber (Hansson and Jerndal 1971), the anterior surface of the iris inserts at the edge of the corneal endothelium, covering the primordial trabecular meshwork (Riordan-Eva 1999, Shields 1983, Anderson 1981) (Figure 19A). The endothelial layer covering the iris and pupillary membrane then progressively disappears in a posterior to anterior direction (Shields 1983, van Burskirk 1981). The endothelial layer is retained as the corneal endothelium and possibly the endothelial lining of the trabecular meshwork as well (Shields 1983, van Burskirk 1981). The peripheral uveal tissues slide posteriorly, deepening the anterior chamber angle and exposing the







**Figure 13.**

A frontal and coronal cut (as indicated by the dotted line) through a mouse embryo at 11 days (equivalent to 36 days human) demonstrating formation of the lens vesicle that pinches off the surface ectoderm. Also visible is the invaginated optic vesicle that forms the bilayered optic cup that remains connected to the forebrain via the optic stalk. Layers of the optic cup will later form the pigmented and neural layers of the retina.

(Reproduced with permission from Dr. K. Sulik, University of North Carolina School of Medicine ([http://www.med.unc.edu/embryo\\_images](http://www.med.unc.edu/embryo_images)))

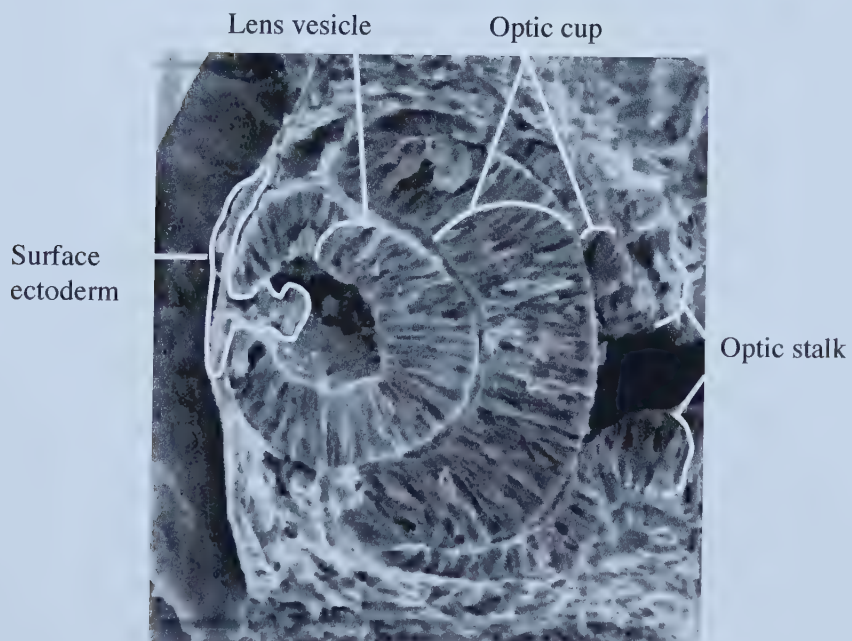






**Figure 14.**

A coronal cut through a 13 day mouse embryo, equivalent to 7 week human fetus.

Following the separation of the lens from the surface ectoderm, the posterior lens fibers elongate to obliterate the lens cavity. The cornea begins to differentiate at this time.

(Reproduced with permission from Dr. K. Sulik, University of North Carolina School of Medicine ([http://www.med.unc.edu/embryo\\_images](http://www.med.unc.edu/embryo_images))).

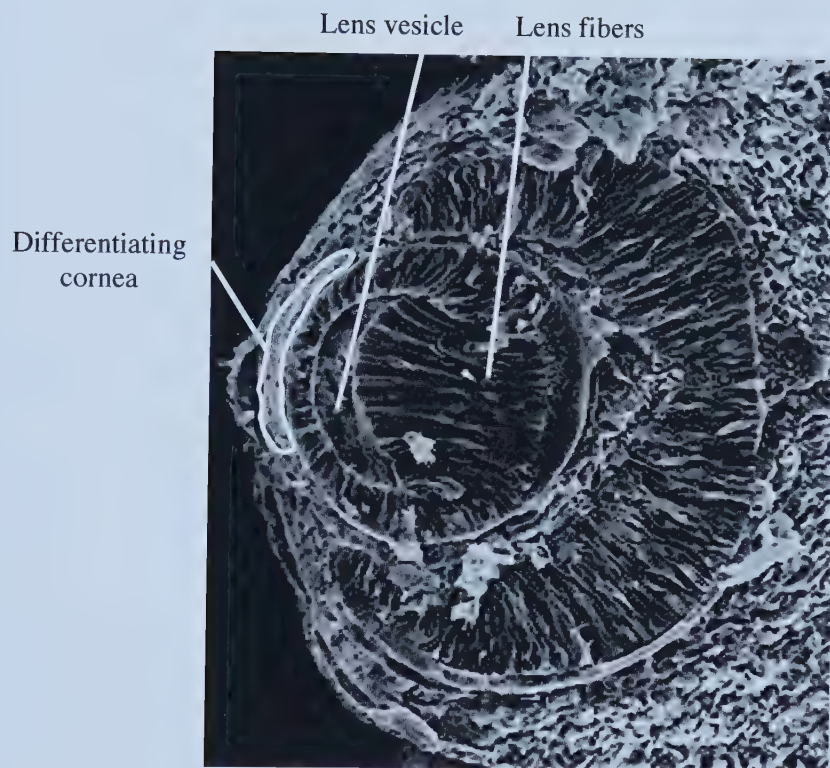








**Figure 15.**

A coronal cut of a day-14 mouse embryo. The outer layer of the optic cup forms the pigment epithelium while the inner layer differentiates into the neural layer of the retina. The anterior chamber of the eye forms as a space develops between the lens and its closely associated iridopupillary membrane and the cornea. The iris partially forms from the outer rim of the optic cup.

(Reproduced with permission from Dr. K. Sulik, University of North Carolina School of Medicine ([http://www.med.unc.edu/embryo\\_images](http://www.med.unc.edu/embryo_images))).

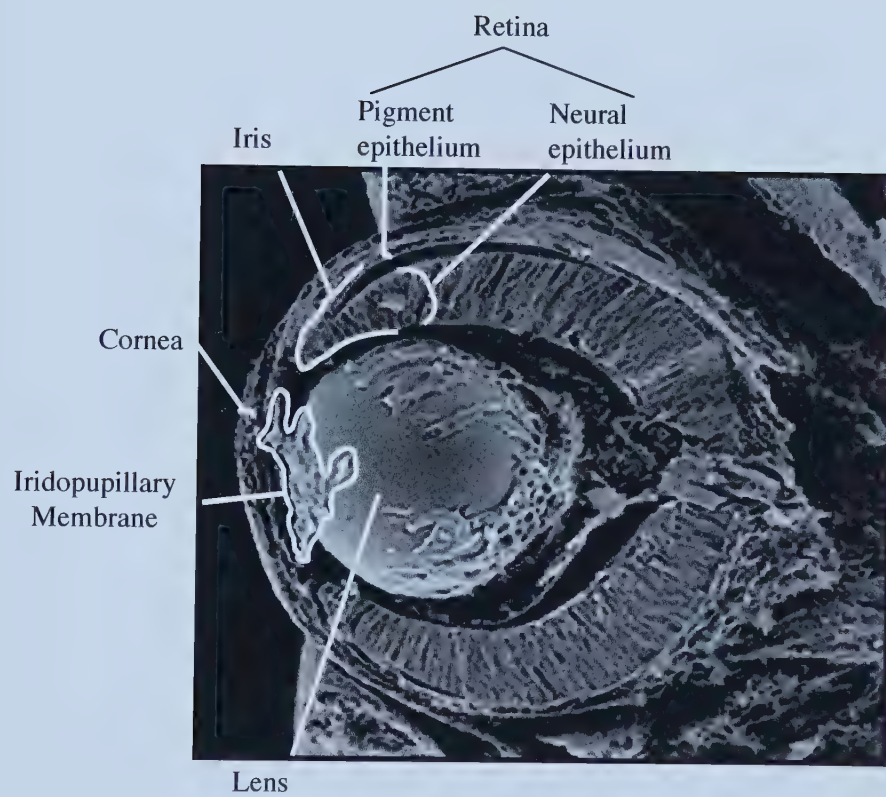






**Figure 16.**

A parasagittal cut at 15 weeks (human fetus) demonstrates folding of the two closely associated layers of the optic cup that results in formation of ciliary processes.

(Reproduced with permission from Dr. K. Sulik, University of North Carolina School of Medicine ([http://www.med.unc.edu/embryo\\_images](http://www.med.unc.edu/embryo_images))).



Ciliary processes







**Figure 17.**

Three migrating waves of neural crest cells form tissues of the anterior segment. The first wave will differentiate into Descemet's membrane and the corneal endothelium. The second wave of cells forms the corneal stroma. The third wave will form the iris stroma and pupillary membrane.

(Adapted from Tripathi 1974).

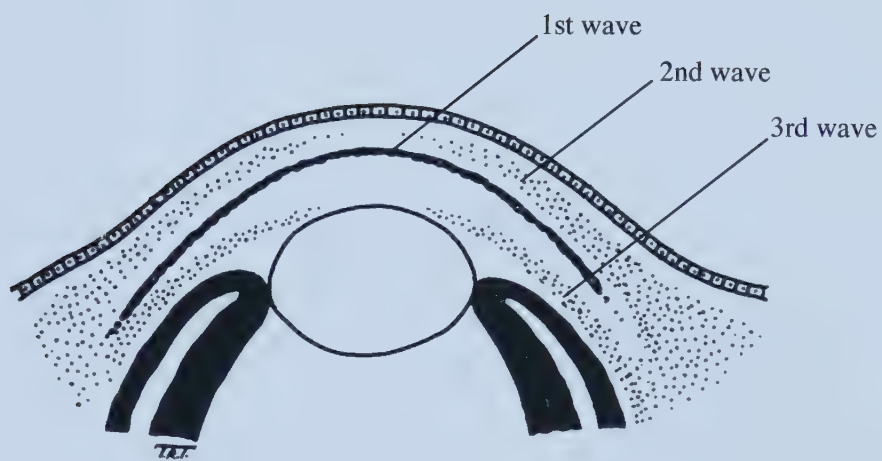






**Figure 18.**

A parasagittal cut of a 8 week-old human fetus shows the cornea that consists of an outer epithelial layer derived from surface ectoderm and inner layers derived from neural crest cells. The pupillary membrane will eventually regress.

(Reproduced with permission from Dr. K. Sulik, University of North Carolina School of Medicine ([http://www.med.unc.edu/embryo\\_images](http://www.med.unc.edu/embryo_images))).

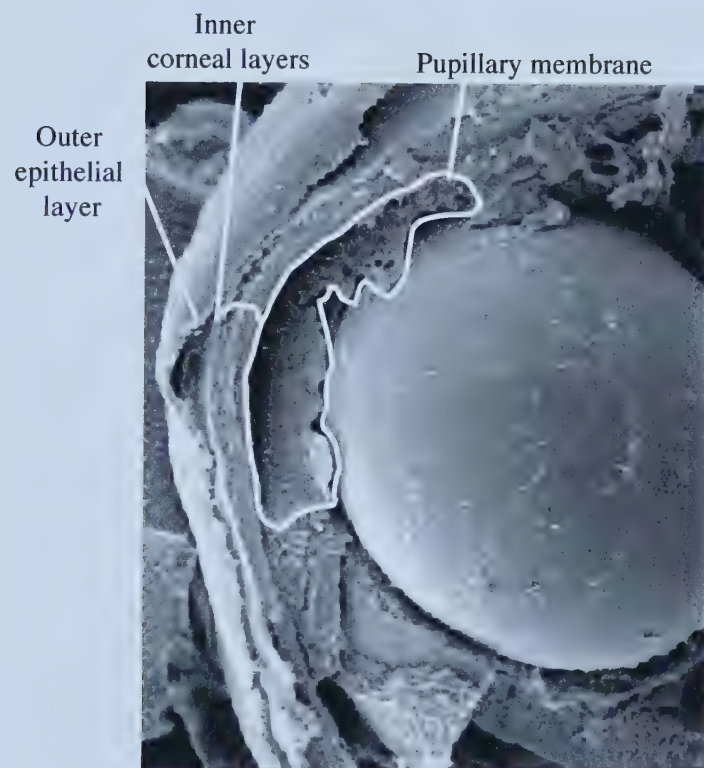






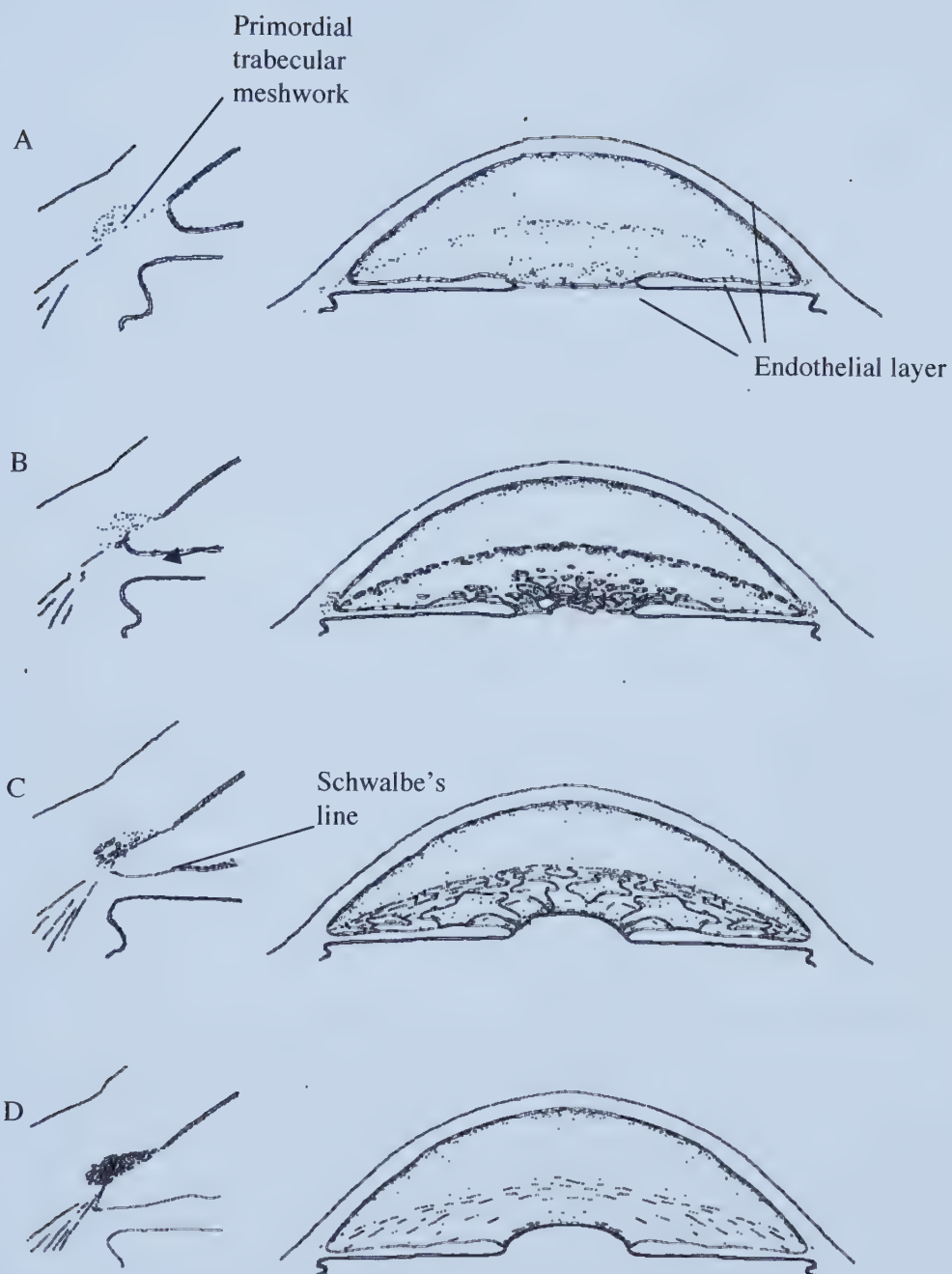


**Figure 19.**

Anterior chamber angle formation.

- A.** At five months gestation the anterior surface of the iris inserts in front of the primordial trabecular meshwork.
- B.** During the last three months of gestation the endothelial layer of the pupillary membrane and iris progressively disappears, and the angle of the anterior segment deepens (arrow).
- C.** Development of the trabecular lamellae and intertrabecular spaces takes place.
- D.** Development of the anterior chamber angle progresses for the first year of life after birth.

(Adapted from Shields 1983).





underlying meshwork (Shields 1983, Anderson 1981) (Figure 19B). The development of trabecular lamellae and intertrabecular spaces begins within the inner and posterior tissues of the primordial trabecular meshwork and progresses towards Schlemm's canal (Shields 1983, Tawara and Inomata 1981) (Figure 19C). As the endothelium of the cornea and the trabecular meshwork begin to differentiate, a distinct demarcation line develops between them to form a primordial Schwalbe's line (Shields 1983, Hansson and Jerndal 1971) (Figure 20). The dilator and pupillary sphincter muscles are derived from the neuroectoderm of the outer layers of the optic cup (Riordan-Eva 1999, Moore 1983). The mesenchyme surrounding the optic cup differentiates into an inner vascular layer, the choroid, and the outer sclera (Riordan-Eva 1999, Moore 1983).

#### Mechanisms of Anterior Segment Dysgenesis

Central defects of the eye (corneal thinning (keratoconus OMIM #148300); Peters anomaly) have been suggested to arise from defects in the first wave of neural crest cells that form the anterior segment (Waring et al. 1975). Peripheral defects of the eye (AR malformations and IGD) have been suggested to result from abnormalities of the second and third waves of cells. I suggest that the anterior segment defects are a progressive spectrum involving the three waves of neural crest cell migration. Iris hypoplasia, occurring alone, likely results from a partial or mild defect of the third wave of neural crest cells which form the iris stroma (and pupillary membrane). Vascular defects of iridic or pupillary blood vessels with thickened basement membrane and functional abnormality (as documented in patients with AR malformations) may lead to decreased blood flow and oxygen deprivation (ischemia) also contributing to iris atrophy (Shields 1983). Defects in the second wave are postulated to result in incomplete maturation of the trabecular meshwork and Schlemm's canal (Waring et al. 1975). Incomplete maturation



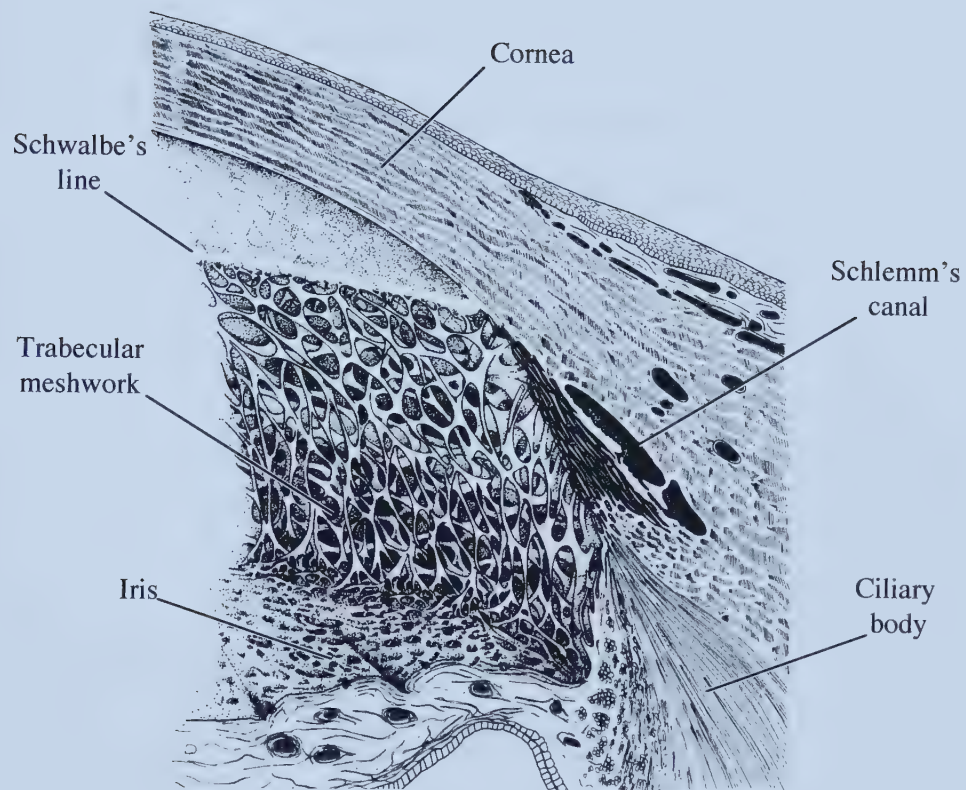




**Figure 20.**

Close-up of the anterior chamber angle of the eye.

(Adapted from Jakobiec 1982).





may lead to the compacted tissue lacking intertrabecular spaces (as documented in cases of AR malformations, Shields 1983). An abnormally retained primordial endothelial layer on portions of the iris and anterior chamber angle is often observed in the eyes of patients with AR malformations (Shields 1983, Alkemade 1969) (Figure 21B). This is likely remnants of the pupillary membrane resulting from a defect in the third wave of cells that is more severe than the defect that results in just iris hypoplasia. Portions of the retained endothelial layer that cross the anterior angle are centrally displaced from the trabecular meshwork during development up until the first years of life either by a contraction of the cellular layer or through different growth rates of the adjacent structures (Shields 1983) (Figure 21B). This displacement in tissue has been suggested to be the cause of the tissue strands that connect Schwalbe's line to the iris (Figure 21C) (Shields 1983). Excessive deposition of basement membrane at an abnormally anterior zone of differentiation between corneal and angle endothelium by the abnormally retained endothelium could result in a prominent and anteriorly displaced Schwalbe's line (Figure 21B) (Shields 1983). Contraction of the remaining endothelial layer on the iris can cause displacement of the pupil toward the contracting tissue, and thinning and tearing in the opposing quadrant(s) of the eye (Figure 21C-D) (Shields 1983). An additional defect in the first wave of neural crest cells would account for the complete loss of Descemet's membrane (Hittner et al. 1982), and the central opacifications and cataracts sometimes associated with AR malformations (Perveen et al. 2000, Doward et al. 1999, Phillips et al. 1996, Holmstrom et al. 1991, Awan 1977). Exclusive, partial defect in the first wave of neural crest cells would account for the central loss, and peripheral preservation, of Descemet's membrane in Peters anomaly (Nakanishi and Brown 1971). This supports the suggestion that Peters anomaly is not a part of the spectrum of anterior segment dysgenesis that includes IH, IGD, AR malformations, and AR malformations with Peters-like features.





**Figure 21.**

A postulated mechanism of anterior segment dysgenesis.

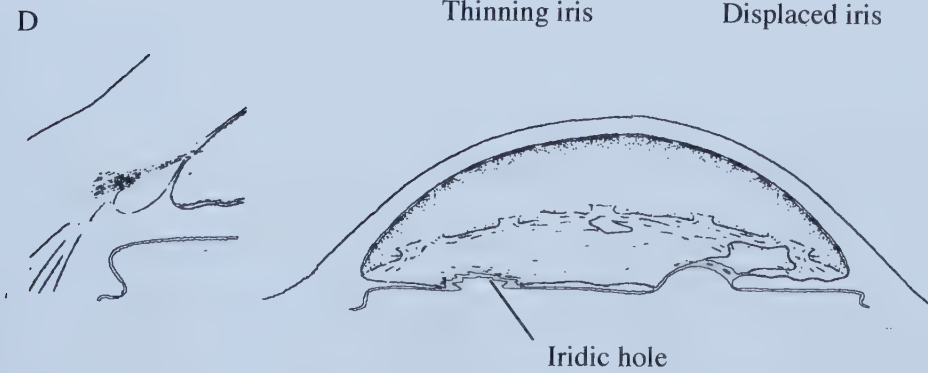
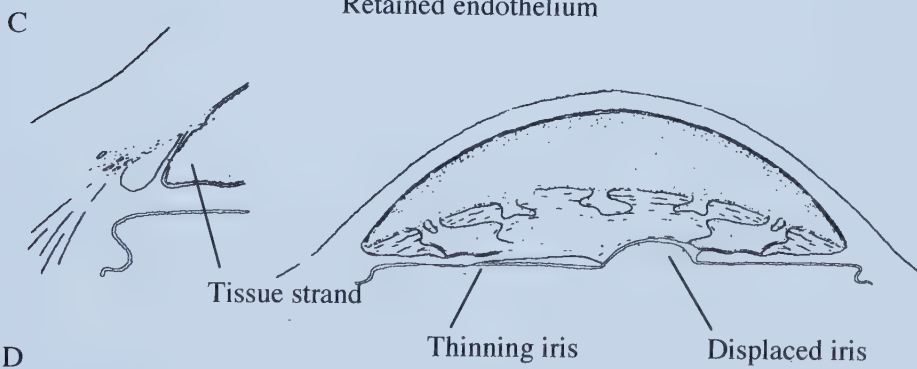
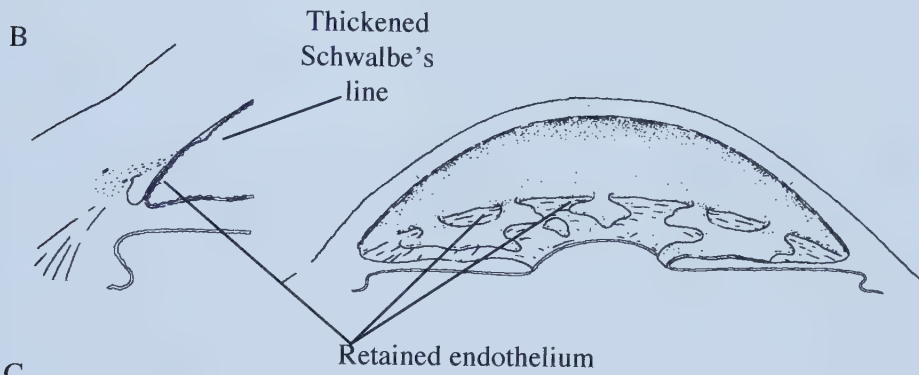
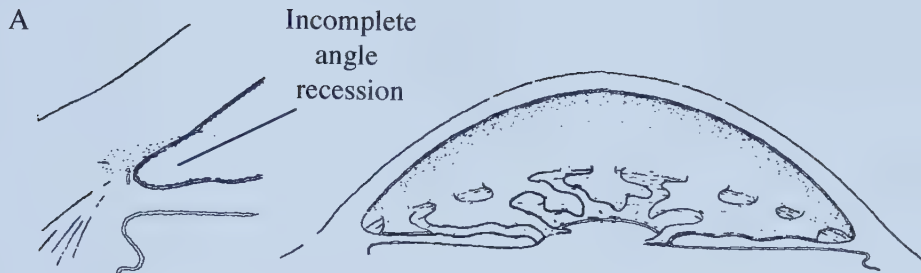
**A.** Incomplete recession of the angle may produce high insertion of the iris over the primordial trabecular meshwork.

**B.** A retained endothelial layer over portions of the iris and trabecular meshwork may be displaced along with underlying iridic tissue from the trabecular meshwork by contraction of the cellular layer or differential growth rates of the adjacent structures. Excessive basement membrane deposition may be responsible for prominence of Schwalbe's line.

**C.** As the endothelial layer disappears, tissue strands extending from the iris to the trabecular meshwork and Schwalbe's line are left behind. Contraction of retained endothelium and these tissue strands may result in a pulling of the pupil towards the contracting tissue, resulting in a displaced pupil.

**D.** Further endothelial contraction may result in iridic thinning and holes in the iris.

(Adapted from Shields 1983).







The neural crest is also responsible for formation of the corneal keratocytes, the ciliary muscle, the fibroblasts of the sclera, the vitreous, and the optic nerve meninges. It is also involved in the formation of the orbital cartilage and bone, the orbital connective tissues and nerves, the extraocular muscles, and the subepidermal layers of the eyelids (Shields 1983, Johnston et al. 1979, Johnston et al. 1973). Note-worthy is that the systemic malformations of pituitary, cranio-facial, and heart tissues associated with the anterior segment disorders have also been shown to be derivatives of neural-crest cells (Shields 1983, Johnston et al. 1979, Johnston et al. 1973).

### Glaucoma

Anterior segment dysgenesis is also associated with the development of glaucoma. Over 50% of patients with IH, IGD, or AR malformations develop early-onset glaucoma by the second decade (Shields 1983). Glaucoma is a group of disorders characterized by progressive damage to the optic nerve of the eye resulting in vision loss. Increased intraocular pressure (IOP) due to decreased or blocked aqueous humor outflow is often associated with glaucoma. An increase in IOP can put stress on optic nerve head resulting in permanent damage of the nerve fibers. Other normal-tension forms of glaucoma are rare and not well understood. Progressive damage to the optic nerve results in first a peripheral, and then a central, loss of vision. Glaucoma can occur as a result of trauma or can have a genetic basis. Hereditary forms of glaucoma are grouped into the three categories of primary, secondary, and congenital glaucoma (Friedman and Walter 1999). Based on the structure of the anterior segment, glaucoma can further be classified as open- or closed-angle glaucoma (Figure 22) (Friedman and Walter 1999). Closed-angle glaucoma indicates the presence of extraneous tissue blocking the trabecular meshwork and thereby preventing normal aqueous humor outflow.





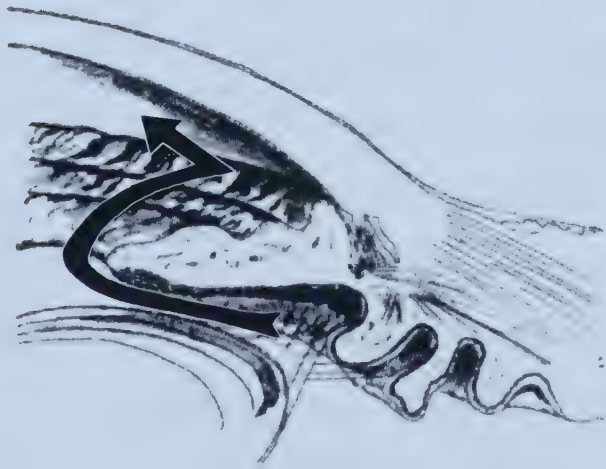
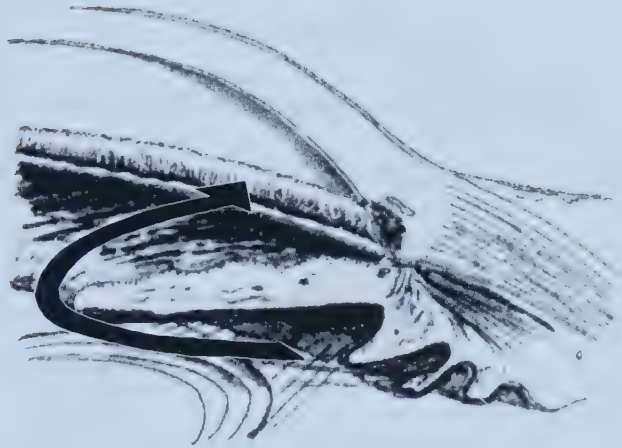
**Figure 22.**

Path of aqueous humor outflow in open- and closed-angle glaucoma.

**A.** In open-angle glaucoma, the aqueous humor (depicted by arrow) produced in the posterior chamber by the ciliary body is able to flow over the lens, through the pupil into the anterior chamber and out through the trabecular meshwork and Schlemm's canal.

**B.** In closed-angle glaucoma, normal outflow of the aqueous humor through the trabecular meshwork and Schlemm's canal is prevented by a blockage of tissue.

(Adapted from Friedman and Walter 1999; original by Dr. I. M. MacDonald, University of Alberta).





Congenital glaucoma is traditionally diagnosed with manifestation before three years of age and has been historically separated from the other 'adult' forms of glaucoma. Primary open-angle glaucoma (POAG) is the most common type of glaucoma. There are no obvious ocular abnormalities, nor any specific systemic diseases related to POAG. Secondary glaucomas can develop as complications of other medical conditions and can result from developmental malformations of the eye, as in the case of AR malformations. Although often considered to be an open-angle form of the glaucoma, the secondary glaucoma associated with AR malformations is probably more appropriately referred to as partially closed due to the presence of adhesions between the iris and Schwalbe's line seen in many patients (Friedman and Walter 1999). However, the presence and severity of glaucoma in AR malformation patients is not correlated with the extent of tissue strands in the angle (Shields 1983). High insertion of the iris into the posterior trabecular meshwork, due to incomplete recession of the peripheral uvea, is seen to be more pronounced in AR patients with glaucoma (Shields 1983, Alkemade 1969, Burian et al. 1954). Transmission electron spectrometry analyses of tissue specimens from patients reveal a compacted trabecular meshwork with reduced or lack of intertrabecular spaces (Shields 1983). It has been proposed that either the high insertion of the iris or compacted trabecular meshwork may be responsible for the obstruction to aqueous humor outflow in the glaucoma of AR malformation patients (Shields 1989). Severe glaucoma in infancy or early childhood in patients with AR malformations is thought to arise mainly from the incomplete development of the trabecular meshwork and Schlemm's canal (Shields 1989). Later development of glaucoma may be a result of compression of the trabecular meshwork from tension exerted by the anteriorly inserted uveal tissue (Shields 1989). The reduced normal aqueous outflow by either mechanism likely results in increased intraocular pressure believed to cause the secondary glaucoma (Shields 1989).





Compacted trabecular meshwork, thought to be due to mechanical compression rather than failed maturation of the tissue, is also seen in congenital and juvenile glaucomas (Anderson 1981, Broughton et al. 1981, Swan 1981). The glaucoma associated with AR malformations has been noted to be particularly difficult to manage and often requires surgical intervention (Shields 1989, Shields 1983, Wyatt et al. 1983). Presymptomatic diagnosis and preventive measures are thus crucial to individuals with AR malformations.

### Genetic Etiology of AR Malformations

Axenfeld-Rieger malformations have long been known to be inherited in an autosomal dominant fashion (Rieger 1934). Translocations, inversions, and deletions within chromosomes 4, 6, 9, 13, 18, and 21 have been associated with AR (Nielson 1984). Four chromosomal loci have been identified by family genetic linkage-based studies on chromosomes 4q25 (Murray et al. 1992), 6p25 (Gould et al. 1997), 13q14 (Phillips et al. 1996) and 16q24 (Nishimura et al. 2000). AR malformation is thus a genetically heterogeneous disorder. The third locus at chromosome 13q14 may represent a clinically distinct phenotype with associated sensorineural hearing loss but no redundancy of the periumbilical skin (Phillips et al. 1996). Mutations of the forkhead transcription factor *FOXC1* on chromosome 6p25 have also been implicated in AR malformations (Mirzayans et al. 2000, Mears et al. 1998, Nishimura et al. 1998). Chromosome 4q25 had shown linkage for a number of affected families, and the epidermal growth factor (*EGF*) gene of the region originally seemed a likely candidate (Murray et al. 1992), but was later excluded (Semina et al. 1996a). In 1996, the transcription factor *RIEG* gene, now called *PITX2*, was identified by positional cloning in the region and its mutation was linked to AR malformations (Semina et al. 1996b). Whole-gene deletion of *PITX2* and interruption



of a regulatory region by a translocation break 90 kb upstream from the gene have also been associated with the disorder (Flomen et al. 1998).

### Allelic Genetic Disorders

In addition to the argument for a developmental relationship between IH, IGD, AR malformations, mutations in *PITX2* link these anterior segment defects genetically. *PITX2* was first found to be mutated in patients with classic AR malformations (Semina et al. 1996b). Missense mutations of the *PITX2* homeodomain have also been documented in patients with IH (Alward et al. 1998) and IGD syndrome (IGDS) (Kulak et al. 1998). The anomaly form of IGD has been excluded from the 4q25 region to this date (Walter et al. 1996) and is linked to 6p25 (Gould et al. 1997).

### The *PITX2* Transcription Factor

The *PITX2* gene spans roughly 18 kilobases (kb) on chromosome 4q25. Three human *PITX2* isoforms have been described that differ at the amino-terminus as proteins of 271 amino acids (aa) (isoform a), 317 aa (isoform b), and 324 aa (isoform c) (Arakawa et al. 1998, Gage and Camper 1997) (Figure 23). Isoform a of *PITX2* has been the most widely studied. All three *PITX2* isoforms maintain a full 60 amino acid homeodomain and identical carboxy-termini. *PITX2* is a member of the *paired-bicoid* class of homeodomain proteins defined by a lysine residue at position 50 of the homeodomain (Figure 24). It has been demonstrated that this lysine residue determines the sequence specificity of the two bases that follow the TAAT core in the DNA-binding sequence TAATCC (Hanes et al. 1994). Members of the *paired-bicoid* group also include *Otd* of *Drosophila*, *unc-30* of *C. elegans* (Jin et al. 1994), the murine *Otx1* and *Otx2* (Simeone et al. 1993), and the human *PITX1* (Lamonerie et al. 1996, Szeto et al. 1996) and *PITX3* (Semina et al. 1997) genes.





**Figure 23.**

Genomic structure of human *PITX2* on chromosome 4q25. Exons are represented as numbered boxes (not representative of actual size). Solid boxes indicate the homeodomain. Underneath are the three known isoforms of *PITX2*.

(Adapted from Arakawa 1998).

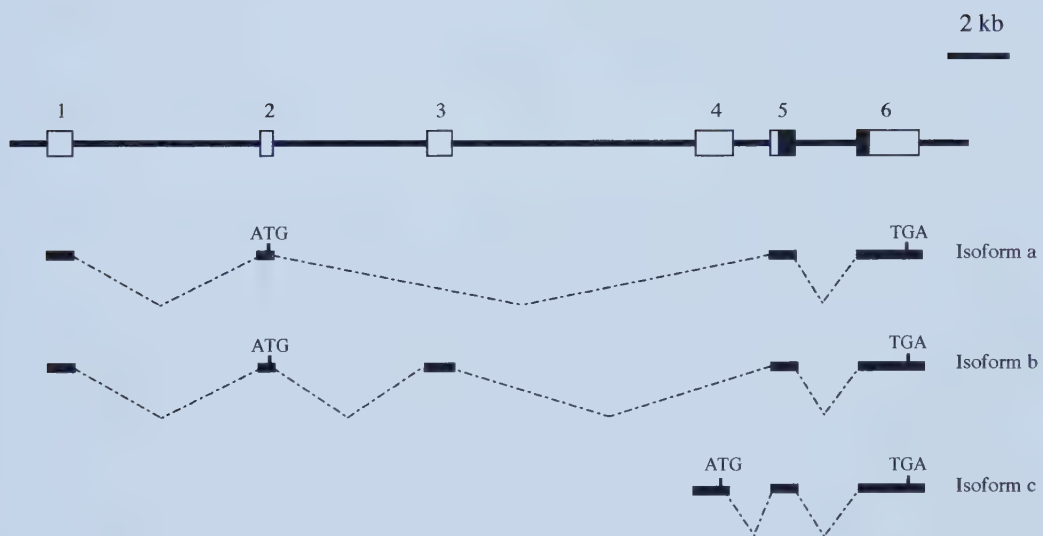








**Figure 24.**

Homeodomain alignment of PITX2 and related transcription factors with percentage identity to the left and the three  $\alpha$ -helices indicated. The *paired-bicoid* class of transcription factors is characterized by a lysine residue at position 50.

% Identity		HELIIX 1										HELIIX 2										HELIIX 3									
		10	20	30	40	50	60	10	20	30	40	50	60	10	20	30	40	50	60												
	PITX2	QRRQRTHFTS	QQLQELEATF	QRNRYPD MST	REEIAVWTNL	TEARVRVWFK	NRRAKWRKRE																								
100	PITX3	-----	-----	-----	-----	-----	-----																								
97	PITX1	-----	-----	-----	-----	-----	-----																								
83	<i>unc-30</i>	P-----	H--T--NW-	S-----	AC-----	-----	IS-----																								
62	<i>Otx-1</i>	---E--T--R	S--DV---L-	AKT-----	IF- ---V-LKI--	P-S--Q----	-----C-QQQ																								
62	<i>Otx-2</i>	---E--T--R	A--DV---L-	AKT-----	IF- ---V-LKI--	P-S--Q----	-----C-QQQ																								
62	<i>otd</i>	---E--T--R	A--DV---L-	GKT-----	IF- ---V-LKI--	P-S--Q----	-----C-QQL																								
60	<i>paired</i>	---C--T-SA	S--D---RA-	E-TQ-----	IY- ---L-QR--	---IQ---S	---RL--QH																								
53	<i>goosecoid</i>	K--H--I--D	E--EA--NL-	-ETK-- --VGT	--QL-RKVH-	R-EK-E----	-----RQK																								
43	<i>Antp</i>	RK-G-QTY-R	Y-TL---KE-	HF---LTRRR	-I---HALC-	--RQIKI--Q	---M--K-EN																								
37	<i>en</i>	EK-P--A-S-	E--AR-KRE-	NE---LTERR	-QQLSSELGL	N--QIKI--Q	-K---IK-ST																								
35	<i>bicoid</i>	P--T--T---	S-IA---QH-	LQGNRYLAPR	LADLSAKLA-	GT-Q-KI---	---RRHKIQS																								



*PITX1*, *PITX2*, and *PITX3* form a group of closely-related transcription factors. *PITX2* and *PITX3* are identical throughout their homeodomains, while the *PITX1* homeodomain differs from that of *PITX2* and *PITX3* by only two residues. The mouse *Pitx1*/*Ptx1* transcription factor was originally characterized and cloned on the basis of its ability to activate transcription of the pro-opiomelanocortin pituitary gene (Lamonerie et al. 1996). Human *PITX1* is located on chromosome 5q31 and is currently not associated with any disorder. Mutation of the *PITX3* gene on chromosome 10q25 is associated with congenital cataracts and anterior segment mesenchymal dysgenesis (ASMD; OMIM #107250) with cataracts (Semina et al. 1998).

The putative helix-turn-helix pattern of the *PITX2* homeodomain (Semina et al. 1996b) represents a classic DNA-binding motif shared by homeodomain proteins such as *bicoid*, *paired*, *engrailed*, and *antennapedia* of *Drosophila melanogaster* (Scott et al. 1989). The presence of a homeodomain in the *PITX2* protein suggests that *PITX2* can bind DNA and influence the transcription of downstream genes during development in a manner similar to the *D. melanogaster* homeotic proteins. Helix 3 of the homeodomain is thought to fit into the major groove of DNA and make DNA base contacts, while helix 2 is thought to contact the DNA phosphate backbone to stabilize the interactions of helix 3 (Burglin 1994) (Figure 25).

### Murine *Pitx2* Expression

The murine *Pitx2* expression profile correlates strongly with the tissues affected in patients with IH, IGD and AR malformations (Gage and Camper 1997, Semina et al. 1996a). *In-situ* hybridization studies of murine *Pitx2* mRNA during embryogenesis show *Pitx2* expression in Rathke's pouch, maxillary and mandibular epithelia, periocular mesenchyme, vitelline and umbilical vessels, limb bud, and dorsal mesentery (Gage and



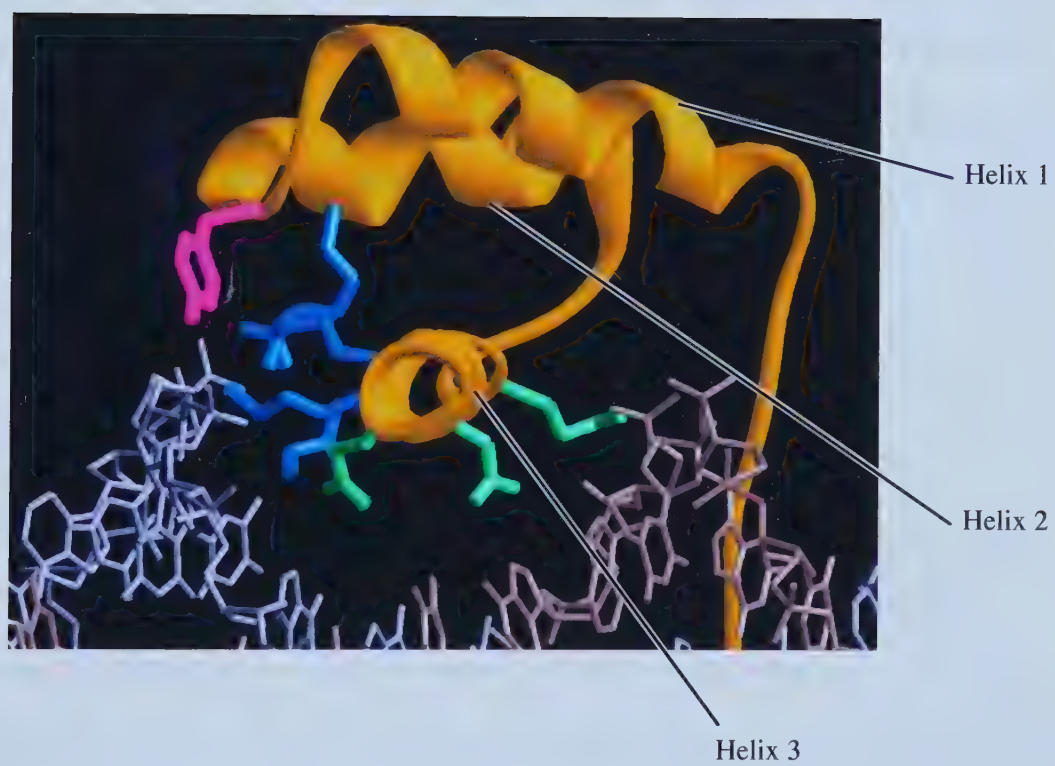




**Figure 25.**

The *engrailed* transcription factor bound to DNA as an example of a helix-turn-helix homeodomain.

(Adapted from [www.expasy.ch](http://www.expasy.ch))





Camper 1997, Semina et al. 1996b) (Figure 26). Recently, murine *Pitx2* has been shown to be expressed as early as 10.5 days following conception in the neural crest surrounding the optic cup and stalk that has begun to migrate across the anterior lens (Gage et al. 2001).

#### Pituitary Expression of *PITX* Transcription Factors

Human *PITX1* is expressed throughout the pituitary while *PITX2* expression is restricted to certain cell lineages, and *PITX3* is not detected. *PITX2* is not seen to be expressed in human corticotroph cells, but is expressed in gonadotroph cells (Pellegrini-Bouiller et al. 1999). *PITX2* is thought to be the first *paired* homeodomain pituitary transcription factor differentially expressed in lactotrophs but not in somatotrophs, indicating a possible role for *PITX2* in the terminal differentiation of these cell lines from a common precursor (Pellegrini-Bouiller et al. 1999).

#### *PITX2* in the Left-Right Pathway

*PITX2* has also been implicated in the developmental pathway of left-right asymmetry. Altered *Pitx2* expression patterns were found in mice with laterality defects that correlated to changes in the visceral symmetry (Piedra et al. 1998). Ectopic expression of *Pitx2* mRNA in chick and *Xenopus* embryos resulted in aberrant looping of the heart and gut and reversed body rotation (Campione et al. 1999, Logan et al. 1998, Ryan et al. 1998). Embryonic-lethal *Pitx2* homozygous null (-/-) mice have incomplete turning of the embryo, defective body wall closure, aberrant heart morphogenesis and/or positioning (but normal looping), right isomerization of the lung, failed pituitary development and tooth organogenesis, and defects in anterior and posterior eye segments (Gage et al. 1999a, Lin et al. 1999, Lu et al. 1999).

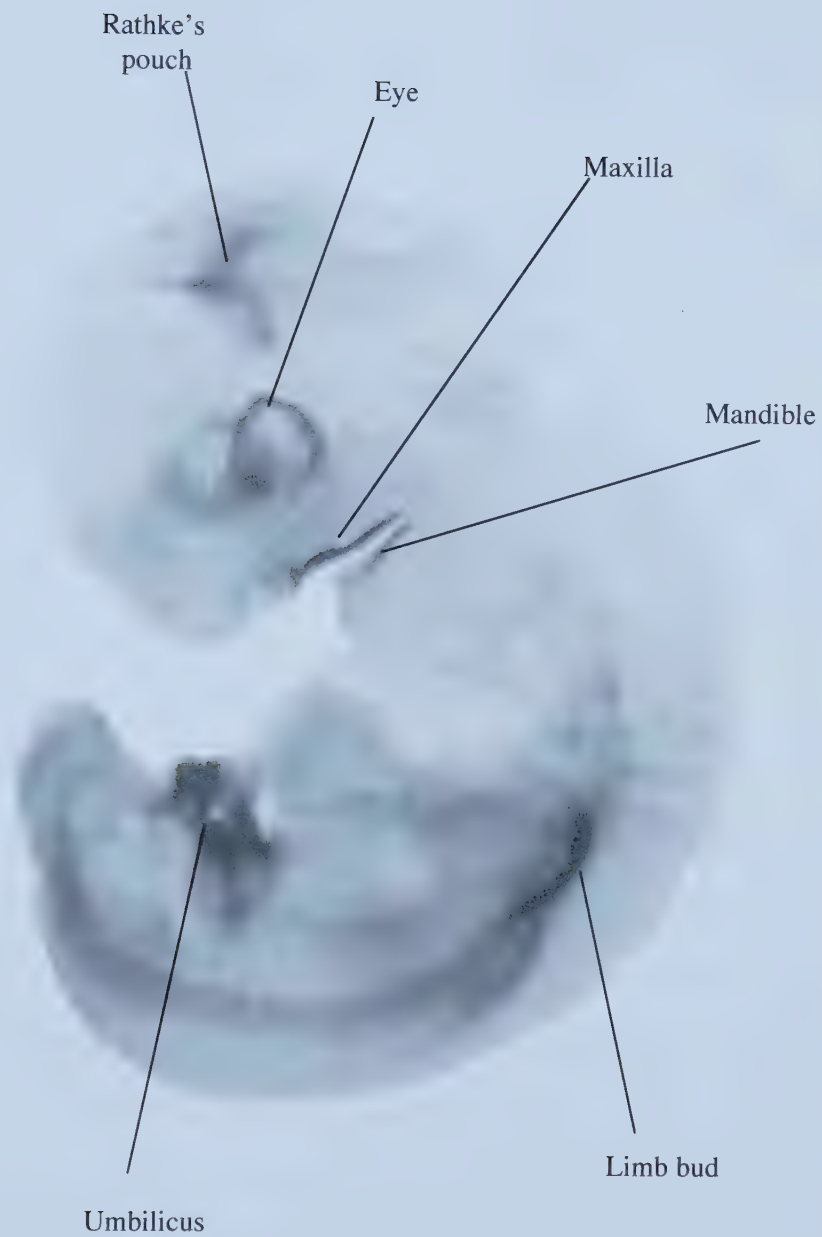




**Figure 26.**

Embryonic expression of *Pitx2* in the mouse at day 11 of gestation.

(Adapted from Semina et al. 1996b)







### Ocular Defects of *Pitx2* Mouse Knock-outs

Heterozygous *Pitx2*<sup>+/-</sup> mice displayed AR malformation-like defects, including small eyes with aberrantly shaped and misplaced pupils, full-thickness iris holes, clouded lens, tooth defects and retarded growth (Gage et al. 1999a). In addition to malpositioned small eyes lacking extrinsic musculature with vestigial lens pits and optic nerve coloboma, *Pitx2*<sup>-/-</sup> null mice presented thickening of both the corneal epithelium and the mesenchyme separating the optic cup rim from the corneal surface ectoderm (Gage et al. 1999a) (Figure 27). Interestingly, undifferentiated mesenchymal cells have been demonstrated in place of a proper cornea in mice null for the *Pitx2* homeodomain (*hd*<sup>-/-</sup>), that also lack the anterior chamber (Lin et al. 1999). Together, these results indicate that PITX2 plays a crucial role in the differentiation of the periocular mesenchyme, loss of which may result in the accumulation of undifferentiated cells and thickening of anterior segment structures.

### Systemic Defects that are Not Seen in Patients

The severity of non-ocular defects and issues of laterality of the homozygous *Pitx2* null (*-/-*) mice are not seen in heterozygous IH, IGD and AR malformation patients. The one wildtype *PITX2* allele carried by patients appears to be sufficient for normal laterality. Functional redundancy may be an additional consideration within certain cell lineages of the pituitary where *Pitx1* exhibits overlapping expression with *Pitx2* during murine development (Gage et al. 1999b, Tremblay et al. 1999, Gage and Camper 1997, Lamonerie et al. 1996). *PITX2* redundancy does not appear to be a consideration within the eye at this time, as there is no evidence of *PITX1* or *PITX3* co-expression with *PITX2* in the same ocular tissues. The lack of *PITX2* redundancy in the developmental pathways





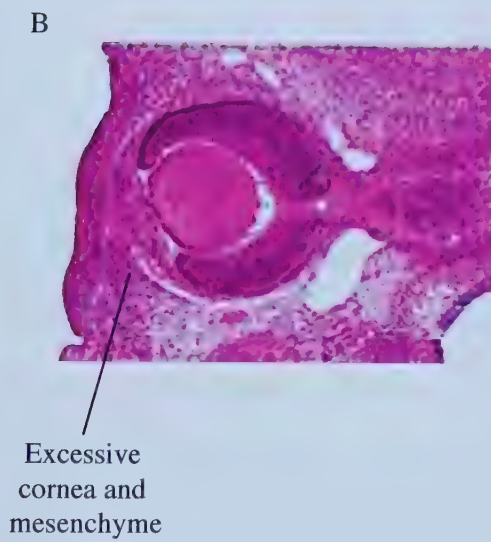
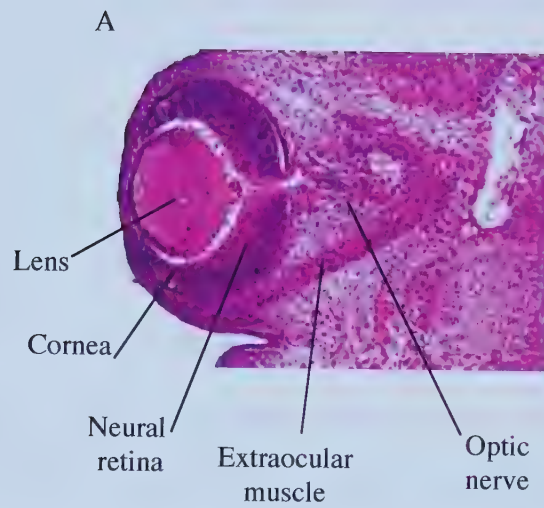
**Figure 27.**

Transverse sections of embryonic murine eyes at day 12.5.

**A.** Wildtype  $+/+$  *Pitx2* eye.

**B and C.** Mutant  $-/-$  *Pitx2* eyes. Note the inappropriate position of the eyes, vestigial lens pit indicating incomplete halted development, and absence of extrinsic ocular muscles. In addition, closure of the optic fissure and stalk are defective (or delayed), and the corneal epithelia and mesenchyme are hypercellular.

(Adapted from Gage et al 1999).





of the anterior segment may partially explain why the eye is more sensitive than the pituitary to *PITX2* mutation.

### Project Description

The purpose of this project was to explore the possible genotype-phenotype correlations of *PITX2* homeodomain mutations and resultant ocular phenotypes within the spectrum of anterior segment dysgenesis. In addition, an attempt was made to identify and examine possible genes downstream of *PITX2* in ocular development, and/or early-onset glaucoma. Patients with AR malformations, IGD, and IH were screened for *PITX2* mutations to add to the list of documented mutations. A larger sampling of *PITX2* mutations will aid in developing genotype-phenotype correlations. As genotype-phenotype correlations had not been possible with mutational data alone, biochemical analyses were required. Missense mutations of the *PITX2* homeodomain documented in the literature were characterized by intracellular localization, DNA-binding ability, and transactivation of a reporter gene. I hypothesized that differences in functional amounts of *PITX2* protein, dependent upon specific *PITX2* mutations, was related to the severity of resultant anterior segment dysgenesis phenotypes. Since the glaucoma associated with anterior segment dysgenesis is not congenital, the possibility that *PITX2* plays a role in the adult eye was also examined briefly by profiling the expression of *PITX2* in adult eye tissues. In addition, the promoter of the *Myocilin* gene involved in glaucoma (Kubota et al. 1998, Stone et al. 1997) was tested as a candidate downstream promoter for transcriptional activation by *PITX2*. Some of the *PITX2* homeodomain mutants were also assessed for their ability to transactivate the *Myocilin* promoter. This thesis will elucidate the role of *PITX2* in the genetic etiology of anterior segment dysgenesis and provide





insight into the genetic pathways of ocular development, and simultaneously, that of other systems.



## **MATERIALS and METHODS:**



## **I: PITX2 Mutational Analysis**

### **Patient DNA**

Genomic DNA of 31 patients with anterior segment dysgenesis (ASD) was available within the Walter laboratory at concentrations of 50 ng/μL for use in PCR. Of the 31 patients with ASD, 12 patients had been diagnosed by their referring ophthalmologists with ARS, 4 with ARA, and 8 with IGD, 6 with Peters anomaly; a single case of uncharacterized anterior segment dysgenesis (ASD) was also included in the study.

### **PCR Amplification, Visualization, and Purification of *PITX2* Exons**

*PITX2* exons were amplified by polymerase chain reaction (PCR) for either automated LI-COR or manual <sup>33</sup>P sequencing. PCR primers were the same as used previously in the Walter laboratory for mutational analysis. One additional primer, 10R, was designed within the 3'UTR to span the sequence encompassed by primer 9R which covers the *PITX2* stop codon. The 10R primer was designed with the aid of the software program GeneWorks 2.2.1 to work with primer 7F. Primers were synthesized by Gibco / BRL Life Sciences. Primer positions and product sizes appear in Figure 28, and primer sequences appear in Table 1. PCR reactions were prepared as follows: 2.5 μL 10x PCR buffer, 2.5 μL 2mM dNTPs, 0.125 μL 100x acetylated BSA, 50 ng genomic template DNA, 0.25 μg of each respective primer (forward and reverse), and sterile distilled H<sub>2</sub>O for a total volume of 25 μL with the addition of home-made Taq polymerase. Recipes for solutions appear in the Materials Appendix. The PCR reactions were amplified using a MJ Research PTC-100 Programmable Thermal Controller. *PITX2* primers pairs 2F and 2R; 3F and 4R; 5F and 7R; 7F and 10R, were used to amplify the intron boundaries and exons of the coding sequence of *PITX2*. PCR amplification used a program consisting of template denaturation at 95°C for 5 minutes, followed by 35 cycles of denaturation for 30







**Figure 28.**

Schematic of the *PITX2* (isoform a) cDNA with the homeodomain indicated in black.

The position of primers used for sequencing exons 2, 5, and 6 are indicated below the cDNA, as are approximated PCR product sizes.

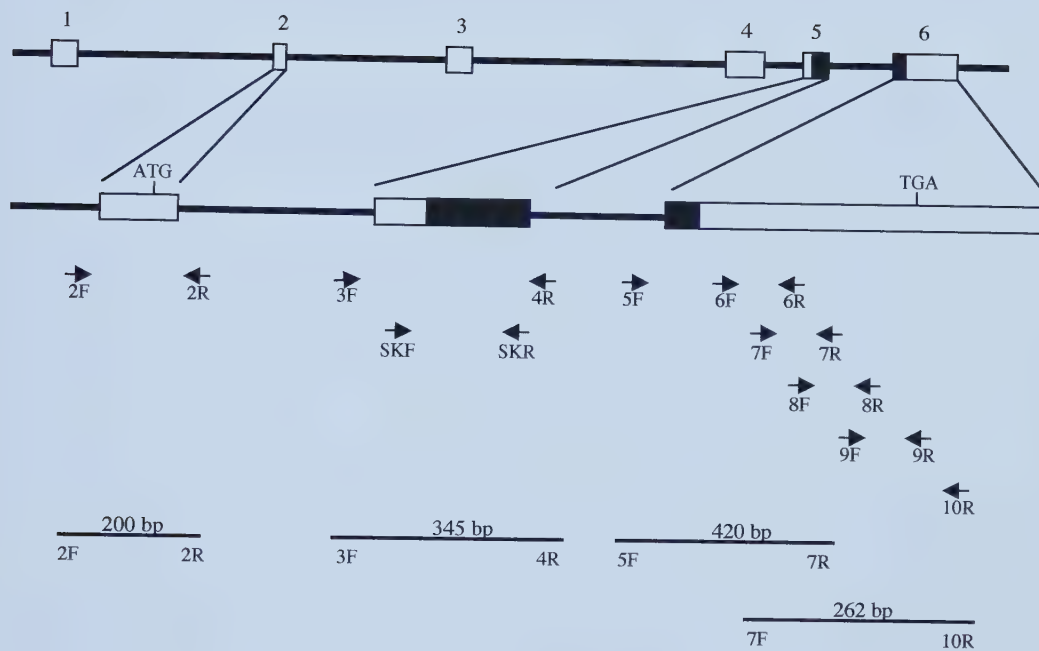




**Table 1.**

Sequence of the *PITX2* PCR primers (forward F and reverse R) used for PCR amplification and sequencing. Annealing temperatures used in sequencing reactions are indicated. See text for annealing temperatures of primer pairs used for PCR amplification.

Primer	Sequence	Annealing Temp. (°C)
2F:	5' CTGAAGCCTAGCACACAGTA	56
3F:	5' CAGCTCTTCCACGGCTTCT	56
SKF:	5' ACCCGTCTAAGAAGAAGCGG	55
5F:	5' GTAATCTGCACTGTGGCATC	56
6F:	5' AGTTCAATGGGCTCATGCAG	56
7F:	5' GCTTCCCCTTCTTCAACTCT	55
8F:	5' ACTCTATCTCGTCCATGAGC	56
9F:	5' GCCGACTCCTCCGTATGTTT	62
2R:	5' GCAGGAGAAGGGGGTTCTTA	56
SKR:	5' GCTTCCGTAAGGTTGGTCC	55
4R:	5' CTCCACATTCTCTCCTGGT	56
6R:	5' GGGGAAAACATGCTCTGTGA	56
7R:	5' GGCTACTCAGGTTGTTCAAG	55
9R:	5' CTGTGGGTGCGGCTCACA	62
10R:	5' TAGTGCCCACGACCTTCTAGC	56



seconds at 95°C, primer annealing for 30 seconds at various temperatures, and product extension for 30 seconds at 72°C, and a final extension step of 7 minutes at 72°C. PCR programs with annealing temperatures of 54°C were used for primers 3F and 4R, 5F and 7R; an annealing temperature of 56°C was used for primers 2F and 2R. A special “touchdown” PCR program was used to optimize amplification with the 7F and 10R primer pair. A touchdown program was designed where the first annealing temperature was 62°C, followed by 15 successive cycles of a 0.5°C decrease in annealing temperature, until a 54°C annealing temperature was reached, followed by a standard PCR program with 35 cycles at an annealing temperature of 54°C.

Amplified PCR products had 5 µL of loading dye added and were sized by electrophoresis on 1% agarose / 1x TBE gels containing ethidium bromide. PCR products were visualized and documented using a Pharmacia Biotech Image Master VDS, and isolated from the gel with aid of a UV transilluminator. PCR products were purified from isolated gel pieces using QIAgen gel extraction columns as per manufacturer instructions.

### <sup>33</sup>P Sequencing

An Amersham <sup>33</sup>P Thermosequenase kit (Amersham Life Sciences) was used to sequence the purified PITX2 PCR products as per manufacturer instructions. Primers used for PCR amplification were also used for *PITX2* sequencing (forward: 2F, 3F, 5F, 7F; reverse: 2R, 4R, 7R, 10R). Additional internal primers were also used (forward: 6F, 8F, 9F; reverse: 6R, 9R) (see Table 1 for sequences and annealing temperatures). Following a 5 minute denaturation step at 95°C 25 rounds of cycle sequencing were performed, with denaturation for 30 seconds at 95°C, primer annealing for 30 seconds at various temperatures, and product extension for 30 seconds at 72°C, and a final extension step of 7 minutes at 72°C. PCR-based sequencing products were separated on 6% denaturing



acrylamide gels for 2 to 6 hrs at 50W. Gels were dried under vacuum and products were visualized by autoradiography on Kodak Biomax film.

### LI-COR Sequencing

Fluorescently labeled sequencing primers were synthesized by LI-COR. *PITX2* forward primers 2F, 3F, 5F, and 7F were labeled with 800 nm detectable fluorescent tags, and reverse primers 2R, and 4R were labeled with 700 nm detectable fluorescent tags, to enable reading of sequence in both directions within the same sequencing reaction. The chemical synthesis of fluorescently-labeled reverse primers 7R and 10R was twice discovered to be imperfect, and the primers were not used for LI-COR sequencing. Reactions contained 0.233  $\mu$ L of each forward and reverse primer (1.0 pmol/ $\mu$ L), 200 ng of template DNA, 2  $\mu$ L of the appropriate ddNTP, and dH<sub>2</sub>O for a final volume of 6  $\mu$ L. Following a 2 minute denaturation at 92°C, 30 cycles of cycle sequencing were performed, with denaturation at 92°C for 30 seconds, primer annealing at 52°C for 15 seconds, and product extension at 72°C for 15 seconds. Reactions were protected from light at all times and were maintained at 4°C until 3  $\mu$ L of stop dye was added. Sequencing reactions were visualized and digitally recorded by a LI-COR Sequencer.

## **II: Functional Analyses of PITX2 Homeodomain Mutants**

### *PITX2* cDNA

The *PITX2* cDNA was a gift from Dr. Jeff Murray, University of Iowa. The *PITX2* cDNA was obtained as a 1.2 kb fragment containing all four exons of *PITX2* (isoform a) and 234 bp of 5' and 153 bp of 3' untranslated DNA. The *PITX2* cDNA was subcloned within the *Eco* R I multiple cloning site of the Bluescript plasmid (pBS) (Figure 29). Transformed *E.coli* cells were provided within an agar gel stab.







**Figure 29.**

Schematic of the *PITX2* cDNA subcloned within the *EcoR* I site of the pBS shuttle vector. Indicated are the *Bam*H I sites used for subcloning into the pcDNA4/His Max A mammalian expression vector. Also denoted is the mutation of a stop codon (TAA) that naturally occurs 5' to the *PITX2* start methionine.

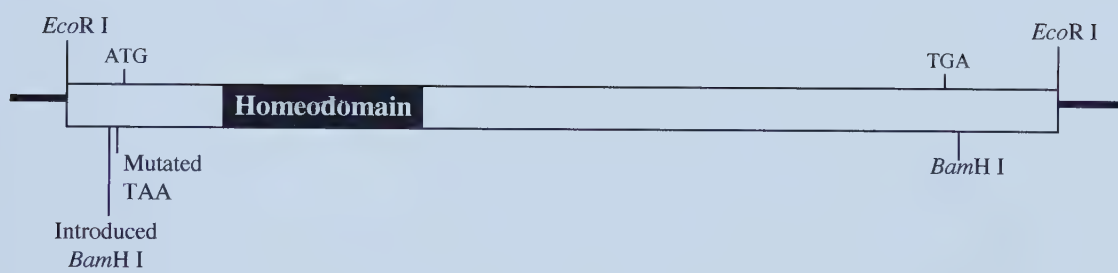






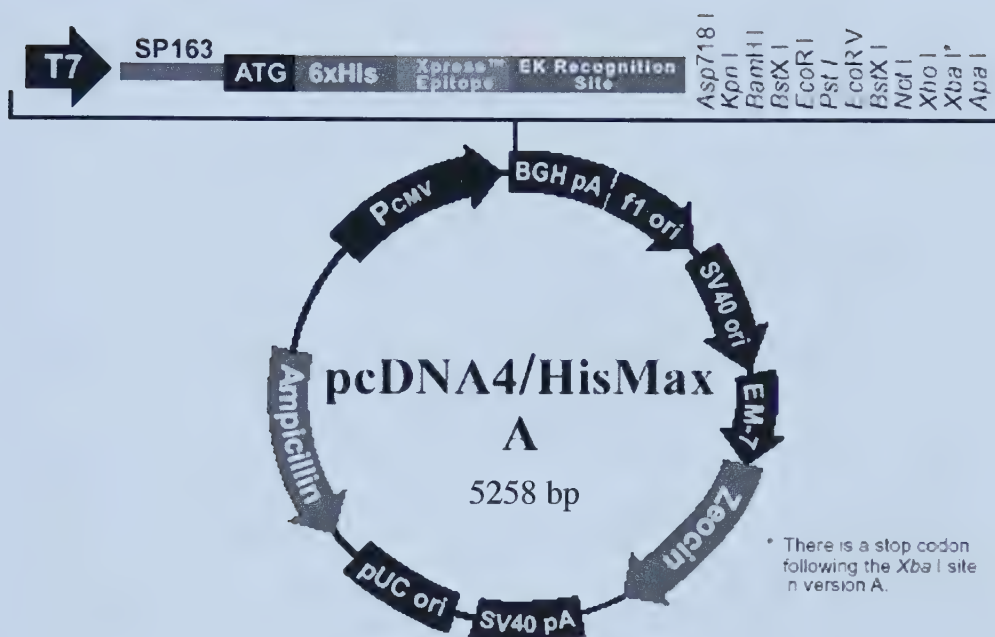
**Figure 30.**

**A.** Schematic of the pcDNA4/HisMax A mammalian expression vector from Invitrogen with main features indicated.

**B.** Sequence of the pcDNA4/HisMax A vector multiple cloning site and other important features.

(From [www.invitrogen.com](http://www.invitrogen.com)).

A



CMV promoter:	bases	232-819
T7 promoter/priming site:	bases	863-882
QBI SP163 translational enhancer:	bases	917-1079
Polyhistidine tag:	bases	1092-1109
Xpress™ epitope:	bases	1149-1172
Enterokinase recognition site:	bases	1158-1172
Multiple cloning site:	bases	1172-1245
pcDNA3.1/BGH reverse priming site:	bases	1268-1495
f1 origin:	bases	1541-1969
SV40 promoter & origin:	bases	1996-2305
EM-7 promoter:	bases	2353-2408
Zeocin resistance gene:	bases	2427-2801
SV40 polyadenylation sequence:	bases	2931-3061
pUC origin:	bases	3444-4117
Ampicillin resistance gene:	bases	4262-5122





## B

```

821 CTGGCTAACT AGAGAACCCA CTGCTTACTG GCTTATCGAA ATTAATACGA CTCACTATAG
                                     T7 promoter/priming site
881 GGAGACCCAA GCTGGCTAGC GTTTAAACTT AAGCTTAGCG CAGAGGCTTG GGGCAGCCGA
                                     QBI SP163 translational enhancer
941 GCGGCAGCCA GGGCCCGGCC CGGGCCTCGG TTCCAGAAGG GAGAGGAGCC CGCCAAGGCG
1001 CGCAAGAGAG CGGGCTGCCT CGCAGTCCGA GCCGGAGAGG GAGCGCGAGC CGCGCCGGCC
1061 CCGGACGGCC TCCGAAACC ATG GGG GGT TCT CAT CAT CAT CAT CAT CAT
    Met Gly Gly Ser His His His His His His His
                                     Polyhistidine Region
1110 GGT ATG GCT AGC ATG ACT GGT GGA CAG CAA ATG GGT CGG GAT CTG TAC
    Gly Met Ala Ser Met Thr Gly Gly Gln Gln Met Gly Arg Asp Leu Tyr
                                     Xpress™ Epitope
1158 GAC GAT GAC GAT AAG GTA CCT AGG ATC CAG TGT GGT GGA ATT CTG CAG
    Asp Asp Asp Asp Lys Val Pro Arg Ile Gln Cys Gly Gly Ile Leu Gln
    Enterokinase recognition site  ▲ EK cleavage site
    EcoR V      BstX I*   Not I    Xho I    Xba I      Apa I
1206 ATA TCC AGC ACA GTG GCG GCC GCT CGA GTC TAG AGGGCCCGTT TAAACCCGCT
    Ile Ser Ser Thr Val Ala Ala Ala Arg Val ***
    pcDNA3.1/BGH reverse priming site
1259 GATCAGCCTC GACTGTGCCT TCTAGTTGCC AGCCATCTGT TGTTTGCCCC TCCCCCGTGC

```



### pcDNA4/HisMax Expression Vector

The mammalian expression vector pcDNA4/HisMax A (Invitrogen) (5258 bp) encoding an N-terminal Xpress epitope (Asp-Leu-Tyr-Asp-Asp-Asp-Asp-Lys) of 4 kDa, was used for protein expression (Figure 30).

### Cloning of *PITX2* cDNA into an Expression Vector

The *PITX2* pBS-subclone was modified prior to subcloning into the pcDNA4/HisMax expression vector. QuikChange (Stratagene Cloning Systems) site-directed mutagenesis was used to introduce a 5' UTR *Bam*H I site and to mutate an upstream stop codon from the *PITX2* cDNA as indicated in Figure 29. Mutagenic primer sequences appear in Table 2.

The new *Bam*H I site was used in conjunction with a pre-existing C-terminal *Bam*H I site for subcloning the *PITX2* cDNA into the mammalian expression vector pcDNA4/HisMax A. Both the pBS-*PITX2* and pcDNA4/HisMax A vectors were digested with the *Bam*H I restriction enzyme. Digested pBS-*PITX2* fragments were size-separated by electrophoresis on 1% agarose gel. A 880 bp fragment containing the *PITX2* cDNA was recovered from the agarose gel using a QIAgen gel extraction column (as per manufacturer's instructions).

Linearized pcDNA4/HisMax A vector was 3' dephosphorylated with Calf Intestinal Alkaline Phosphatase (CIAP). Dephosphorylated plasmid DNA was then purified by ethanol precipitation with 2x volume 95% Ethanol (ice-cold) and 0.1x volume (after addition of ethanol) 3M NaOAc at -80°C overnight. Centrifugation at 13 000 rpm for 15 minutes (4°C) produced a DNA pellet that was washed with 70% Ethanol (ice-cold), air-dried, and resuspended in dH<sub>2</sub>O.



**Table 2.**

Sequence of the various mutagenesis primers used with the *PITX2* cDNA subcloned in pBS. In brackets is the methodology used for identifying clones carrying the intended mutation.

**New *Bam*H I: (differential *Bam*H I digest of the plasmid)**

Forward: 5' GCAGTGGGACGCGGATCCAGCAGCTCTCTCCC

Reverse: 5' GGGAGAGAGCTGCTGGATCCGCGTCCCCTG

**Stop Codon Mutation: (differential *Eco*R V digest of the plasmid)**

Forward: 5' CCGGTAGCCGATATCGGGGAATGGAGACC

Reverse: 5' GGTCTCCATTCCCCGATATCGGCTACCGG

**Arg31His (IGD) (*Bst*U I restriction site lost in digest of SKF-SKR PCR product)**

Forward: 5'-GGACATGTCCACACACGAAGAAATCG

Reverse: 5'-CGATTTCTTCGTGTGTGGACATGTCC

**Arg46Trp (IH) (*Msp* I restriction site lost in digest of 4F-6R PCR product)**

Forward: 5'-GGAAGCCCGAGTCTGGGTTTGGTTCAAGAATCG

Reverse: 5'-CGATTCTTGAACCAAACCCAGACTCGGGCTTCC

**7aaDup (AR-1) (differential *Eco*O 109 restriction digest of the plasmid)**

Forward: 5' CGGCAAAGGCGGCAGCGGACTCACTTTACCAGCCAGCAGACT  
CACTTTACCAGCCAGCAGCTCCAGGAGCTGGAGGCC

Reverse: 5' GGCCTCCAGCTCCTGGAGCTGGCTGGTAAAGTGAGTCTGCTGGC  
TGGTAAAGTGAGTCCGCTGCCGCCTTTGCCGC



**Table 2 Continued.**

**Leu16Gln (AR-2) (*Alu* I restriction site lost in digest of SKF-SKR PCR product)**

Forward: 5'-GCAGCTCCAGGAGCAGGAGGCCACTTTCC

Reverse: 5'-GGAAAGTGGCCTCCTGCTCCTGGAGCTGC

**Thr30Pro (AR-3) (confirmed by sequencing plasmid with 4F)**

Forward: 5'-CCCGGACATGTCCCCACGCGAAGAAATCGC

Reverse: 5'-GCGATTTCTTCGCGTGGGGACATGTCCGGG

**Val45Leu (AR-4) (*Ava* I restriction site lost in digest of plasmid)**

Forward: 5'-CCTTACGGAAGCCCGACTCCGGGTTTGG

Reverse: 5'-CCAAACCCGGAGTCGGGCTTCCGTAAGG

**Arg53Pro (AR-5) (*Msp* I restriction site lost in digest of 4F-6R PCR product)**

Forward: 5'-GGTTCAAGAATCGTCCGGCCAAATGGAGAAAGAGG

Reverse: 5'-CCTCTTTCTCCATTTGGCCGGACGATTCTTGAACC

**Δ NLS: (size 4F-SKR PCR product and sequence with 4F)**

Forward: 5' CGAGGACCCGTCTCAAAGGCGGCAGC

Reverse: 5' GCTGCCGCCTTTGAGACGGGTCCTCG





Ligations of *PITX2* cDNA and pcDNA4/HisMax A plasmid were carried out at 2:1, 1:1, and 1:2 ratios overnight at 15°C. 50 µL of competent *E.coli* XL1 Blue cells were transformed with ~25 ng DNA of the ligation mix in 10 µL total volume. Following incubation for 30 minutes on ice cells were heat shocked for 90 seconds at 42°C and 500 µL of warm LB was added. Cells were shaken for 1 hr at 37°C and 250 µl plated on LB agar plates with appropriate ampicillin selection and incubated overnight at 37°C. Isolated colonies were grown in LB with ampicillin at 37°C overnight with shaking.

Plasmid was prepared from the bacterial cultures by standard plasmid miniprep procedures. Bacterial cells were pelleted from 1.5 mL of overnight culture by centrifugation for 60 seconds. The majority of media was poured off and pellets were resuspended by vortexing in the remaining 50 – 100 µL media. 300 µL TENS was added, followed by 150 µL 3 M NaOAc, and 3-4 slow inversions. Proteins and cellular debris were pelleted by centrifugation for 6 minutes. Supernatant was removed to a new tube, and 900 µL ice-cold 95% ethanol was added, followed by centrifugation for 10-15 minutes at 4°C. Pellets were washed with 500 µL ice-cold 70% ethanol, centrifuged for 3 minutes, air dried and resuspended in 30 µL dH<sub>2</sub>O.

The size of the *PITX2* cDNA insert was confirmed by *EcoR* I digest of the plasmid preparations with electrophoresis on 1% agarose. Selected clones were grown in maxi-cultures for preparation and purification of plasmid DNA using a QIAGEN MaxiPrep Column. QIAGEN maxiprep protocols were slightly altered; 500 mL instead of 100 mL of overnight culture were used, and volumes of resuspension, lysis, and neutralization buffers supplied by QIAGEN were correspondingly increased to 30-40 mLs, depending upon size of bacterial pellet following initial centrifugation. The *PITX2* cDNA subclone was fully sequenced prior to use in transfection with *PITX2* primers as used for patient mutational analysis.



### PITX2 Homeodomain Mutants

Mutations of the PITX2 homeodomain, documented in the literature, were introduced into wildtype *PITX2* cDNA for expression and characterization. A total of seven mutants were re-created for this study, including one found in a patient with IH (Arg46Trp), one described in a patient with IGD (Arg31His), and five found in ARS patients (a seven amino acid duplication (7aaDup, AR-1), and four missense mutations: Leu16Gln (AR-2); Thr30Pro (AR-3); Val45Leu (AR-4); and Arg53Pro (AR-5)). The mutations were introduced into the PITX2-pcDNA4/HisMax expression construct using the QuikChange Site-Directed Mutagenesis Kit with the mutagenic primers that appear in Table 2 as per manufacturer's instructions. *E. coli* cells were transformed with the mutagenesis reactions and isolated colonies grown under ampicillin selection were subjected to miniculture and plasmid preparation. The PITX2 homeodomain region was PCR-amplified using various *PITX2* primer pairs from the plasmid preparations to identify mutations by restriction enzyme digestion and sizing of PCR products (see Table 2 for specific details). Clones deemed to carry the intended mutation and free of all other secondary mutations were cultured and plasmid DNA was prepared and purified with QIAgen maxiprep columns. Prior to transfection experiments, maxiprep DNA was re-sequenced.

### Tissue Culture Cells

Mammalian COS-7 and HeLa cells, originally obtained from ATCC, were maintained as frozen stocks.

### Immunofluorescence

To determine intracellular localization by immunofluorescence, mammalian COS-7 cells were seeded at  $2 \times 10^5$  cells per well in 2 mLs Dulbecco's Modified Eagle Media (DMEM)



+ 10% fetal bovine serum (FBS) on coverslips in 6-well plates (30 mm x 10 mm). A mixture of 3  $\mu$ L FuGENE 6 transfection reagent (Roche Molecular Biochemicals) and 97  $\mu$ L of DMEM, incubated for 15 minutes, was added to ~60 ng of PITX2-pcDNA4/HisMax DNA and incubated for an additional hour. The FuGENE-DNA mix was then added to the COS-7 cells grown to 40-50% confluency.

72 hours following transfection, COS-7 cells were washed with 1x PBS, fixed with 1% paraformaldehyde (1x PBS) for 6 minutes, washed 3 times with 1x PBS, permeated by 0.05% TritonX-100 (1x PBS) for ten minutes, washed 5 times with 1x PBS, and blocked with 5% bovine serum albumin (1x PBS) for one hour, followed by 3 washes with 1% BSA/ 1x PBS (Adapted from Shin et al. 1999). Anti-Xpress (Invitrogen), a mouse monoclonal antibody, was used to detect the Xpress epitope encoded by the expression vector carried by the recombinant PITX2 proteins. Cells were incubated for 45 minutes with the anti-Xpress antibody at 1:400 dilution in 1% BSA/1x PBS. A secondary rabbit-anti-mouse antibody linked to fluorescent Cy3 (Jackson ImmunoResearch Laboratories) was used at a 1:400 dilution for a 45 minute incubation. Each incubation was followed by 5-6 washes with 1% BSA/1x PBS. Nuclei were counterstained with mounting media containing DAPI dye. Coverslips were sealed onto glass microscope slides with either rubber cement or clear nail polish. Cells were examined by fluorescent microscopy (Leica Mikroskopie und Systeme GmbH, Germany) with a TRITC filter (Chroma Technology Corporation).

### PITX2 Protein Expression

For large scale protein expression, COS-7 cells were seeded at  $2 \times 10^6$  in 16 mLs DMEM + 10% FBS per 100 mm plate. A mixture of 24  $\mu$ L FuGENE 6 transfection reagent (Roche Molecular Biochemicals) and 776  $\mu$ L of DMEM was added to ~500ng of the





various PITX2-pcDNA4/HisMax constructs for introduction into the COS-7 cells grown to roughly 50-70% confluency.

COS-7 cells were harvested by scraping 72 hours post transfection. Cells were rinsed with cold 1x PBS and pelleted by centrifugation. Cells of each 100 mm plate were resuspended in 200 µl of lysis buffer and allowed to swell on ice for 15 minutes. Cells were sonicated with 3 sets of 6 pulses at 1.5 Watts. Homogenized extracts were used for western analysis and in EMSAs. Extracts were stored at -80°C.

#### Deletion of Putative PITX2 NLS

The putative N-terminal nuclear localization signal (NLS), Lys-Lys-Lys-Arg, at residues 35 to 38 of the PITX2 protein, was removed from the PITX2-pcDNA4/HisMax A construct using site-directed mutagenesis  $\Delta$ NLS primers (sequence appears in Table 2). Following transformation, culture, and plasmid preparation, deletion of the putative NLS was established by PCR product sizing with primers 4F and SKR (55°C annealing temperature) and confirmed by sequencing with primer 4F. Intracellular localization of the  $\Delta$ NLS PITX2 protein was examined by immunofluorescence of transfected COS-7 cells.

#### Western Analysis

Whole cell protein extracts were electrophoresed on SDS-PAGE gels in 1x Electrophoresis Buffer and transferred overnight at 4°C at 100V in 1x Towbin buffer to PVDF membrane (Bio-Rad Laboratories). Membranes were incubated with a minimal amount of Ponceau Stain (Sigma) for 10 minutes, followed by rinses with dH<sub>2</sub>O, to visually examine the separation and transfer of protein prior to Western blotting. Membranes were blocked with a 5% dry skim milk/ 1x PBS solution for 20 minutes.





The western blot was incubated for 1 hour with a 1:5000 dilution in 1% milk / 1x PBS of the  $\alpha$ -Xpress antibody to detect recombinant PITX2 proteins. The secondary antibody, goat-anti-mouse linked to horseradish peroxidase (Pierce) was incubated for 1 hour at a 1:2500 dilution in 1% milk / 1x PBS-T. Each incubation with antibody was followed by three 5 minute washes with 1x PBS-T; prior to detection one 5 minute wash with 1x PBS was used. SuperSignal, West Pico Chemiluminescent Substrate (Pierce) was used to detect the secondary antibody. Chemiluminescence was visualized by exposure to autoradiographic Kodak BioMax film.

### Electrophoretic Mobility Shift Assays (EMSAs)

DNA-binding experiments were designed to exploit the high homology of PITX2 with PITX1. PITX2 and PITX1 differ only at two residues within their homeodomains: position 3 of the 2nd helix and position 2 of helix 3. Murine Pitx1 was first identified as a transcriptional activator of the pro-opiomelanocortin (POMC) gene, binding to the CE-3 regulatory region of the POMC promoter (Tremblay et al. 1999, Drouin et al. 1998, Lamonerie et al. 1996). Based on the presumption that similar homeodomains will bind to similar DNA sequences, PITX2 DNA-binding was assayed using an oligonucleotide containing the CE-3 Pitx1 DNA-binding sequence. Whole cell protein extracts from transfected COS-7 cells, standardized by western analysis to 1x wtPITX2 protein, were used in EMSAs with the double-stranded  $^{32}$ P labeled CE-3 probe. The 71-mer probe 5'CAGGTCAGTTCAGCGGATCCTGTGCGACCAGGATGC**TAAGCC**TCTGTC AGGCGAATTCAGTGCAACTGCAGC -3' containing the CE-3 element (indicated in bold) and internal Pitx1 binding site (boxed) was synthesized and  $^{32}$ P-labeled by PCR with forward and reverse primers to the oligonucleotide (underlined). A 52.5 °C annealing temperature was used in a standard PCR reaction.



Protein extracts were added to 100 ng CE-3 probe within a 40  $\mu$ L binding reaction of 5% glycerol, 20 mM Hepes (pH 7.5), 1 mM EDTA, 0.5  $\mu$ g poly(dI-dC), 1 mM dithiothreitol and 50 mM NaCl (Modified from Amendt et al. 1998). Binding reactions were placed on ice for twenty minutes prior to addition of protein extracts, and then incubated on ice for an additional 60 minutes. Wildtype PITX2 protein extracts were titrated from 0.1x to 20x; mutant IH (Arg46Trp), IGD (Arg31His), and AR-1 (7aaDup) from 1x to 20x; AR-2 (Leu16Gln), AR-3 (Thr30Pro), and AR-5 (Arg53Pro) from 1x to 200x; and AR-4 (Val45Leu) from 1x to 100x. EMSAs were replicated three times for wtPITX2 and the IH and IGD protein extracts, and twice for the AR-mutant PITX2 extracts, each extract representing a separate transfection of COS-7 cells. Competition assays were performed with 100-1000 ng unlabeled probe added to binding reactions five minutes prior to addition of protein. Unlabeled CE-3 oligonucleotide probe competitor was prepared as above. Similar assays were performed with the double-stranded unrelated-DNA fragments 5'-AGTTCAATGGGCTCATGCAGCCCTACGACGACATGTACCCAGGCTATTCCTACAACAACTGG-3' and 5'-GCTTCCCCTTCTTCAACTCTATGAACGTCAACCCCCTGTCATCACAGAGCATGTTTTCCCC-3'. Binding reactions (with the addition of 5  $\mu$ L loading dye) were electrophoresed on 8% PAGE (non-denaturing) gels, 0.25x TBE, for 6-7 hours at 250V (4°C).

### pGL3 Luciferase Reporter Vectors

Basic and SV-40 Promoter pGL3 Luciferase reporter vectors from Promega were used in transactivation assays.



### βGal Control Vector

A pSV-βGal control vector, used as an internal transfection control, was purchased from Promega. Another vector, pCMV-βGal from Clontech, was also tried.

### Transactivation Assays with the CE-3 Element

A CE-3 luciferase reporter construct was developed by first annealing the single-stranded CE-3 oligonucleotides (F: 5'-GATCTACCAGGATGCTAAGCCTCTGTCA-3' R: 5'-GATCTGACAGAGGCTTAGCATCCTGGTA-3'). The oligonucleotides were designed with overhanging *Bgl* II restriction sites to allow oligomerization of the CE-3 element in a ligation reaction. Ligation reactions were size-separated by electrophoresis on a 3% agarose gel and tetramers of the CE-3 element were isolated and purified by QIAGEN column. The CE-3 tetramers were subcloned into the *Bgl* II cloning site directly 5' to the SV-40 promoter of the pGL3 vector encoding the firefly luciferase gene (Promega). Minipreps of the transformed *E. coli* cells were sequenced with the pGL3 vector RV3 primer (5'-CTAGCAAAATAGGCTGTCCC-3'). A clone was selected with four tandem copies of the CE-3 element, three copies in sense orientation were flanked by one copy in anti-sense orientation (++++). The selected clone was grown in a maxi-culture for preparation and purification of plasmid DNA using a QIAGEN MaxiPrep Column.

Wildtype and mutant *PITX2* cDNA constructs within the pcDNA4/HisMax A vector (500 ng) were co-transfected with 50 ng of the CE-3 (++++-) pGL3-Promoter vector into mammalian HeLa cells ( $2 \times 10^5$  cells per well in 2 mLs DMEM + 10% fetal bovine serum) with 3 μl FuGENE 6 transfection reagent (Roche Molecular Biochemicals). Cells were harvested with 50 μL of a 1x Passive Lysis Buffer (Promega), 40 hours post-transfection. 20 μL of protein lysate was added to 100 μL of the LARII



reagent (Promega), and firefly luciferase activity was measured by luminometer (Turner Designs). Transfections were repeated three times for the IH and IGD mutants and twice for the AR mutants and the wtPITX2 construct. For the Val45Leu and 7aaDup experiments, a  $\beta$ gal-CMV control vector (100 ng DNA) was co-transfected along with the PITX2 expression constructs and the luciferase reporter vector.  $\beta$ gal activity was measured with a commercial  $\beta$ gal assay kit (Promega). Transfections were repeated eight times for the Val45Leu mutants and seven times for the 7aaDup mutants. Transactivation with an empty pGL3-vector, not containing the CE-3 oligonucleotide, was examined to determine whether CE-3 is required for transactivation, or whether Val45Leu is able to use a pre-existing site within the pGL3 vector for transactivation. Transfected HeLa cells were also examined by immunofluorescence, as above, to measure transfection efficiency of the *PITX2* constructs.

### **III: PITX2 in the Adult Eye**

#### Eye Tissue cDNA Libraries and Pools

Human adult trabecular meshwork and retina cDNA pools, and a iris cDNA library, were available within the Walter laboratory. These were prepared by another graduate student, James Friedman, from the RNA of dissected human eye tissues. A lymphoblast cDNA pool was also made available.

#### *PITX2* and *PIT1* Expression in the Adult Eye

Prepared cDNA libraries or pools of human adult trabecular meshwork, iris, retina, and lymphoblast tissues were analyzed for existence of *PITX2* cDNAs. Standard PCR reactions were performed with 50 ng of each individual cDNA pool and *PITX2* primers





7F and 10R. PCR reactions were compared to that of genomic DNA with the same *PITX2* primers performed at the same time. To test expression of *PIT1* in the adult eye, *PIT1* primers were designed to exon 6 of *PIT1* (encompassing the C-terminus and partial 3' UTR) using GeneWorks 2.2.1 (Forward: 5'-CGGGTGAAAACAAGTCTG-3', Reverse: 5'-CCCATACTCATATGTCTGCG-3'). An annealing temperature of 52°C was used with the *PIT1* primers for PCR reactions with the cDNA pools as performed for *PITX2*.

### *MYOC* Promoter Constructs

pGL3 Basic vectors containing Human (-1052/+54 and -234/+54), Mouse (-2258/+51), and Rat (-510/+62) *Myocilin* promoters were provided by Dr. Tomarev (NIH) dried on filter paper.

### Transactivation Assays with the *Myocilin* Promoter

Human (-1052/+54 and -234/+54), Mouse (-2258/+51), and Rat (-510/+62) *Myocilin* promoters subcloned within the pGL3 Basic vectors were reconstituted from dried filter paper for transformation of *E.coli* J109 bacterial cells. Isolated colonies were cultured, maxipreped with QIAgen columns, and sequenced with RV-primer 3 (Figure 30B) to confirm the identity of the inserts. *MYOC* promoter constructs (50 ng DNA) were introduced into HeLa cells with the *PITX2*-pcDNAHisMax construct (500ng DNA) to examine whether *PITX2* protein can regulate transactivation of the different *MYOC* promoters. The  $\beta$ gal CMV vector (100ng DNA) was used as an internal control for transfection efficiency. The CE-3-pGL3 construct was used for comparison. Wt*PITX2*, AR-3 (Arg30Pro), and AR-4 (Val45Leu) constructs were assayed for *MYOC* transactivation activity. Luciferase and  $\beta$ gal expression was measured as for the transactivation experiments utilizing the CE-3 element above.



### FOXC1 Expression and Transactivation Reporter Constructs

Fellow graduate student, R. Saleem of the Walter Laboratory, prepared and made available all FOXC1 materials for use in transactivation studies. *WtFOXC1* cDNA and associated FOXC1 binding and transactivating null mutant Ser131Leu (Saleem et al. 2001), of the FOXC1 forkhead domain, were available as pcDNA4/HisMax mammalian expression constructs. A transactivation reporter construct containing three copies (+ -- orientation) of an oligonucleotide 5'-CTAGCCAAGGTAAATAAACAACAGCAAA GTAAATAAACAACAGG- 3' each containing two of the proposed FOXC1 BS 1-2 binding site elements (underlined), subcloned into the pGL3 TK promoter vector, was also available for comparison to the *MYOC* promoters. The BS 1-2 FOXC1 site had previously been tested for its ability to be bound by FOXC1 in EMSA experiments by R. Saleem (Saleem et al. 2001).



## **RESULTS:**

### **Note:**

Much of the work presented herein has been previously published, and appears in Kozlowski and Walter 2000, and Priston et al. 2001.



## **I: PITX2 Mutational Analysis**

The genomic DNA of 31 individuals with anterior segment dysmorphism (ASD) was screened for mutation in the *PITX2* gene. Of these 31 patients, 12 had been diagnosed with ARS, 4 with ARA, 8 with IGD, 6 with Peters anomaly, and 1 individual with uncharacterized ASD. The three coding exons of *PITX2* were PCR-amplified to include the intron/exon boundaries from genomic DNA. PCR products were screened for *PITX2* mutations using a combination of manual <sup>33</sup>P and LI-COR fluorescent sequencing.

One mutation, a G to a T change (bold) in the sequence 5'-tttcagttt**cag**AG AAA GAT AAA AGC- 3' at the invariant splice acceptor site (underlined) of exon 3 at nucleotide position -1 was found in a patient of mixed Korean and Mexican decent with AR malformations (Figures 31 and 32). Clinical description for this patient includes displacement of both pupils, with the left pupil being pinpoint in size, and the iris irregular in contour. Facial dysmorphism included a mildly depressed nasal bridge and small chin and a under-development of the maxilla. Redundant peri-umbilical skin and an anteriorly displaced anus were also noted. Anomalies of the heart or gut were not apparent, and hearing was normal. DNA of the patient's mother was also screened and found to be normal at that position (Figure 32). The patient's father was unavailable for screening at the time. It is thus unknown whether the mutation carried by this patient is *de novo* or paternally inherited. No other changes were found in the coding regions of *PITX2* for this patient. This splice-site mutation of *PITX2* is therefore concluded to be disease-causing in this patient. The splice-site mutation is predicted to result in truncated *PITX2* protein. It is expected that loss of the homeodomain, in whole or in part, results in a non-functional protein.

No other patients displayed changes within the coding regions of *PITX2*. Combining this study with previous mutational analysis studies of *PITX2* indicates that a







**Figure 31.**

Three generation pedigree of the patient with AR malformations found to carry the 'g to t' -1 splice site mutation of *PITX2* intron 2. The filled circle indicates the affected individual. Small triangles indicate spontaneous abortions.

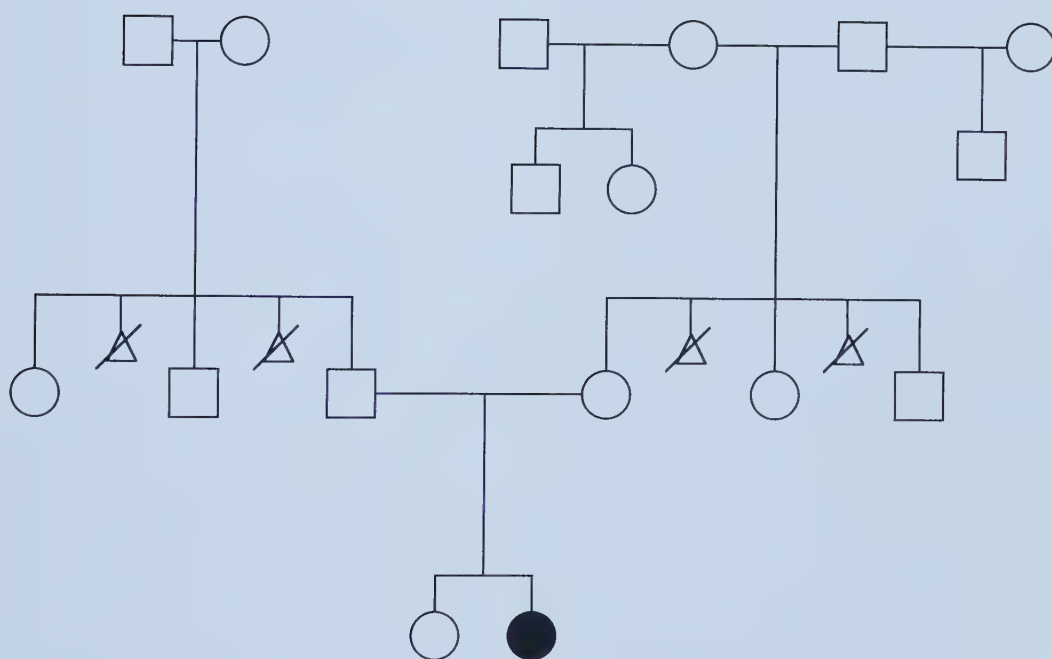


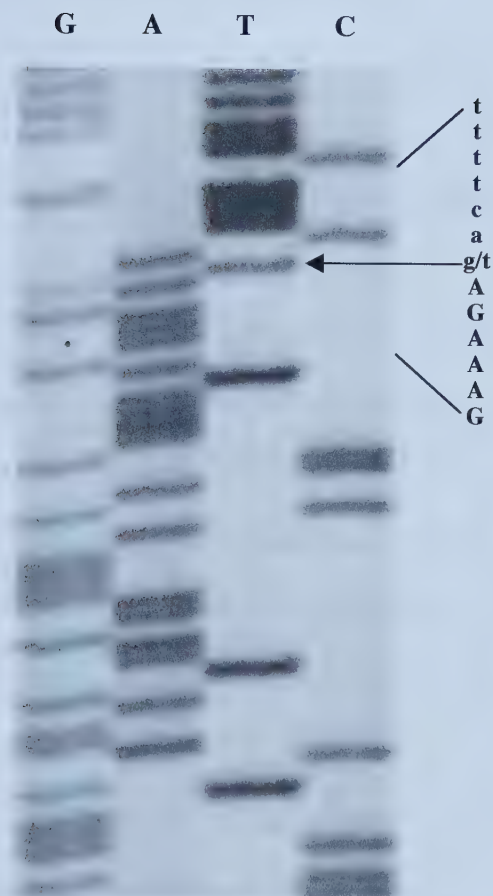




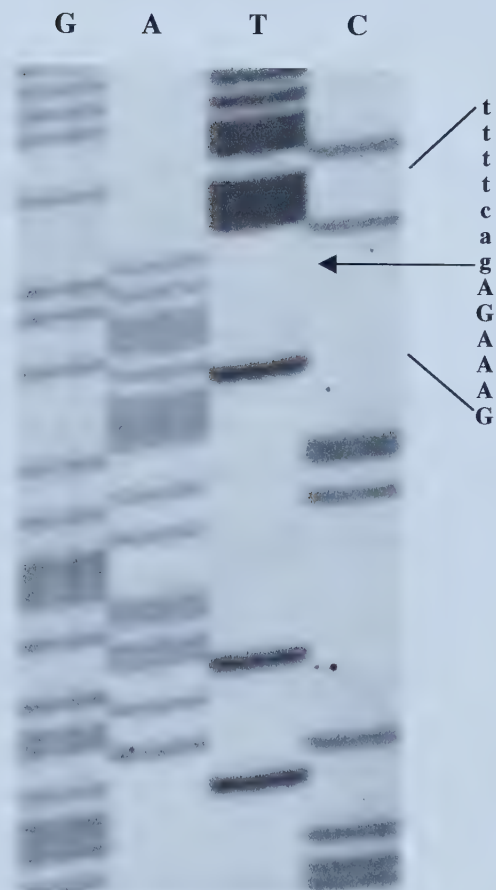
**Figure 32.**

<sup>33</sup>P sequencing autoradiograph demonstrating the heterozygous mutation of the splice acceptor site 'cag' to 'cat' at position -1 of *PITX2* intron 2 (indicated by arrow).

Affected child



Unaffected mother







*PITX2* mutation has been found in approximately 28% of patients with ARS (Table 3). No *PITX2* mutations were found in patients with IH, IGD, or Peters anomaly in this study. *PITX2* mutations have only been documented for IH and IGD once each (Alward et al. 1998, Kulak et al. 1998), and twice in patients with AR malformations with additional Peters-like features (Perveen et al. 2000, Doward et al. 1999). Combined results thus indicate an incidence of *PITX2* mutation in approximately 9% of patients within the spectrum of ASD phenotypes (Table 3).

## **II: Analyses of PITX2 Homeodomain Mutants**

### ***PITX2* Expression Constructs**

A *wtPITX2* expression construct was made by subcloning the *PITX2* (isoform a) cDNA into the pcDNA4/His Max mammalian expression vector. Site-directed mutagenesis was used to introduce mutations of the *PITX2* homeodomain as documented in the literature in patients with AR malformations, IGD, and IH (Priston et al. 2001, Alward et al. 1998, Kulak et al. 1998, Semina et al. 1996b). Seven different *PITX2* mutations were introduced into the *wtPITX2*-pcDNA4/HisMax expression vector (Figure 33).

### **Intracellular Localization**

Immunofluorescence of the COS-7 cells transfected with the various *PITX2*-pcDNA4/HisMax expression constructs demonstrated stable recombinant wildtype and mutant *PITX2* proteins (Figure 34). Recombinant proteins were detected with an  $\alpha$ -Xpress antibody to the Xpress epitope carried by the pcDNA4/HisMax expression vector. Cells transfected with the *wtPITX2* construct showed full nuclear localization of the recombinant protein. Of the 1000 transfected cells assayed by immunofluorescence for each mutant *PITX2* construct, 23% Arg46Trp (IH),



**Table 3.**

Incidence of *PITX2* mutation in patients with ARS and anterior segment dysgenesis (ASD) as indicated by various *PITX2* mutational studies.

Study	# mutations found	ARS	ASD
<u>Kulak 1998, 1999</u>			
5 ARS →	1		
4 ARA		1/5 20%	2/14 14%
5 IGD →	1		
<u>Perveen 2000</u>			
19 ARS →	8		
57 (ARA IGD IH Peters)		8/19 42%	8/76 10%
<u>Priston 2001</u>			
21 ARS →	3		
9 ARA 5 IH 3 Peters		3/21 14%	3/38 8%
<u>Kozlowski 2001</u>			
12 ARS →	1		
4 ARA 8 IGD 6 Peters 1 ASD		1/12 8%	1/31 3%
		13/57 28%	14/159 9%





**Figure 33.**

Schematic of PITX2 cDNA subcloned in the pcDN4/HisMax expression vector with the homeodomain mutations studied indicated.

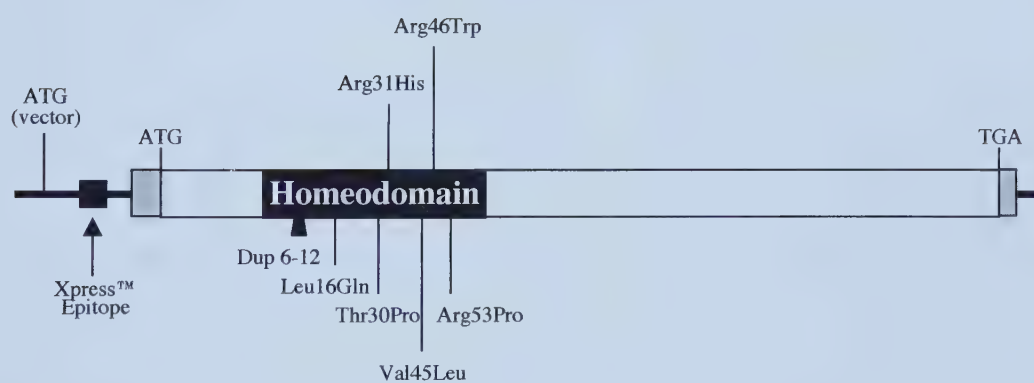








**Figure 34.**

Immunofluorescence of COS-7 cells expressing various pcDNA4/HisMax constructs. Cy3 staining of Xpress tagged proteins is on the left, and DAPI staining of the nuclei is on the right.

**A.** Control transfection with the LacZ pcDNA4/HisMax construct demonstrates expression throughout the cell.

**B.** wtPITX2 expression is restricted to the nucleus.

**C- H.** The majority of the cells transfected with the various mutant *PITX2* constructs demonstrate nuclear localization of protein.

**I.** The Arg53Pro PITX2 mutant protein is localized to both the nucleus and the cytoplasm.

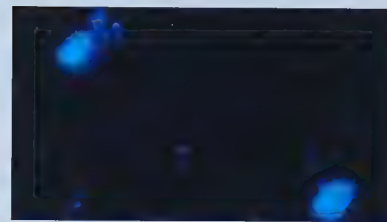
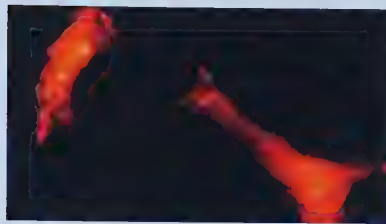
**J.** The  $\Delta$ NLS PITX2 protein is restricted in localization to the nucleus, but less so than the Arg53Pro mutant.

**Cy3 Staining of PITX2**

**DAPI Staining of Nuclei**

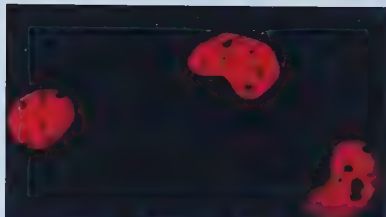
**A**

LacZ



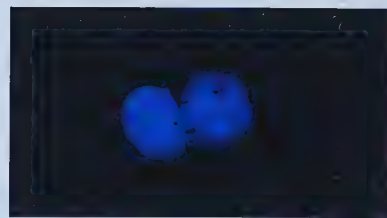
**B**

wtPITX2



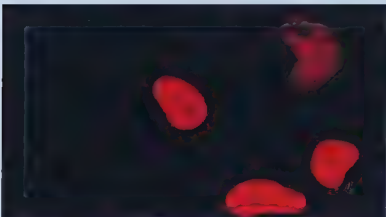
**C**

IH  
Arg46Trp



**D**

IGD  
Arg31His



**E**

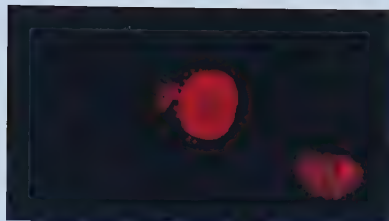
AR-1  
7aaDup





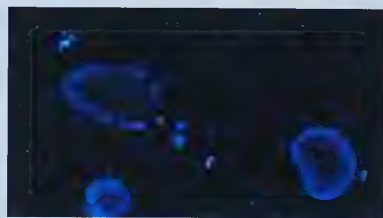
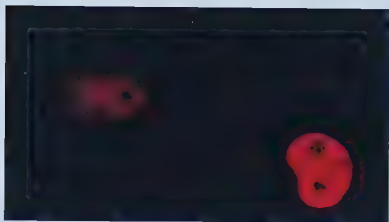
**F**

AR-2  
Leu16Gln



**G**

AR-3  
Thr30Pro



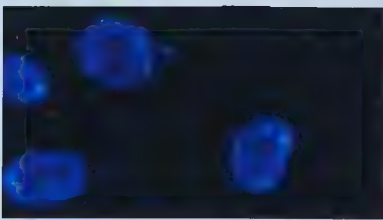
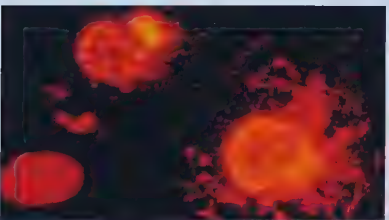
**H**

AR-4  
Val45Leu



**I**

AR-5  
Arg53Pro



**J**

$\Delta$ NLS





30% Leu16Gln (AR-2), 18% Thr30Pro (AR-3), and 64% Arg53Pro (AR-5) of cells displayed cytoplasmic staining in addition to nuclear localization. Examination by immunofluorescence of similar numbers of cells transfected with the other PITX2 mutant constructs (Arg31His (IGD), 7aaDup (AR-1) and Val45Leu (AR-4)) showed complete nuclear localization of the recombinant proteins.

#### Deletion of the Putative N-terminal PITX2 Nuclear Localization Signal

The Arg53Pro (AR-5) PITX2 mutation resulted in partial exclusion from the nucleus, indicating it may be part of a nuclear localization signal (NLS) (Figure 34I). Amino acid residues Lys-Lys-Lys-Arg at positions 35-38 of the PITX2 protein, immediately N-terminal to the homeodomain, has previously been postulated to be an NLS (Lindberg et al. 1998, Gage and Camper 1997, Dingwall and Laskey 1991). To determine if the putative N-terminal NLS is sufficient for nuclear localization of PITX2, residues 35-38 (a total of 21 bp) were deleted by site-directed mutagenesis from the *wtPITX2* expression construct. Immunofluorescence of COS-7 cells transfected with the  $\Delta$  NLS construct resulted in some exclusion of PITX2 protein from the nucleus. In comparison to the Arg53Pro AR-5 mutant that displayed heavy extra-nuclear staining (Figure 34), very little actual cytoplasmic staining was present in the COS-7 cells transfected with the  $\Delta$  NLS PITX2 construct (Figure 34J). In addition, transfection efficiency was low (below 5%) and many of the nuclei appeared to be undergoing apoptosis. It is unknown whether that was directly related to the mutation itself, or a problem with the cells. Regardless, the postulated NLS at positions 35-38 did not appear to be fully responsible for nuclear localization of PITX2.





### Protein Expression and Western Analysis

Mammalian COS-7 cells were used to express recombinant PITX2 proteins from the wildtype, IH, IGD and AR-mutant *PITX2* expression constructs. Whole cell protein extracts of transfected COS-7 cells were size-separated by SDS-PAGE. Subsequent western analysis with a commercial antibody to the vector-encoded Xpress epitope (Invitrogen) demonstrated a stable 35 kilodalton (kDa) band for wildtype and mutant PITX2 protein extracts, representing the 4 kDa Xpress epitope tag and expected 31 kDa PITX2 protein (Figure 35). Band intensities of the western blots were used to determine equivalent amounts of the various recombinant PITX2 protein extracts for future experiments.

### DNA-binding Assays

Electrophoretic Mobility Shift Assays (EMSAs) were used to test the DNA-binding ability of the PITX2 recombinant protein extracts with the CE-3 oligonucleotide probe. Untransfected COS-7 cell extracts were used as a control to demonstrate that endogenous COS-7 cell proteins were unable to bind the CE-3 probe (Figure 36A, lane 2). To demonstrate that the Xpress epitope did not provide DNA-binding ability to the recombinant PITX2 proteins, a Xpress-LacZ fusion protein was used as a control (Figure 36A, lane 3). Addition of recombinant wtPITX2 protein extract to the CE-3 probe produced a retarded electrophoretic mobility shift in the labeled CE-3 probe, indicating the formation of DNA-protein complexes (Figure 36A, lane 4). Specificity of CE-3 probe binding by PITX2 protein was demonstrated by the addition of unrelated and unlabeled oligonucleotides that were unable to effectively compete with the CE-3 probe (Figure 36A, lanes 5-7). DNA-binding by the PITX2 protein was shown to be specific for double-stranded DNA as the addition of single-stranded CE-3 oligonucleotides (forward and





**Figure 35.**

Western blot analysis demonstrates that all the mutant PITX2 proteins expressed in COS-7 from the pcDNA4/HisMax vector cells are stable. LacZ protein is shown as a control to demonstrate specificity of the  $\alpha$ -Xpress antibody.

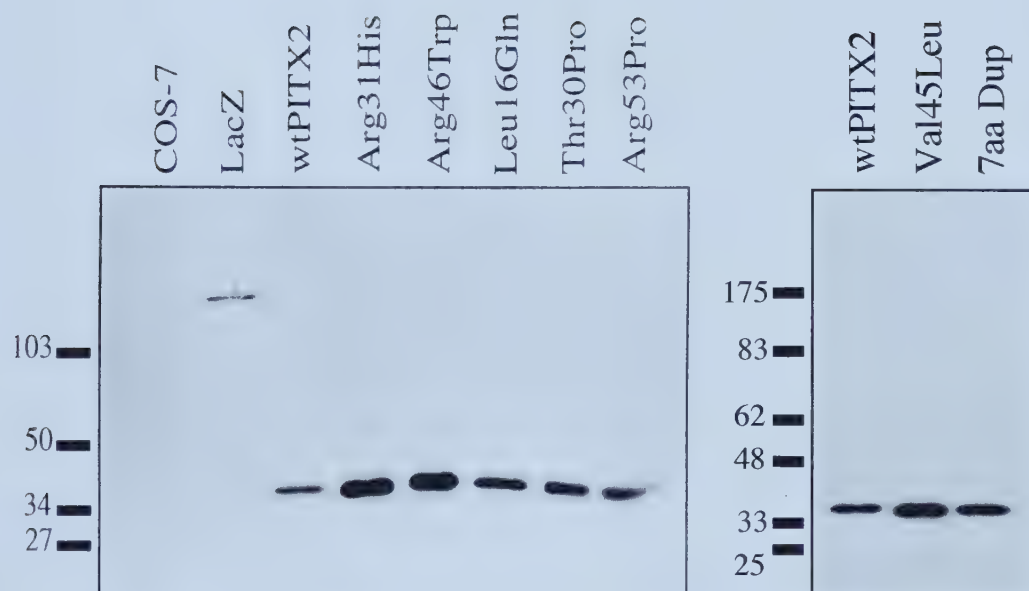








### **Figure 36.**

EMSAs with the CE-3 probe. Arrowheads represent the DNA-protein complexes.

**A-B.** CE-3 probe ·protein complex formation is specific for PITX2 protein and is sequence specific for double-stranded (ds) DNA.

**A.** Proteins native to COS-7 cells (lane 2), and other recombinant proteins that carry the Xpress epitope (like LacZ, lane 3) do not bind the CE-3 probe. Unlabeled oligonucleotides of unrelated sequence (5 to 20X) (lanes 4-7), and unlabeled single-stranded CE-3 oligonucleotides (50X) (lanes 8-9), are unable to effectively compete with labeled ds CE-3 probe for binding of PITX2 protein.

**B.** Unlabeled ds CE-3 oligonucleotides (1 to 10X) were able to efficiently compete with the labeled CE-3 probe for binding of the PITX2 protein.

**C.** DNA-binding of the CE-3 probe with titrated amounts (0.1 to 20x) of wildtype PITX2 protein extract.

**D-J.** The left-most lane of each mutant-PITX2 EMSA represents a control of 1x wtPITX2 protein; the second lane contains only probe and no protein in the reaction.

**D.** DNA-binding by the Arg46Trp IH PITX2-mutant protein extract (5 to 200x).

Approximately 20x of the mutant PITX2 protein is required for binding equivalent to that of 1x wtPITX2.

**E.** DNA-binding by the Arg31His IGD PITX2-mutant protein extract (titrated from 5 to 200x). Approximately 200x of the mutant PITX2 protein is required for binding equivalent to that of 1x wtPITX2.

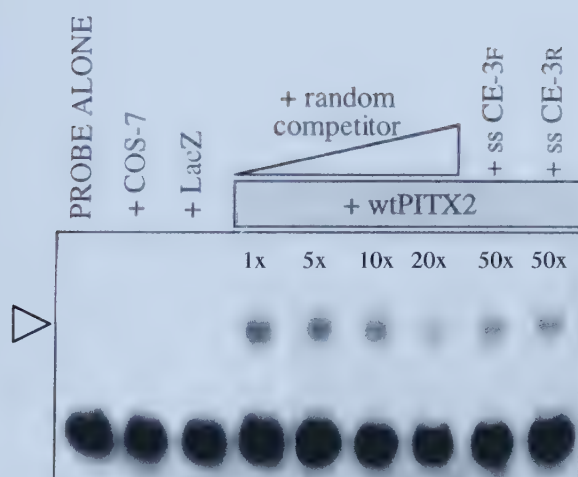
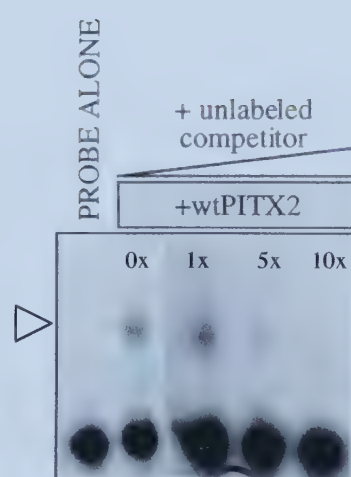


**Figure 36 Continued.**

**F.** DNA-binding by the 7aa Dup AR-1 PITX2-mutant protein extract (titrated from 1 to 100x). 100x of the protein is required to produce DNA-binding that is approximately only 1/5 as strong as 1x wtPITX2. Also note the slower migration of the DNA-protein complex that may be a result of the additional seven amino acids.

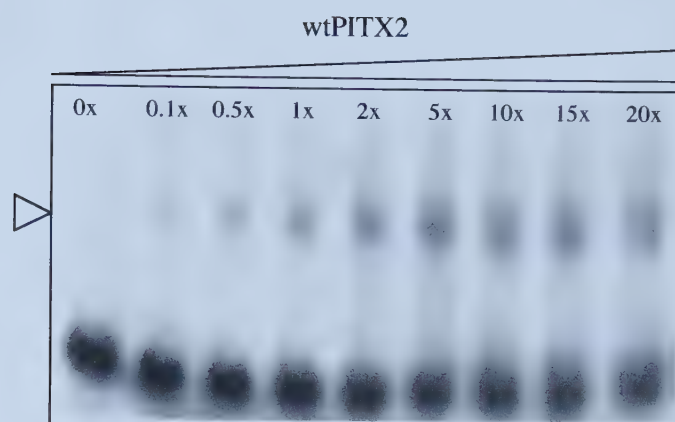
**G, H, J.** Three of the AR-mutant PITX2 proteins (Leu16Gln, Thr30Pro, Arg53Pro) (titrated from 1 to 200x) do not display visible binding of the CE-3 probe.

**I.** The Val45Leu (AR-4) mutant, titrated from 1 to 20x. Less than 10x of the mutant is required for binding equivalent to that of 1x wtPITX2.

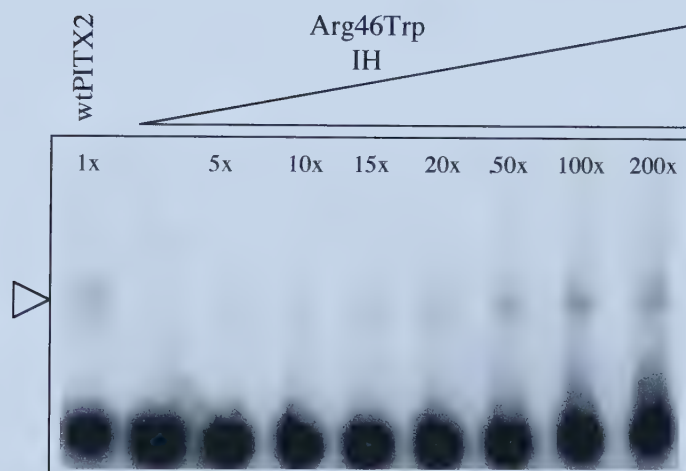
**A****B**



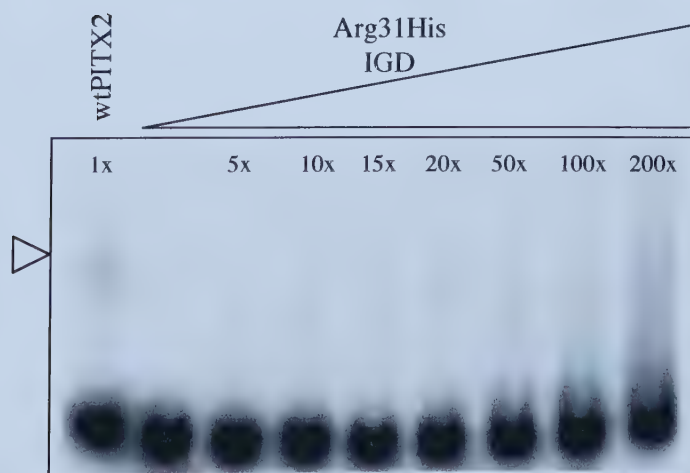
**C**



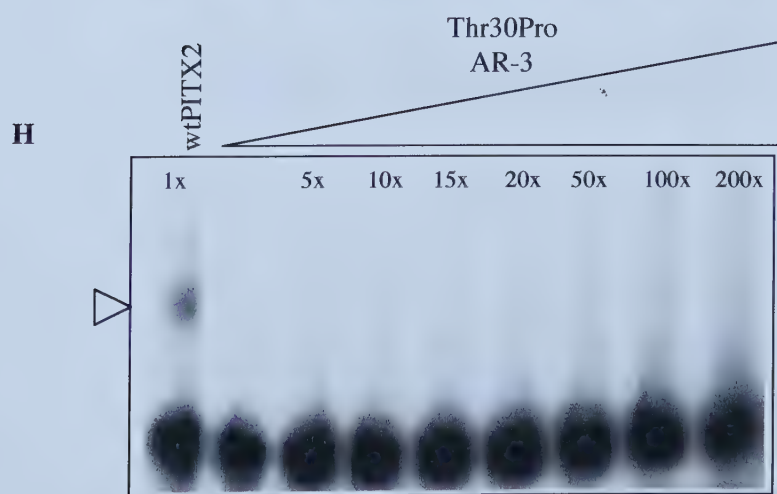
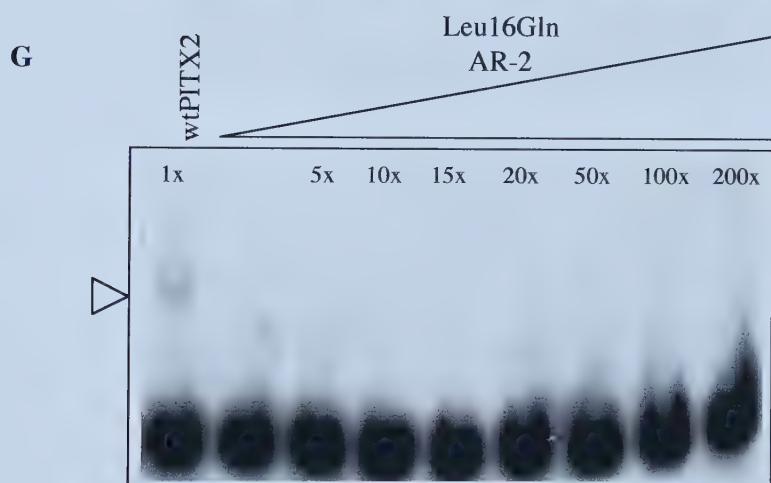
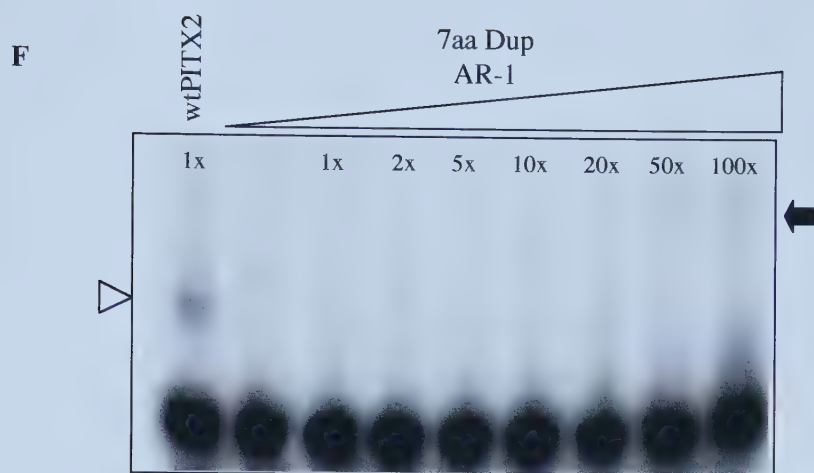
**D**



**E**



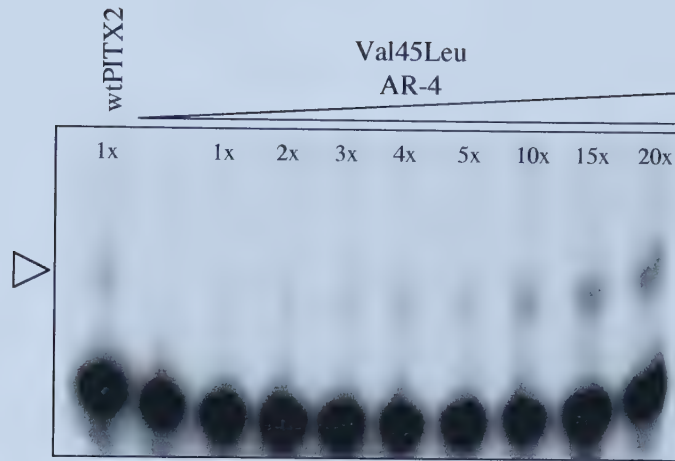




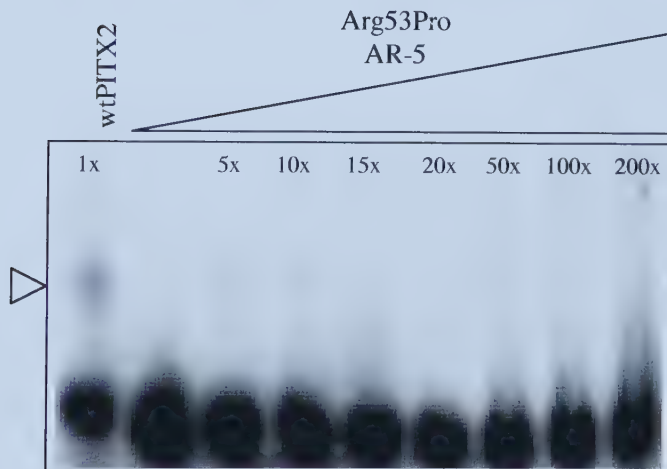




**I**



**J**





reverse) did not affect binding of the double-stranded CE-3 probe by the PITX2 protein (Figure 36A, lanes 8-9). Addition of unlabeled CE-3 probe successfully competed and reduced the visible PITX2 protein-CE-3 complex (Figure 36B).

EMSAs with titrated amounts of mutant PITX2 protein extracts showed that the AR-4 mutant (Val45Leu) retained the greatest amount of residual DNA-binding of the CE-3 oligonucleotide as compared to wildtype PITX2 (Figure 36I). The IH and IGD mutant retained lower amounts of residual DNA-binding activity (Figure 36D-E) compared to the AR-4 mutant. In between 2x and 7.5x (depending on the particular experiment) of the Val45Leu (AR-4), 20x of the Arg46Trp (IH) and 200x of the Arg31His (IGD) mutant-PITX2 protein extracts were necessary to achieve binding of the CE-3 probe equivalent to that of 1x wtPITX2 protein. Faint DNA-binding (much less than that exhibited by 1x wtPITX2) was achieved with approximately 100x of the 7aaDup (AR-1) protein extract (Figure 36F). The other AR mutants Leu16Gln (AR-2), Thr30Pro (AR-3), and Arg53Pro (AR-5) mutant PITX2 proteins were not able to bind the CE-3 probe at detectable levels (Figure 36G,H,J). EMSAs were replicated three times, with new protein extracts from independently transfected cells, for wtPITX2 protein and the IH and IGD extracts, and twice for the AR-mutant PITX2 extracts, with similar results each time.

#### Transactivation of The CE-3 Luciferase-Reporter Construct

Co-transfection of the pGL3-Promoter vector containing four copies of the CE-3 oligonucleotide (+++-), (Figure 37A), with the PITX2-pcDNA4/HisMax constructs demonstrated varying levels of firefly Luciferase reporter gene transactivation by the different PITX2 mutants. Experiments were done in two sets: wtPITX2, the IH, IGD, and





**Figure 37.**

Transactivational studies of wildtype and mutant PITX2 proteins with the CE-3 Luciferase reporter construct.

**A.** The CE-3 (+++-) pGL3-Promoter construct.

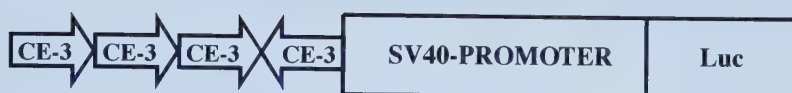
**B.** Transactivation studies demonstrating the relative effectiveness of the PITX2 mutant proteins studied as compared to wtPITX2 ability to transactivate the luciferase reporter gene from the CE-3 (+++-) pGL3-Promoter construct when co-transfected into HeLa cells. \*Transactivation for the Arg53Pro mutant is actually closer to 6.9% because of the lowered transfection efficiency of the mutant.

**C.** Transactivation studies with the 7aaDup and Val45Leu PITX2 mutants compared to wtPITX2 ability to transactivate the Luciferase reporter gene from the CE-3 (+++-) pGL3-Promoter construct when co-transfected into HeLa cells. Values are represented as Luciferase/ $\beta$ gal ratios with a baseline of 1.0x represented by transactivation with an Empty expression vector.

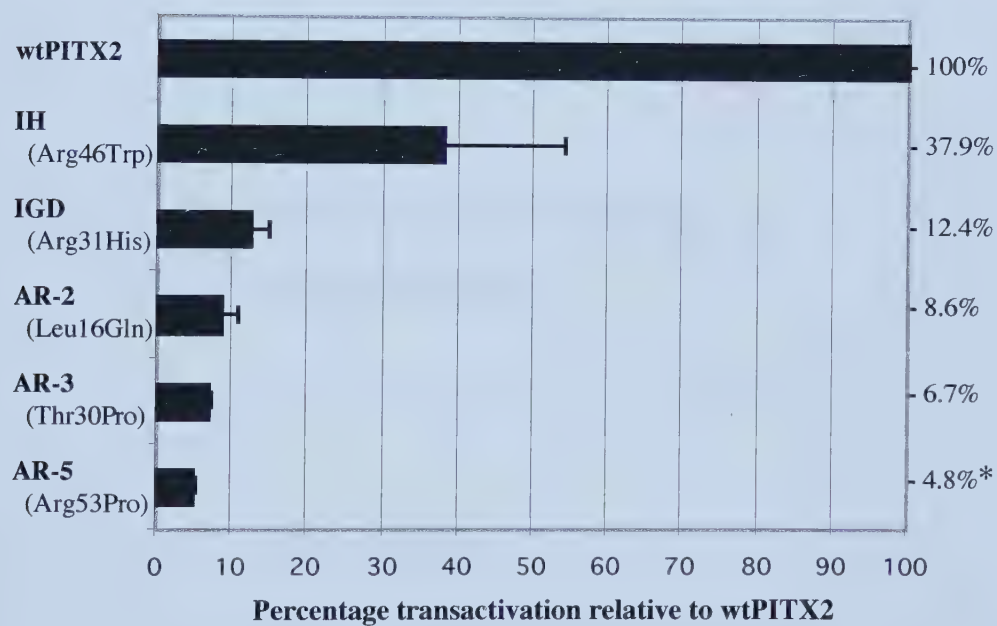
**D.** Co-transfection of wtPITX2 and Val45Leu together in transactivation assays, with comparison to 2x of each, to examine possible interactions and use of binding sites. No evidence of dominate-negative or synergistic interactions were found, and the two forms of PITX2 appear to compete for the same binding site.

**E.** The Val45Leu PITX2 mutant is unable to transactivate the control pGL3 SV-40 vector not containing the CE-3 element.

**A**



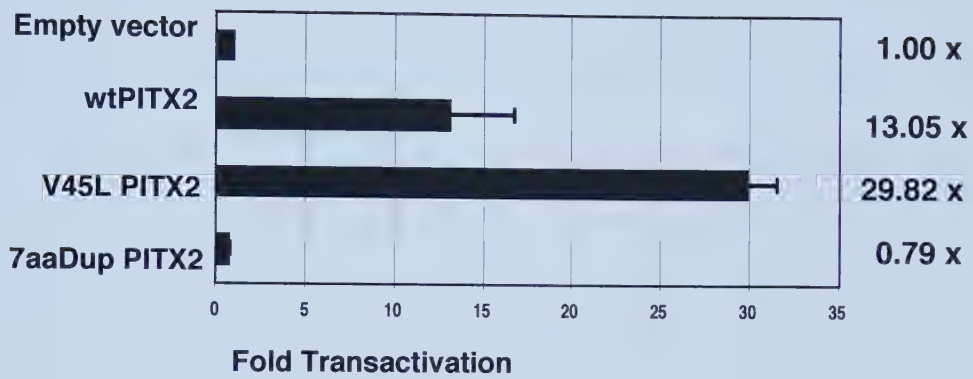
**B**



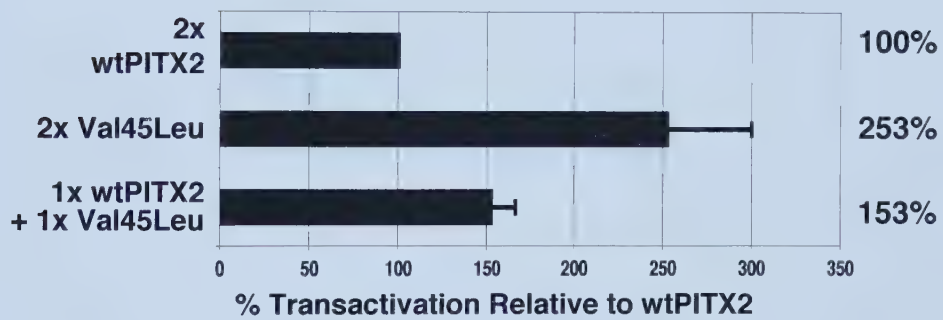




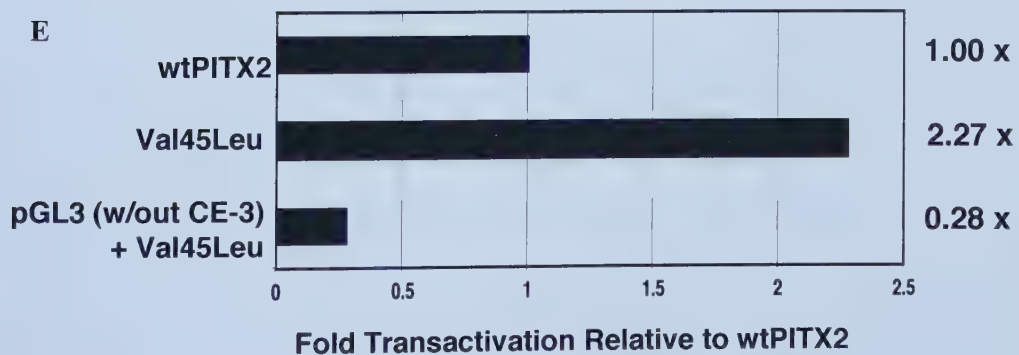
**C**



**D**



**E**





AR-2, AR-3, and AR-5 mutants in the first set (Figure 37B), and wtPITX2, AR-1 and AR-4 mutants in the second set (Figure 37C).

The use of an internal  $\beta$ gal control (pCMV $\beta$ , Clontech) was attempted with the first set of transactivation experiments, but the  $\beta$ gal control vector chosen proved to be responsive to PITX2 transactivation. This became apparent when levels of  $\beta$ gal were lower for the mutants than for wtPITX2. This was confirmed when the control LacZ expression vector was tested and also had lower  $\beta$ gal activity than the wtPITX2 construct. It was then determined that the  $\beta$ gal vector actually contained a potential PITX2 DNA-binding site (5'-CTAATCC-3') at position -410 in front of the origin of replication. This  $\beta$ gal vector was thus deemed to be an inappropriate transfection control in the presence of wtPITX2. As a result, immunofluorescence was used to gauge transfection efficiency, and Luciferase reporter transactivation was compared directly between the constructs for the first set of experiments. To ensure that equal amounts of the wt, IH, IGD, and AR-2, AR-3, and AR-5 PITX2 proteins were being assayed, transfected HeLa cells were examined by immunofluorescence. Transfection efficiencies of the PITX2 constructs were approximately equal, with the exception of the AR-5 (Arg53Pro) construct, which was expressed at approximately 70% of the other PITX2 proteins. Within this set of experiments, the IH mutant (Arg46Trp) retained the greatest amount of residual transactivation ability, representing 37.9% of wtPITX2 activity (Figure 37B). The IGD mutant (Arg31His) maintained 12.4% of wtPITX2 transactivational ability, while the AR mutations (Leu16Gln, Thr30Pro, Arg53Pro) retained 8.6, 6.7, and 4.8% activity, respectively. When the reduced transactivation efficiency of the Arg53Pro mutant is taken into account, transactivation is actually 6.9% of wtPITX2 levels.



A new  $\beta$ gal internal control vector (pSV- $\beta$ -Galactosidase, Promega) was purchased for the second set of experiments and was found to be non-responsive to PITX2. A ratio was prepared between Luciferase activity and the expression of  $\beta$ -galactosidase by the new internal transfection control. Mutant AR-1 (7aaDup) was unable to transactivate above baseline levels, as determined by an Empty (containing no PITX2) pcDNA4/HisMax vector, which were set to a value of 1.0 (Figure 37C). Remarkably, the AR-4 mutant, Val45Leu, was able to transactivate above wtPITX2 levels, averaging at 228.5% of wtPITX2 activity.

With the increased transactivation by the Val45Leu mutant, possible interaction between wtPITX2 and the Val45Leu mutant was examined for evidence of synergy or a dominant negative effect. Co-transfection of the wtPITX2 and Val45Leu expression constructs with the CE-3 Luciferase reporter resulted in transactivation at levels between that of 2x wtPITX2 and 2x Val45Leu (Figure 37D). This indicates independence of the two forms of PITX2 being tested. To test whether the Val45Leu mutant was using a binding site other than CE-3 within the pGL3 Luciferase reporter vector, the Val45Leu mutant was co-transfected with the Basic pGL3-SV40 Promoter Luciferase reporter vector not containing the CE-3 oligonucleotide (Figure 37E). The Val45Leu mutant was unable to transactivate the Basic Luciferase reporter. The transactivation activity of the Val45Leu mutant is therefore dependent upon presence of the CE-3 oligonucleotide in these studies.

### **III: PITX2 Expression and Activity in the Adult Eye**

#### **PITX2 is expressed in the Adult Human Anterior Segment**

PITX2 was determined to be expressed, by means of PCR with PITX2 primers, in cDNA pools/libraries of human adult eye tissues. PITX2 primers 7F and 10R were used to







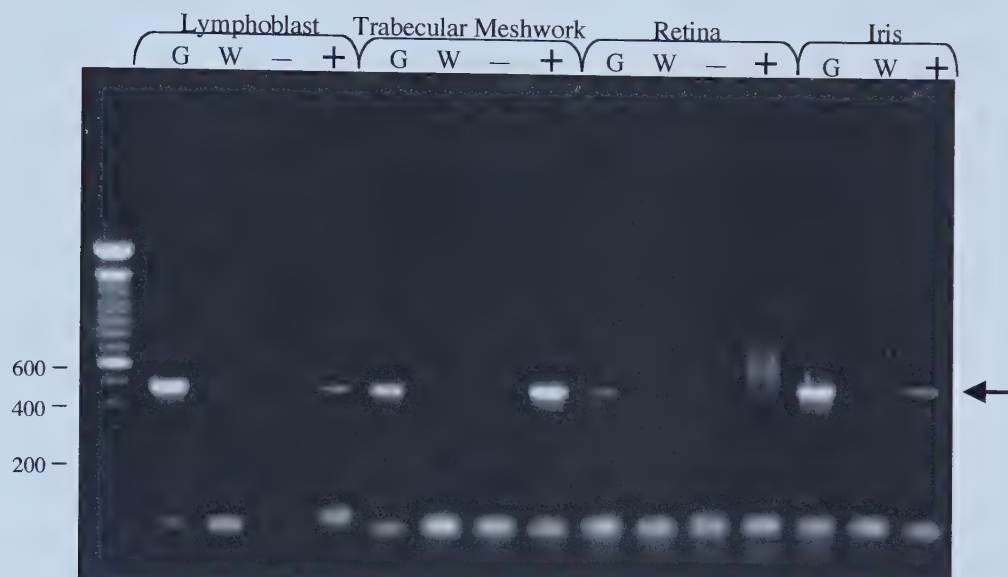
**Figure 38.**

*PITX2*, but not *PIT1*, is expressed in adult eye tissues, including the trabecular meshwork and iris.

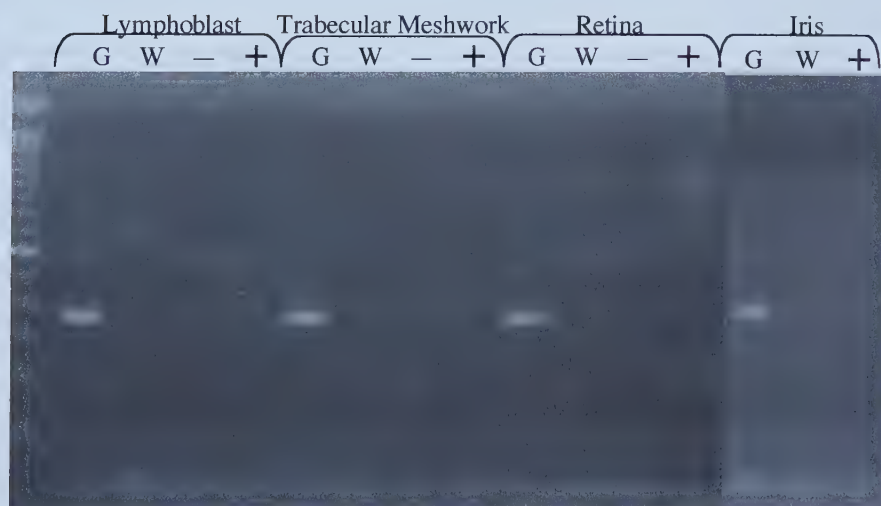
**A.** PCR with *PITX2* primers on genomic DNA (G), dH<sub>2</sub>O (W), and human adult eye tissues and lymphoblasts cDNA pools (– or + reverse transcriptase) demonstrates the expected 471 base pair band (arrow).

**B.** Similar PCR reactions with *PIT1* primers demonstrate that the *PIT1* cDNA is not expressed in adult eye tissues.

**A**



**B**





amplify the *PITX2* cDNA. The human adult trabecular meshwork cDNA pool and iris cDNA library tested positive for *PITX2* expression by this method (Figure 38A). PCR product sizes matched that given by a genomic control. There was some question as to whether *PITX2* is expressed in the adult retina, as PCR with *PITX2* primers produced a smear (possibly due to degradation of the cDNAs). *PITX2* also appears to be expressed within lymphoblasts. These same cDNA pools were tested for expression of *PIT1*. PCR tests revealed that *PIT1* is likely not expressed along with *PITX2* in the adult eye tissues tested (Figure 38B).

#### Possible Down-stream Targets of PITX2

Among the promoters that contain a putative PITX2 binding site TAAGCC (as identified by post doctoral fellow Dr. Fred Berry using the TargetFinder program), was the promoter of the *Myocilin* (*MYOC*) gene. *MYOC* is an excellent candidate for downstream regulation by PITX2 because of its ocular expression and implication in late-onset glaucoma (Kubota et al. 1998, Stone et al. 1997). A number of potential sites that resemble the Pitx1 DNA-binding sequence consensus of **T/c,A/t/c,A,T/G,C,C/T** (Tremblay et al. 1998) that may be bound by PITX2 as well, exist within the *MYOC* promoter. In the 3 species of *MYOC* promoter provided to us by our collaborator, Dr. Tomarev, are four potential PITX2 binding sites potentially conserved between the three species (Figure 39). The three species of *MYOC* promoters were also examined for potential FOXC1 binding sites (**A/G,T,A,A,A,C/T,A**). There are two potentially conserved FOXC1 binding sites among the three species of promoter (Figure 39). Order and spacing of the potentially conserved PITX2 and FOXC1 binding sites is similar among the three promoters.





**Figure 39.**

Putative PITX2 and FOXC1 binding sites in the *MYOC* promoters. Possible binding sites of PITX2 (blue) and FOXC1 (green) are indicated for the different *MYOC* promoters (note different scale for each). Underlined sequence indicates a match with the consensus binding sequences that appear in the box in the lower right. Other sites that vary from the consensus slightly (indicated in red) are included in an attempt to find conserved sites. Lines above the schematic for each promoter indicate a possible site in the forward sequence, lines below the schematics indicate sites (represented 5' to 3') on the opposite strand. Bold lines indicate possible conservation between species of a binding site at that approximate position.







### Transactivation of the *MYOC* Promoters by wtPITX2

Three species (human, mouse, and rat) of *MYOC* promoters were assayed for their ability to be transactivated by wtPITX2. The *MYOC* promoter fragments had been subcloned within the pGL3 Basic Luciferase reporter vector. Two human *MYOC* promoter constructs of different lengths were made available, one spanned nucleotides -1062/+54 and the other -234/+54. The mouse *MYOC* promoter spanned nucleotides -2258/+51, while the rat promoter construct spanned -510/+62. For assay of each promoter construct, HeLa cells were co-transfected with a *MYOC* promoter construct, a pcDNA4/HisMax expression construct, and a  $\beta$ Gal CMV vector as a internal control. Transactivation was measured as a ratio of Luciferase to  $\beta$ Gal. A baseline level of transactivation was established with an empty pcDNA4/HisMax expression vector. WtPITX2 was able to transactivate each of the *MYOC* promoters above baseline levels. Transactivation ranged from 6.9x for the human -1062/+54 promoter, to 18.2x for the rat promoter (Figure 40A). To test the validity of the transactivation by PITX2 of the *MYOC* promoters, the PITX2 null mutant Arg30Pro (AR-3) was tested for transactivation of the *MYOC* promoters. Arg30Pro was not able to transactivate the *MYOC* promoters, indicating that transactivation by wtPITX2 was specific.

### Increased Transactivation of the *MYOC* Promoters by Val45Leu

To determine whether the increased transacting activity of the AR-4 (Val45Leu) PITX2 mutant, seen with the CE-3 reporter construct, is applicable to a potential *in vivo* target, the Val45Leu mutant was tested for ability to transactivate the different *MYOC* promoter constructs. The Val45Leu PITX2 mutant is over 300% more effective than wtPITX2 in transactivating the rat *MYOC* construct, and nearly 200% more effective than wtPITX2 in transactivating both the human 1062/+54 and mouse constructs (Figure 40B). Val45Leu





## Figure 40.

Transactivation of the *MYOC* promoters by PITX2 and FOXC1.

**A.** WtPITX2 is able to transactivate the four different *MYOC* promoter · Luciferase reporter constructs. The Rat -510/+62 *MYOC* construct gives the highest levels of transactivation. An empty pcDNA4/HisMax vector and AR-3 mutant Arg30Pro are shown as controls. Neither is able to transactivate the *MYOC* promoter constructs. The CE-3 reporter construct is shown for comparison.

**B.** The Val45Leu mutant is over 300% more effective than wtPITX2 in transactivating the Rat *MYOC* construct, and nearly 200% more effective than wtPITX2 in transactivating both the Human 1062/+54 and Mouse constructs. The CE-3 construct is shown as a control.

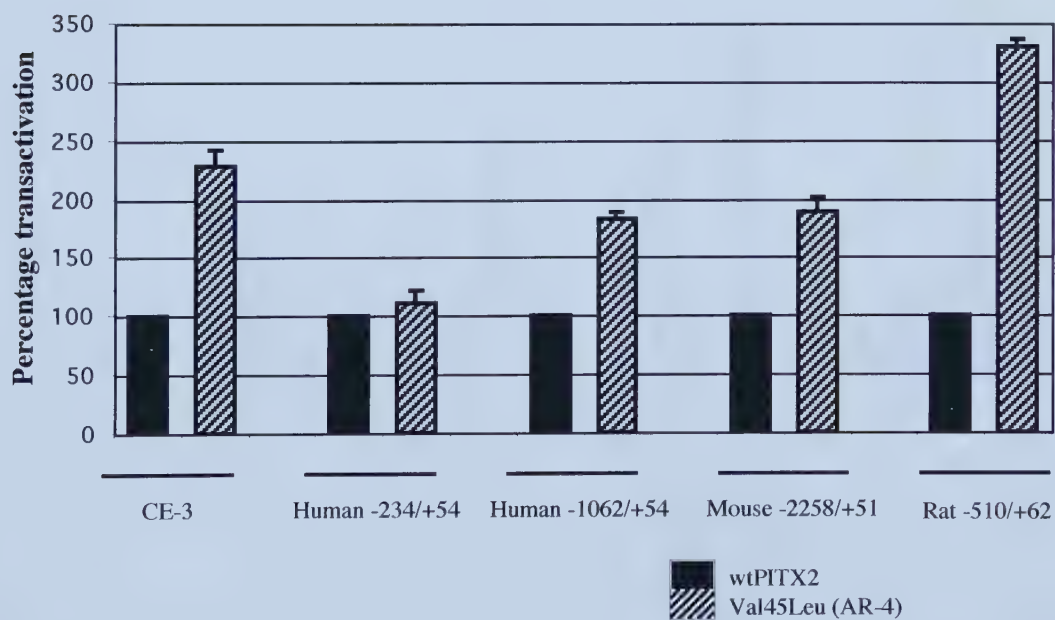
**C.** WtFOXC1 is also able to transactivate all four *MYOC* constructs tested; the Mouse -2258/+51 *MYOC* construct gives the highest levels of transactivation. The Ser131Leu FOXC1 mutant is not able to transactivate the *MYOC* promoter constructs. A reporter construct containing copies of the FOXC1 BS 1-2 binding site is shown for comparison.

**D.** Investigation of the interactions of wtPITX2 and wtFOXC1 and impact on transactivation of the different *MYOC* promoter constructs. Co-transfection of 1x wtPITX2 and 1x wtFOXC1 with the different *MYOC* constructs reveals that they act independently. Transactivation levels of the co-transfection experiments are in-between that seen with transfections of 2x wtPITX2 and 2xwtFOXC1. Transfection results with 1x DNA are shown as controls.

**A**

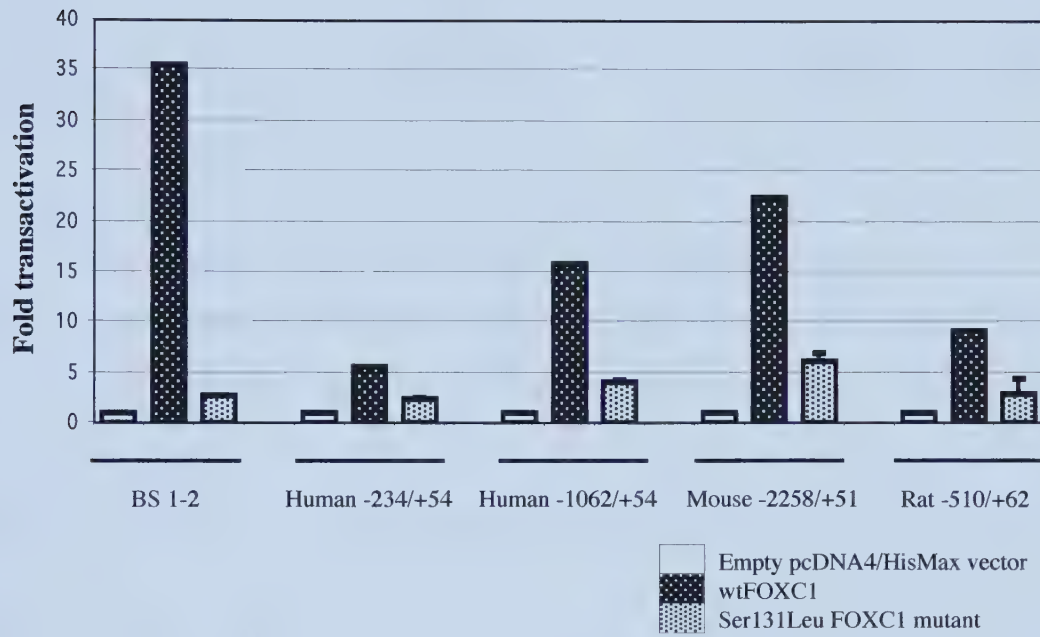


**B**

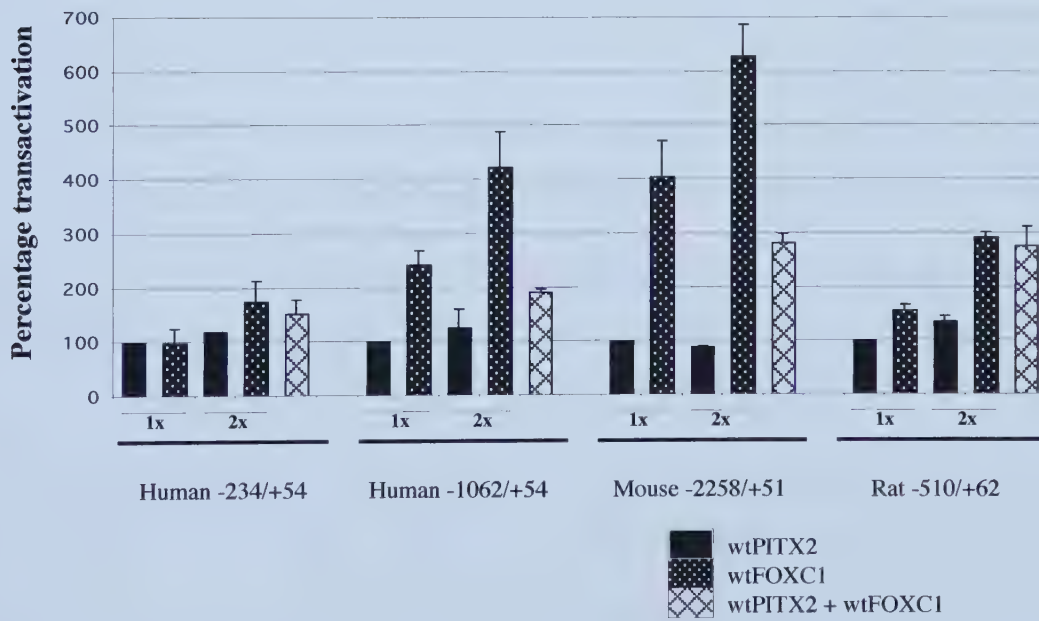




**C**



**D**







is slightly more effective than wtPITX2 in transactivating the -234/+54 human construct. Increased transactivation of the *MYOC* promoters by Val45Leu is consistent with the results seen with the synthetic promoter CE-3 reporter construct (Figure 37C). Furthermore, it suggests that the Val45Leu mutant may indeed increase transactivation of relevant *in vivo* promoters.

#### Transactivation of the *MYOC* Promoters by FOXC1

Earlier sequence analysis of the *MYOC* promoter constructs revealed potential FOXC1 binding sites (Figure 39). Therefore, a wtFOXC1-pcDNA4/HisMax expression construct was also examined for its ability to transactivate the different species of *MYOC* promoters. WtFOXC1 was determined to be able to transactivate the different *MYOC* promoters above baseline levels (Figure 40C). Of the four *MYOC* promoters being tested, FOXC1 was able to transactivate the mouse *MYOC* promoter best, approximately 23 times above baseline levels. The FOXC1 Ser131Leu DNA-binding null mutant was also tested, and was found to be unable to transactivate the *MYOC* promoters. For comparison the BS 1-2 Luciferase reporter construct containing six copies of the FOXC1 binding site was also tested. In comparison to the BS 1-2 construct, the mouse *MYOC* promoter was about ~60% as efficient, indicating that the synthetic enhancer element is more potent than the *MYOC* promoters for FOXC1 as well as for PITX2.

#### PITX2 and FOXC1 Do Not Interact in Transactivation of the *MYOC* Promoter

Since both PITX2 and FOXC1 binding sites appear within the *MYOC* promoters (Figure 39), and both are individually capable of transactivating the *MYOC* promoter constructs (Figure 40 A,C), wtPITX2 and wtFOXC1 were assayed together to assess possible interactions between them in the transactivation of the *MYOC* promoters. Co-transfection



of wtPITX2 and wtFOXC1 with the various *MYOC* promoter constructs resulted in transactivation levels that fall between that of the experiments with wtPITX2 and wtFOXC1 when assayed separately (Figure 40D). No interactions, whether additive or subtractive, were noted for PITX2 and FOXC1 in the transactivation of the *MYOC* promoters.



## **DISCUSSION:**



## **I: PITX2 Mutational Analysis**

### **Incidence of PITX2 mutation**

Thirty-one patients with AR malformations, IGD, and IH, Peters and ASD were screened for *PITX2* mutations. One 'g' to 't' mutation at the invariant -1 position of the splice acceptor site of the second intron was detected in one of the twelve patients with AR malformations. This small study suggests a *PITX2* mutation frequency of 8% (1/12) for AR malformations, and a frequency of 3% (1/31) for anterior segment dysgenesis. The *PITX2* gene has been found to be mutated in a total of 18 patients with classic AR malformations to date, including the one mutation reported herein (Table 4). Two *PITX2* mutations have been reported in patients with AR malformations with additional Peters-like findings (Perveen et al. 2000, Doward et al. 1999). Missense mutations of the *PITX2* homeodomain have also been documented in patients with IGD (Kulak et al. 1998) and IH (Alward et al. 1998). Table 3 shows the incidence of mutations in patients with AR malformations and anterior segment dysgenesis as reported in various studies including this one. The combination of the studies to date would indicate a *PITX2* mutation frequency of 23% in patients with AR syndrome, and a frequency of 9% for anterior segment dysgenesis. This number does not include the data in the original *PITX2* mutational study by Semina et. al. (Semina et al. 1996a) where four out of the six mutations occurred in families already linked to chromosome 4q25. Chromosomal abnormalities of 4q25 and mutations that impact upon positional affects, promoter mutations, gene duplication and deletion, and *PITX2* mutations that affect the splicing of alternate exons, may also account for some cases of AR malformations. Mutation in *FOXC1* accounts for at least an additional 12% of ASD cases (Nishimura et al. 2001, Mears et al. 1998, Nishimura et al. 1998, J. Marshall -Walter lab, personal communication). Furthermore, duplication or deletion of *FOXC1* may account for many





**Table 4.**

The 22 known *PITX2* mutations identified to date.

Nucleotide Change	Reference	Nucleotide Position	Amino Acid Position	Amino Acid Change	Position in Homeodomain
<b>ARS</b>					
1. g to c	Perveen et al. 2000	-1 2nd intron		Splice	
2. g to t	Kozlowski 2001	-1 2nd intron		Splice	
3. Ins 21bp	Priston et al. 2001	712-732	44-50	Duplication	6-12
4. T to A	Semina et al. 1996b	744	54	Leu to Gln	16
5. T to C	Semina et al. 1996b	785	68	Thr to Pro	30
6. g to c	Semina et al. 1996b	+5 3rd intron		Splice	
7. a to g	Semina et al. 1996b	-11 3rd intron		Splice	
8. G to C	Priston et al. 2001	830	83	Val to Leu	45
9. A to T	Perveen et al. 2000	845	88	Lys to Gln	50
10. C to T	Perveen et al. 2000	851	90	Arg to Cys	52
11. G to C	Priston et al. 2001	854	91	Arg to Pro	53
12. G to C	Semina et al. 1996b	855	91	Arg to Pro	53
13. Del AA	Perveen et al. 2000	868-869	96	Frameshift	58
14. Del A	Perveen et al. 2000	938	119	Frameshift	
15. G to A	Semina et al. 1996b	981	133	Nonsense	
16. Del C	Kulak 1999	998	139	Frameshift	
17. TA to AAG	Perveen et al. 2000	1234-35	218	Nonsense	
18. Del T	Richards et al. 2001	1261	227	Frameshift	
<b>ARS + Peters-like</b>					
1. a to t	Perveen et al. 2000 Doward et al. 1998	-2 3rd intron		Splice	
2. Ins C	Perveen et al. 2000	1083	167	Frameshift	
<b>IGD</b>					
1. G to A	Kulak et al. 1998	789	69	Arg to His	31
<b>IH</b>					
1. C to T	Alward et al. 1998	833	84	Arg to Trp	46



more cases than previously assumed (Lehmann et al. 2000, Smith et al. 2000, F. Mirzayans –Walter lab, personal communication). It is unknown how many cases might be associated with the yet uncloned AR malformation loci at chromosomes 13q14 and 16q24 (Nishimura et al. 2000, Phillips et al. 1996). It is also possible that there are as of yet uncloned loci in the genome. It is possible that the different genes involved in the genetically heterogeneous disorders of AR malformations and anterior segment dysgenesis reflect common stop points reached by the genes in different parts of a common genetic pathway. Alternatively, the genes may represent different pathways of eye development that have common end-points.

#### Types of *PITX2* Mutations Identified to Date

A variety of *PITX2* mutations associated with anterior segment dysgenesis have been reported in the literature. Mutations of *PITX2* include missense, nonsense, frameshift, and splicing mutations, and a duplication within the homeodomain (Priston et al. 2001). Nine missense mutations that cause non-conservative amino acid changes have been documented throughout the homeodomain (Perveen et al. 2000, Priston et al. 2001, Semina et al. 1996a). Missense mutations have to this date been limited to the DNA-binding homeodomain of *PITX2*. Mutations have been found within all three helices of the homeodomain spanning exons 3 and 4. These mutations of the homeodomain likely indicate residues important to the function of the DNA-binding domain. Two nonsense mutations that truncate the *PITX2* protein prematurely have been reported (Perveen et al. 2000, Semina et al. 1996a). Two mutations have been described at position –1 affecting the same splice acceptor site of intron 2. One of these mutations is the g/t alteration described herein. A different g/c mutation at the same position has been previously identified in another patient with AR malformations (Perveen et al. 2000). Three splicing



mutations of the intron dividing the homeobox sequence have also been described (Perveen et al. 2000, Doward et al. 1999, Semina et al. 1996a). Five frameshift mutations have been documented, all occurring after the homeodomain with the exception of one that occurs near the very end of the homeodomain at position 58 (Richards et al. 2001, Perveen et al. 2000, Kulak 1999).

### Important Residues of the Homeodomain

To appreciate how the missense mutations of the PITX2 homeodomain may impact upon DNA-binding function, the PITX2 homeodomain was compared with the sequence and three-dimensional DNA-complexed crystal structures of the classic helix-turn-helix homeodomain proteins *Antennapedia* (*Antp*) and *Engrailed* (*en*) (Gehring et al. 1994, Billeter et al. 1993, Kissinger et al. 1990) (Figure 25). X-ray crystallographic and nuclear magnetic resonance spectroscopic studies have indicated a compact globular structure of three folded helical domains with a N-terminal extension. Helices 1 and 2 lie parallel to each other and across helix 3. Many of the amino acids of *Antp* and *en* that have been determined by crystallographic analysis to be important to homeodomain structure and function are conserved in PITX2 (Figure 41). Leu16, Phe20, Trp 48, and Phe 49 are demonstrated in *Antp* and *en* to make up the hydrophobic pocket between helices 1 and 3 that regulates and stabilizes the folding of the homeodomain, and are invariant among all homeodomains (Wilson et al. 1996, Scott et al. 1989), including PITX2. Threading analysis of the PITX2 homeodomain through the co-ordinates of the *en* homeodomain indicates that the most favorable hydrophobic interactions involve Phe8, Leu13, Leu16, Ile34, Leu40, Val45, Trp 48, and Phe49 (Banerjee-Basu and Baxevanis 1999). Within the N-terminal arm preceding helix 1 that slides into the minor DNA groove in *Antp* and *en* studies, amino acid residues Arg3, Arg5, and Thr6 are conserved in PITX2. Important







**Figure 41.**

Homeodomain alignment of PITX2 and related transcription factors with the three  $\alpha$ -helices indicated. Potential PITX2 protein-DNA contact points as based upon conserved *Antp* and *en* residues are indicated (closed arrowheads: DNA-base contact points; open arrowheads: DNA-backbone sugar/phosphate contacts; circles: residues of the hydrophobic core). Missense mutations of the PITX2 homeodomain found in IH, IGD, and AR malformation patients are in bold.

	HELIX 1										HELIX 2										HELIX 3																																											
	10					20					30					40					50					60																																						
	▽	▽	▽			○		○			▽	▽	▽								▽	▽	▽	○	○	▽	▽	▽	▽	▽	▽	▽																																
PITX2	Q	R	R	Q	R	T	H	F	T	S	Q	Q	L	Q	E	L	E	A	T	F	Q	R	N	R	Y	P	D	M	S	T	R	E	E	I	A	V	W	T	N	L	T	E	A	R	V	R	V	W	F	K	N	R	R	A	K	W	R	K	R	E				
<i>Antp</i>	R	K	-	G	-	Q	T	-	R	-	Y	-	T	L	-	-	-	K	-	E	H	F	-	-	-	L	T	R	R	R	-	I	-	-	-	H	A	L	C	-	-	-	R	Q	I	K	I	-	-	Q	-	-	-	M	-	-	K	-	E	-				
<i>en</i>	E	K	-	P	-	-	A	-	S	-	E	-	-	A	R	-	K	R	E	-	N	E	-	-	-	L	T	E	R	R	-	Q	Q	L	S	S	E	L	G	-	N	-	-	Q	I	K	I	-	-	Q	-	K	-	-	-	I	K	-	S	-				
<i>paired</i>	-	-	-	C	-	-	T	-	S	A	S	-	-	D	-	-	-	R	A	-	E	-	T	Q	-	-	-	I	Y	-	-	-	-	L	-	Q	R	-	-	-	-	-	-	I	Q	-	-	-	S	-	-	-	-	-	-	-	-	-	R	L	-	-	Q	-
<i>goosecoid</i>	K	-	-	H	-	-	I	-	-	D	E	-	-	E	A	-	-	N	L	-	-	E	T	K	-	-	-	V	G	-	-	Q	L	-	R	K	V	H	-	-	R	-	E	K	-	E	-	-	-	-	-	-	-	-	-	-	-	-	R	Q	K	-	-	
<i>bicoid</i>	P	-	-	T	-	-	T	-	-	-	S	-	I	A	-	-	-	Q	H	-	L	Q	G	N	R	Y	L	A	P	R	L	A	D	L	S	A	K	L	A	-	G	T	-	Q	-	K	I	-	-	-	-	-	-	R	R	H	K	I	Q	-				



helix 2 amino acid residues Tyr25 and Arg31 are also conserved, which in *Antp* and *en* stabilize the interactions of helix 3 by contacting the DNA phosphate backbone. Helix 3 amino acid residues 47, 50, 51, 57 involved in DNA sequence recognition and specificity are divergent among the three homeodomains, with the exception of the invariant Asn51 residue (Wilson et al. 1996, Scott et al. 1989), which makes a critical DNA-base contact. Also conserved between *Antp/en* and PITX2 are a number of helix 3 amino acid residues (residues 48, 53, 55) that make important DNA-phosphate contacts, especially Arg53 which is invariant among all homeodomains (Scott et al. 1989). Thereby, three of the tested PITX2 mutations (Leu16Glu, Arg31His, and Arg53Pro) occur at known key residues while the remainder fall adjacent to, or within critical helical sites or domains (Figure 42). Mutations of the PITX2 homeodomain have also been analyzed by theoretical threading techniques where the homeodomain sequence is threaded through the atomic coordinates of the X-ray structure of *en* to examine possible changes to the relative energies of hydrophobic interactions that direct PITX2 homeodomain folding (Banerjee-Basu and Baxevanis 1999). Based on the above analysis of important residues, homeodomain mutations of PITX2 likely disrupt DNA-binding either directly or indirectly through impaired homeodomain folding, which may also result in protein instability.

## **II: Characterization of PITX2 Homeodomain Mutations**

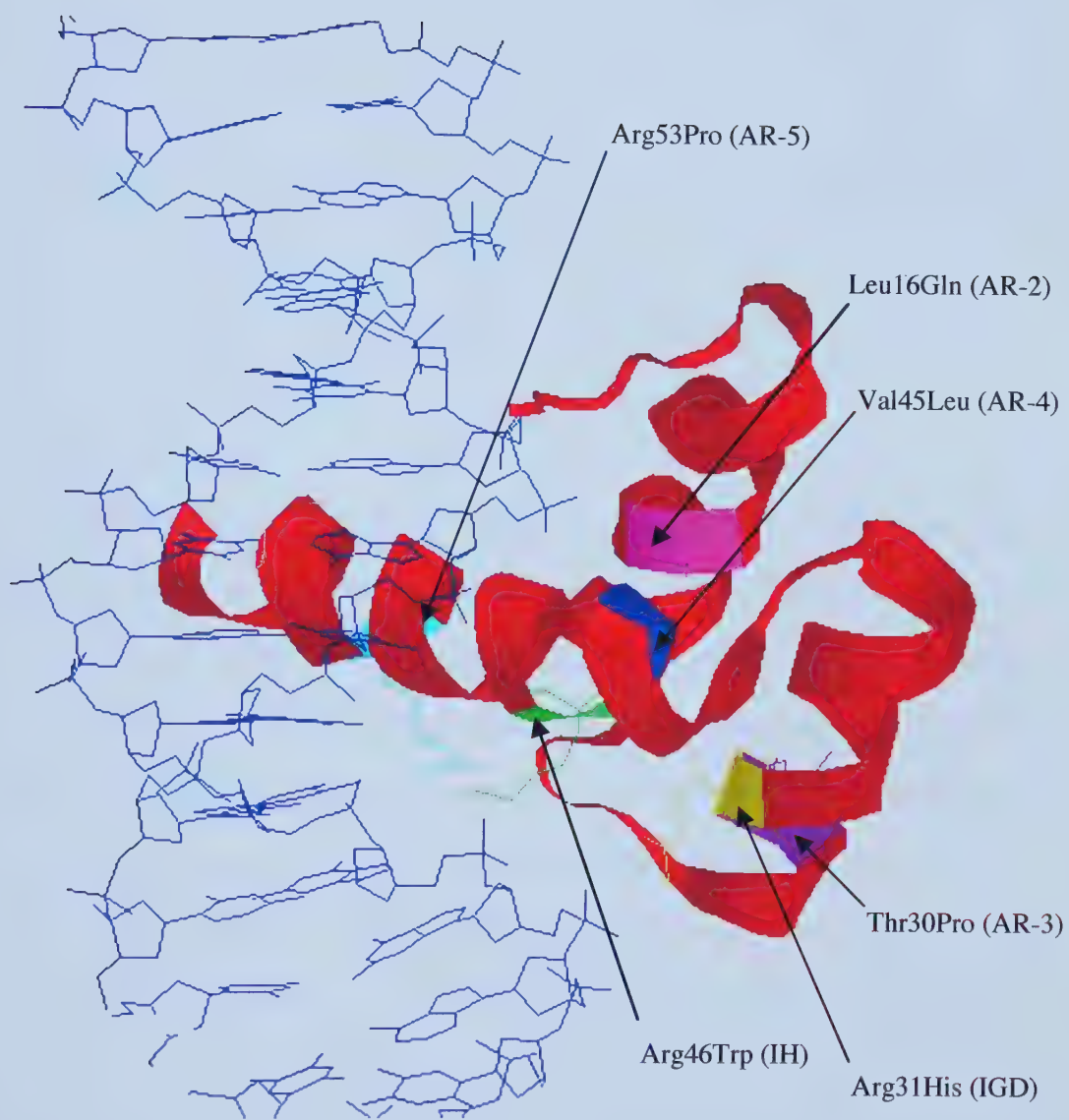
In the present study, homeodomain mutations of the PITX2 transcription factor identified in patients with IH, IGD, and AR malformations were analyzed to investigate a possible genotype-phenotype correlation. Of the nine unique PITX2 homeodomain mutations documented to date (Table 4), seven are studied herein: Arg46Trp associated with IH; Arg31His associated with IGD; and Leu16Gln, Thr30Pro, Val45Leu, Arg53Pro,





**Figure 42.**

*Engrailed* homeodomain, homologous to PITX2, complexed with DNA, modeled from crystallographic data. The positions of the five missense mutations of the PITX2 homeodomain studied (Leu16Gln, Thr30Pro, Arg31His, Val45Leu, Arg46Trp, Arg53Pro) are highlighted.







and a seven amino acid duplication of residues six through twelve of the homeodomain, all associated with AR. Splice-site, frameshift and nonsense mutations of PITX2 were not studied. Partial or complete loss of the PITX2 homeodomain by splice-site mutations is expected to result in non-functional proteins. It is predicted that prematurely truncated PITX2 proteins are likely targeted for early degradation. The remaining two homeodomain mutations (Lys50Gln and Arg52Cys (Perveen et al. 2000)) had not yet been identified during the time of the molecular analyses presented herein and have therefore not yet undergone study. A brief discussion of the possible mechanisms of disease-action for these mutations will now be included however.

### Lys50Gln

A very recent report of a Lys50Gln missense mutation of the homeodomain suggests a dominant negative mechanism of action (Saadi et al. 2001). This novel mutation was identified in a sporadic patient with bilateral iris hypoplasia, prominent Schwalbe's line, and corneal opacities with iris adhesions that originally was misdiagnosed as Peters anomaly (Saadi et al. 2001, Perveen et al. 2000). The ocular defects were noted as being more severe than those noted in most patients with AR malformations. Non-ocular features included midline abdominal defects, diastases recta, a protuberant umbilicus, hyperflexive joints, bifid uvula, and submucous cleft palate. Lys50 is the homeodomain residue that imparts the DNA-binding specificity of the *paired-bicoid* group of homeodomains. DNA-binding of a *bicoid* probe by the Lys50Gln mutant is reduced, as is the transactivation of a *bicoid* reporter construct. *In vitro* transactivation assays of the prolactin promoter with wtPITX2 in the presence of the Lys50Gln mutation and PIT1 results in a suppression of the synergism normally seen between wtPITX2 and PIT1 (Amendt et al. 1998). The suppression is dependent upon the presence of the C-terminal



39aa of wtPITX2 that likely represents a homo-dimerization domain. This domain may be responsible for other protein-protein interactions, as it is required for synergism with PIT1 in some cell lines (COS-7 and HeLa), but not others (CHO, LS8, N2A). Synergism between PITX2 and PIT1 does not require the transactivation domain of PIT1, nor the proposed N-terminal protein-binding domain, but does require the PIT1 DNA-binding (POU) domain. This implies that although PITX2 and PIT1 do not appear to interact throughout their protein-protein interaction domains, binding of the Lys50Gln mutant to the PITX2 dimerization/protein-binding domain prohibits synergism of PITX2 with PIT1. It is possible that the PITX2 homodimer interacts with PIT1 either through a third intermediary factor, through yet uncharacterized protein-protein interaction domains, or through their respective DNA-binding domains. The requirement of the PIT1 DNA-binding domain supports this last notion, which has been previously demonstrated for other homeodomains (Fortin et al. 1998, Wilson et al. 1993). Introduction of the Lys50Gln mutant into the pituitary adenoma GH3 cell line that naturally expresses both PITX2 and PIT1 also results in the suppression of the prolactin promoter. This implies the physiological relevance of Lys50Gln activity in the pituitary, but is confusing in the light of the observation that no pituitary defects have been associated with this mutation. There is no evidence for PIT1 expression in the eye (Figure 38), but a similar dominant-negative mode of action that inhibits the normal transcriptional activation activity of PITX2 may be present in ocular tissue with a different transcription factor.

### Arg52Cys

Arg52Cys is another recently identified PITX2 homeodomain mutation (Perveen et al. 2000) that was not available for characterization during the time of the studies. The mutation was found in a family with AR malformations, dental abnormalities, umbilical



abnormalities, cleft palate, endentulous cleft uvula, and learning difficulties. Arg52 is a highly conserved residue not known to occur as a cysteine (Scott et al. 1989) and is thought to make two phosphate contacts in *Antp* (Gehring et al. 1994). Conversion of a homeodomain residue to cysteine may result in a new interaction with the other six cysteine residues that naturally occur outside of the PITX2 homeodomain. Alteration to the pattern of cysteine bridges could result in a mis-folded and unstable PITX2 protein.

#### Molecular Characterization of the Selected PITX2 Homeodomain Mutations

Constructs containing IH, IGD and AR mutations of the PITX2 transcription factor (Figure 33) were examined for protein stability and functional activity. Intracellular localization, electrophoretic mobility shift assays, and transactivation studies were used to test nuclear signaling, DNA-binding, and transcriptional activation, respectively, as required by functional transcription factors. PITX2 DNA-binding was assayed using an oligonucleotide containing the Pitx1 CE-3 DNA-binding sequence. The CE-3 element was also used in a Luciferase reporter construct to examine the transactivation of the PITX2 mutants. A variation in the amount of PITX2 protein function may account for the phenotypic differences within the spectrum of anterior segment dysgenesis that result from PITX2 mutation. The molecular characterization of each homeodomain mutation will now be discussed individually with accompanying comments on possible mechanism.

#### IH Mutant (Arg46Trp)

The Arg46Trp PITX2 mutation was found in 15 affected individuals of a five generation pedigree diagnosed with IH (Alward et al. 1998, Héon et al. 1995). Ten individuals presented with glaucoma, six had prominent vascular loops, and four had fine translucent





iris processes to normally localized Schwalbe's lines. One individual presented with dental anomalies, maxillary hypoplasia, and redundant periumbilical skin.

Western analysis and immunofluorescence demonstrated that the Arg46Trp protein was stable, and nuclearly localized. Additional cytoplasmic localization was seen in 23% of transfected cells. DNA-binding analysis with the CE-3 oligonucleotide revealed a 20-fold reduction in DNA-binding as compared to wildtype PITX2, and 38% of wildtype transactivation of the pGL3-CE-3 reporter construct maintained.

It is possible that replacement of Arg46 on the hydrophilic face of helix 3 with a hydrophobic and bulky tryptophan may interfere with the stability of the protein-DNA complex, potentially explaining the partial loss of DNA-binding and transactivation ability of the Arg46Trp (IH) mutant PITX2 protein. Arg46 may be important for contacting a sugar residue of the DNA backbone just as Lys46 of *en* does, since the two side-chains have the same overall structure and chemistry. Although threading analysis does not imply a significant difference in folding energy it does predict a removal of the negative interaction between the two positive arginine residues at positions 31 and 46 of the homeodomain (Banerjee-Basu and Baxeavanis 1999). Substitution of the hydrophobic tryptophan for arginine at position 46 likely removes the repulsion slightly altering conformation of the homeodomain.

#### IGD Mutant (Arg31His)

The Arg31His PITX2 mutation was described in 13 individuals of a five generation pedigree diagnosed with IGD (Pearce et al. 1999, Walter et al. 1996, Chisholm and Chudley 1983). At least six individuals also had glaucoma, and 11 members were described with maxillary hypoplasia and dental anomalies, while nine had redundant periumbilical skin. One eye displayed a displaced pupil due to localized adhesion to the





posterior periphery of the cornea with membrane-like tissue over the iris root despite an otherwise open-angle. Histological examination of another glaucomatous eye donated from this family for study revealed nodular thickening of a normally localized Schwalbe's line (Pearce et al. 1999).

Western analysis and immunofluorescence demonstrated that the Arg31His protein was stable, and almost completely localized to the nucleus (3% on transfected cells showed additional cytoplasmic staining). DNA binding of the Arg31His mutant was reduced 200-fold and transactivation was reduced to 12.4% of wildtype levels.

The greater reduction in DNA-binding and transactivation by the Arg31His (IGD) PITX2 mutant protein may represent a more severe mutation than Arg46Trp (Figures 36 and 37). Although threading analysis did not predict a significant alteration in energy for the Arg31His mutant (Banerjee-Basu and Baxevanis 1999), the Arg31His mutation occurs on the hydrophilic face of helix 2 at a critical phosphate backbone contact position required by both *Ant* and *en* for efficient DNA-binding. While arginine and histidine are both basic residues, the shorter ring structure of the histidine residue may be inappropriate for proper contact with the DNA backbone, resulting in instability of the complex.

#### AR Mutant 1 (7aa Duplication)

A *de novo* duplication of amino acids six through twelve of the PITX2 homeodomain was found in an AR patient described with iris atrophy, iris processes to 360° of the surrounding cornea, a prominent Schwalbe's line, narrow anterior segment angles, glaucoma (diagnosed at 19 years of age), and maxillary hypoplasia.

Protein stability and nuclear localization of the 7aaDup-mutant PITX2 protein were normal (Figures 34E and 35). The 7aaDup-mutant PITX2 protein demonstrated



nominal levels of DNA-binding activity, approximately 500x 7aaDup protein is required for DNA-binding equivalent to that of wtPITX2 protein (Figure 36F). Despite evidence of some residual binding of the CE-3 oligonucleotide probe in EMSAs, the 7aaDup mutant was unable to transactivate the pGL3-CE-3 reporter construct tested (Figure 37C).

The duplicated amino acid residues 6-12 of the PITX2 homeodomain are part of a proposed N-terminal arm that is thought to fit into the minor DNA groove. Interactions between the N-terminal arm and the DNA supplement the contacts made by helix 3 for DNA recognition and high DNA binding affinity (Gehring et al. 1994, Kissinger et al. 1990). This duplication of the N-terminal arm may inhibit proper binding of PITX2 with the DNA target, interfering with the docking of helix 3 in the DNA major groove. The duplication may also alter the conformational folding of the homeodomain, thereby preventing DNA-binding. Threading analysis is not possible for the duplication mutation (Dr. Banerjee-Basu, NIH, personal communication).

#### AR Mutant 2 (Leu16Gln)

While less clinical data has been published by other groups on the precise AR families found to carry PITX2 mutations, it has been reported that at least one member of each family displayed the three cardinal features of AR that include abnormal anterior segments (generally accepted to include glaucoma, iris hypoplasia, a prominent Schwalbe's line and occasionally, distorted and displaced pupils due to iris processes, and glaucoma), hypodontia, and failure of the periumbilical skin to involute (Semina et al. 1996b, Semina et al. 1996a, Murray et al. 1992).

Leu16Gln mutant PITX2 protein had previously been shown to be unstable in bacteria (Amendt et al. 1998). Our production of stable Leu16Gln mutant PITX2 protein may reflect our use of a mammalian expression system rather than a bacterial system.



Immunofluorescence of transfected COS-7 cells shows that 30% of Leu16Gln transfected cells showed cytoplasmic staining in addition to nuclear localization (Figure 34F). DNA-binding ability of the Leu16Gln mutant PITX2 protein was undetectable (Figure 36G). The Leu16Gln (AR-2) mutation occurs within a critical component of the homeodomain hydrophobic core. Leu16 is normally invariant between homeodomains (Wilson et al. 1996, Scott et al. 1989), and substitution by a hydrophilic glutamine within the hydrophobic core might disrupt the packing of helix 1 against helix 3. This is supported by threading analysis that predicts a significant alteration in folding energies due to predicted loss of the interactions that normally occur between Leu16 and Phe8, Val45, Trp 48, and Phe 49 (Banerjee-Basu and Baxeavanis 1999).

#### AR Mutant 3 (Thr30Pro)

The Thr30Pro PITX2 mutant produced stable protein detectable by western analysis (Figure 35). Immunofluorescence showed that approximately 18% of Thr30Pro (AR-3) transfected cells showed cytoplasmic staining in addition to nuclear localization (Figure 34G). DNA binding of the Thr30Pro mutant was non-detectable and transactivation was reduced to 6.7% of wildtype PITX2 levels (Figures 36H and 37B).

Mutation to proline residues, described in AR as Thr30Pro and Arg53Pro mutations, represent substitutions highly disruptive to the formation of alpha-helices (O'Neil and DeGrado 1990). Furthermore, these proline mutations likely occur at important positions within the homeodomain by comparison to *Ant* and *en* crystal structures. The Thr30Pro (AR-3) mutation occurs on a hydrophilic face between amino acids Arg25 and Arg31 which are required to make phosphate contacts with the DNA backbone to stabilize helix 3 within the DNA-major groove. Conformational disruptions may account for the reduced nuclear localization and loss of DNA-binding.





#### AR Mutant 4 (Val45Leu)

One individual, diagnosed with AR, has been shown to carry a Val45Leu PITX2 mutation. Clinical details include iris hypoplasia, corectopia, Schwalbe's line visible for 180° of the angle, no glaucoma at age 6, maxillary hypoplasia, dental anomalies, and a prominent umbilicus.

The Val45Leu mutant is seen to be a stable protein with full nuclear localization (Figure 35H). DNA-binding analysis with the CE-3 oligonucleotide and recombinant Val45Leu mutant PITX2 protein demonstrated a two- to seven-fold reduction in DNA-binding ability (Figure 36I). Transactivation studies demonstrated that the Val45Leu mutant showed a two-fold increase in transactivation activity over that of wtPITX2 (Figure 37C). Control transactivation studies using the standard pGL3-SV40 Luciferase reporter construct (without the CE-3 insert) revealed that both wtPITX2 and Val45Leu require the CE-3 binding site for transactivation, being unable to transactivate the empty pGL3-SV40 construct (Figure 37F). Co-transfection experiments with wtPITX2 and Val45Leu result in transactivation levels somewhere between the two alone, indicating that wtPITX2 and Val45Leu proteins are likely competing for binding sites (Figure 37E). The results also indicate that the Val45Leu PITX2 mutation is not likely to represent a direct dominant negative mutation, as the addition of Val45Leu protein does not reduce the ability of wtPITX2 protein to transactivate when the two are assayed together. However, it is not known whether the Val45Leu mutant is capable of inhibiting wtPITX2 synergism with other factors, in the manner of the Lys50Gln mutation. WtPITX2 and Val45Leu do not appear to interact synergistically either, as co-transfection of wtPITX2 and Val45Leu together does not result in transactivation levels above and beyond that of Val45Leu.





Substitution of valine with leucine would generally be considered a conservative mutation. Leucine differs from valine by containing one extra methyl group within its main chain. Position 45 occurs within the hydrophobic core between helices 1 and 3 of the homeodomain, shown to be responsible for directing proper homeodomain folding (Qian et al. 1993), and is conserved in over 97.5% all homeodomains. Of the nearly 800 homeodomains entered into the NIH homeodomain database (<http://genome.nhgri.nih.gov/homeodomain>), only 19 examples (with four that are orthologues) were found with a leucine at position 45 of the homeodomain (Figure 43). Biochemical studies mutating different residues of the *antennapedia* homeodomain found that position 45 is under high levels of steric hindrance (Billeter et al. 1993) and therefore extension of the main methyl chain may not be a conservative change at this position within most homeodomains. The 15 homeodomains with a leucine at position 45 are divergent from eukaryotic homeodomain sequences (Scott et al. 1989), particularly within the hydrophobic core (Qian et al. 1989), and at positions of significant steric hindrance within helices 1 and 2 (Qian et al. 1993). This may reflect homeodomain conformations with greater potential for accommodating the larger leucine side-chain at position 45 of helix 3. Threading analysis did not demonstrate significant changes in energies (Dr. Banerjee-Basu, NIH, personal communication).

A number of mechanisms have been proposed to explain increased transactivational activity for other mutated transcription factors. Altered patterns of phosphorylation due to the elimination of phosphorylation sites (Huang et al. 2000, Ray-Gallet and Moreau-Gachelin 1999), or alternatively, introduction of residues (i.e. glutamate and aspartate) that mimic phosphorylation (Saeki et al. 1999, Lin et al. 1998, M. Nohaile et al. 1997), have been demonstrated to result in constitutively active forms of transcription factors. Leucine, however is not a residue that would mimic





### Figure 43.

Homeodomain alignment of PITX2 and the 19 homeodomains with a leucine at position 45. Percentage identity is shown to the left, and the three  $\alpha$ -helices are indicated above. Genbank numbers and species are shown below. Dashes indicate identity of amino acid residues with PITX2. Note that many of the residues of the homeodomains that naturally contain a leucine at position 45 are divergent (highlighted in gray) from the consensus for homeodomains of higher eukaryotes (Qian et al. 1989). These divergent residues tend to occur at residues of the hydrophobic core (indicated by circles) (Scott et al. 1989), and at positions determined to encounter steric hindrance (empty and filled squares represent moderate and high levels of steric hindrance, respectively) (Qian et al. 1993). Divergence at residues of the hydrophobic core and at residues that encounter internal steric hindrance within helices 1 and 2 may represent conformations with greater potential for accepting the larger leucine side-chain at position 45.

% Identity

Identity		HELIIX 1										HELIIX 2										HELIIX 3									
		10	20	30	40	50	60																								
100	PITX2	QRRQRTHFTS	QQLQELEATF	QRNRYPDMST	REEIAVWTNL	TEARVRVWFK	NRRAKWRKRE																								
33	<i>Apterous</i>	TK-M--S-KH	H--RTMKS-	AI-HN--AKD	LKQLSQK-G-	PKRVLQ---Q	-A-A---RMM																								
33	<i>LHX2</i>	TK-M--S-KH	H--RTMKS-	AI-HN--AKD	LKQL-QK-G-	TKRVLQ---Q	-A-A-F-RNL																								
33	<i>LHX9</i>	TK-M--S-KH	H--RTMKS-	AI-HN--AKD	LKQL-QK-G-	TKRVLQ---Q	-A-A-F-RNL																								
31	<i>MTP1</i>	V-G-CSKC-K	PH-MRWLLH	YD-P--SN-E	FYDLSAA-G-	RTQL-N--S	---R																								
25	<i>CUP9</i>	R-SNLPKE-V	QI-NTWLLNH	LN-P--TQQE	KR-LLIK-G-	KIQLSN--I	-V-RRKIFSD																								
21	<i>YR63 (ORF)</i>	K--R--TDAE	AT-L-QYFLK	TPKPSLIERQ	ELSKKLSKSM	PRELQI--Q	-K-QSL-R																								
13	<i>B2</i>	HFLHTLDNPF	PTQE-K-GLV	RLTNESTARV	GLSK-NRPP-	EVHQLTL--I	-A-RRSGWSH																								
15	<i>B3</i>	HFLHTLENPF	PTQE-K-GLV	RLTNESTARI	-PSN-IRPP-	EVHQLTL--I	-A-RRSGWSH																								
13	<i>B4</i>	HFLHTLENPF	PTQE-K-TLV	RLTNESTARV	GQS-VNRPP-	EVHQLTL--I	-A-RRSGWSH																								
10	<i>B5</i>	HFLHTLDNPF	PTQE-KQNLV	RLTNESTVRV	GSSNPAPPP-	EVHQLTL--I	-A-RRSGWSH																								
12	<i>B6</i>	HFLHTLDSPY	PTQE-K-TLV	RLTNESTARV	GQSSVNRPP-	EVHQLTL--I	-A-RRSGWSH																								
13	<i>B7</i>	HFLHTLDSPY	PTQE-K-GLV	RLTNESTARV	GLSN-TRPP-	EVHQLTL--I	-A-RRSGWSH																								
8	<i>HM26</i>	SSSMLTPMHL	RKAKLMFFYT	RYPNSNLLKS	YFPDIRFNKN	NT-QLVK--S	-F-EFYYNQM																								
8	<i>PROX 1</i>	MQEGLSPNHL	KKAKLMFFYT	RYPSSNMLK-	YPSDVKFNRC	ITSOLIK--S	-F-EFYIYQM																								
8	<i>Prospero</i>	HSSTLTTPMHL	RKAKLMFFVW	RYPSSAVLKM	YFPDIKFNRKN	NT-QLVK--S	-F-EFYIYQM																								
			o	o		o						o	o	o		o	o					o	o								
			■	■		■						■	■	■		■	■					■	■								

Gene	Species	Genbank Number
PITX2	Human	AF238048
<i>Apterous</i>	<i>Drosophila melanogaster</i>	P29673
<i>LHX2</i>	Human/Mouse/Rat	P50458/Q9Z0S2/P36198
<i>LHX9</i>	Mouse	Q9WUH2
<i>MTP1</i>	<i>Schizosaccharomyces pombe</i>	P10842
<i>CUP9</i>	<i>Saccharomyces cerevisiae</i>	P41817
<i>YR63 (ORF)</i>	<i>Schizosaccharomyces pombe</i>	P40923
<i>B2</i>	<i>Ustilago maydis</i>	P22016
<i>B3</i>	<i>Ustilago maydis</i>	P22017
<i>B4</i>	<i>Ustilago maydis</i>	P22018
<i>B5</i>	<i>Ustilago maydis</i>	P22019
<i>B6</i>	<i>Ustilago maydis</i>	P22020
<i>B7</i>	<i>Ustilago maydis</i>	P22021
<i>HM26</i>	<i>Caenorhabditis elegans</i>	P34522
<i>PROX 1</i>	Human/Mouse/Chick	Q92786/P48437//Q91018
<i>Prospero</i>	<i>Drosophila melanogaster</i>	P29617



phosphorylation, and residue 45 is not within any predicted phosphorylation sequence (as determined by the NetPhos 2.0 Prediction program at the Centre For Biological Sequence Analysis at ( [www.cbs.dtu.dk](http://www.cbs.dtu.dk) )). Therefore, altered phosphorylation is likely not responsible for increased transactivation activity of the Val45Leu PITX2 mutant.

An equally subtle mutation of a leucine to a valine residue has been documented in the transcription factor *AreA* of *asperigillus nidulans* at a conserved residue of its DNA-binding domain (Ravagnani et al. 1997). In the case of *AreA* the leucine to valine mutation alters DNA-specificity and results in decreased transcriptional activation of some promoters while increasing the transactivation of other promoters. Altered DNA-specificity has not yet been demonstrated for the Val45Leu mutant. Even though DNA-binding of Val45Leu is reduced with the CE-3 element, the increased transactivation activity was not due to use of a site other than CE-3, because removal of the CE-3 binding sites from the Luciferase reporter construct resulted in loss of transcriptional activation (Figure 37F). Therefore, a mechanism other than altered DNA specificity is likely responsible for the increased transactivation seen with the Val45Leu PITX2 mutant in the present set of experiments. Illegitimate transcriptional activation by the Val45Leu mutant of novel promoters would probably result in a different clinical phenotype, which was not detected in this patient who presented with the typical ocular and non-ocular features associated with AR malformations. Even if altered DNA-binding specificity does exist for the Val45Leu mutant it seems to be of little physiological importance.

Another possibility is that the substitution of valine with leucine at position 45 affects homeodomain conformation such that it intrinsically affects DNA-binding and transactivation differently. The altered conformation may result in reduced binding ability or affinity for DNA. The same conformational change could theoretically increase the ability of PITX2 to recruit transcriptional machinery, or increase the affinity of





protein-protein interactions. Studies on the glucocorticoid receptor have demonstrated that substitution of leucine with a valine residue within the transactivation domain results in decreased transactivation (Almlof et al. 1997). The authors postulated that the hydrophobicity and helix-forming propensity of residues of the transactivation domain are important to activity. It could be that introduction of a leucine residue at position 45 of the PITX2 homeodomain improves transactivation activity in a direct manner for PITX2. However, conservation of the valine residue may be indicative of its importance to homeodomain folding and structure that is required for proper DNA-binding, as it is reduced in the Val45Leu mutant (Figure 36I).

These data indicate that the DNA-binding and transcriptional activities of PITX2 are separable, and that mutation of residue 45 has separate consequences for both functions. Separable DNA-binding and transactivation abilities have also very recently been indicated for FOXC1 (Saleem et al. 2001). In the case of FOXC1, proteins with either Phe121Ser or Ile126Met mutations of the FOXC1 DNA-binding domain are able to bind DNA at nearly wildtype levels, but exhibit severe reduction in transcriptional activation potential.

The decrease in DNA-binding found with the Val45Leu PITX2 mutant is likely not disease-causing in this AR patient. The levels of residual DNA-binding are much higher in the Val45Leu mutant (14-50%) than with the Arg46Trp PITX2 mutant (only 5% residual activity) that has the milder IH phenotype (Kozlowski and Walter 2000). The increased transcriptional activation of the Val45Leu PITX2 mutant may result in AR malformations by aberrantly increasing transcription of genes downstream of PITX2 in the ocular development pathways. This suggestion is supported by recent studies demonstrating that three copies of FOXC1 result in ocular defects similar to those seen in patients with AR malformations (Lehmann et al. 2000, Nishimura et al. 2001,



F. Mirzayans –Walter lab, personal communication). Studies of PAX6 have also demonstrated that three copies of PAX6 also result in disturbances in ocular development (Aalfs et al. 1997). This suggests that too much of a downstream factor, possibly common to the pathways of PITX2 and FOXC1, results in aberrant ocular development.

#### AR Mutant 5 (Arg53Pro)

The Arg53Pro mutation has been independently documented in the literature twice (Table 4). The first report documents a patient with classic AR malformations with syndromic features (Semina et al. 1996a). The second report describes an apparently unrelated patient with iris hypoplasia and polycoria, corectopia, prominent Schwalbe's line, prominent iris processes, without glaucoma at age 12 (Priston et al. 2001). Non-ocular features included maxillary hypoplasia, dental anomalies, and a prominent umbilicus.

The Arg53Pro mutant results in a stable protein, with nuclear (36% of transfected cells) or nuclear + cytoplasmic staining (64% of transfected cells) (Figures 34I and 35). DNA binding was non-detectable and transactivation reduced to 4.8% for the mutant (Figures 36J and 37B). Similar results have been recently been confirmed by other investigators (Saadi et al. 2001).

The Arg53Pro mutation potentially disrupts helix 3 structure by introducing a kink in the helix. This may affect the packing of helix 3 against helix 1, thereby inhibiting DNA binding. Furthermore, this proline mutation occurs at a conserved helix 3 residue responsible for making two critical phosphate contacts and is surrounded by a number of DNA contact and recognition points, including those made by amino acids Lys50 and Asn51. Because Arg53 is not part of the hydrophobic core, threading analysis was not able to determine a change in energies (Banerjee-Basu and Baxevanis 1999).



Immunofluorescence shows that approximately 64% of Arg53Pro (AR-5) transfected cells showed cytoplasmic staining in addition to nuclear localization (Figure 34I). A reduction in protein stability introduced by prolines within the alpha-helix as in the Thr30Pro (AR-3) and Arg53Pro (AR-5) mutations may cause the reduced nuclear localization observed. However, the more extensive reduction to nuclear targeting by the Arg53Pro mutation may be more complex than that for Thr30Pro. Disruption to helix 3 could interfere with packing against helix 1, destabilizing the homeodomain further, but it may also represent an impaired nuclear localization signal (NLS) within helix 3. This is supported by similarity of this PITX2 region to the NLS of the homeodomain transcription factor PDX-1 (Figure 44) (Hessabi et al. 1999). The third helices of PITX2 and PDX-1 are very similar, with three clusters of basic amino acids similarly spaced. The central cluster (Arg53 and Arg54; both conserved in PITX2) is critical to the PDX-1 NLS, mutation of which effectively blocked PDX-1 nuclear import. Reduced nuclear localization is also seen with the Arg46Trp (IH) PITX2 mutation, indicating amino acid residue Arg46 and nearby Arg44 may also be part of a PITX2 NLS within helix 3. Basic residues are often characteristic of nuclear localization signals (Gorlich 1997, Dingwall and Laskey 1991), and basic residues Arg43 and His44 of PDX-1 are found to contribute to proper cellular targeting, impairing nuclear localization when mutated to leucine residues. PITX2 is also has sequence similarities with the C-terminal end of the PDX-1 NLS. Arg58 and Lys59 of PITX2 may be functionally equivalent to the two PDX-1 lysine residues at positions 58 and 59, which when mutated along with Arg53/Arg54 further excluded PDX-1 from the nucleus. This would be the first description of a C-terminal PITX2 nuclear localization signal that may also exist in homeodomains such as PITX1 and *unc-30* (Figure 44). A second putative NLS (Lys-Lys-Lys-Arg) has been predicted immediately N-terminal to helix 1 of the homeodomain (Lindberg et al. 1998,







**Figure 44.**

Homeodomain alignment of PITX2 and related transcription factors with the three  $\alpha$ -helices indicated. The putative C-terminal nuclear localization signals of PITX2 and PDX-1 are boxed. Amino acids determined to be important to the PDX-1 NLS are shaded, along with possible counter-residues in PITX2. Potential PITX2 protein-DNA contact points (as based upon conserved *Antp* and *en* residues) are also indicated along with the missense mutations of the PITX2 homeodomain found in patients in an effort to determine other possible reasons for impaired nuclear localization of some of the mutants.





Gage and Camper 1997, Dingwall and Laskey 1991). This N-terminal NLS would appear to be secondary to the C-terminal NLS, as deletion of these four amino acids had little effect on subcellular localization (Figure 34J). More work needs to be done to determine the regulation of PITX2 nuclear localization.

### **III: PITX2 in the Adult Eye**

It has been proposed that either the high insertion of the iris or compacted trabecular meshwork may be responsible for the obstruction to aqueous humor outflow in the glaucoma of AR patients (Shields 1989). Severe glaucoma in infancy or early childhood seen in some patients is thought to arise mainly from the incomplete development of the trabecular meshwork and Schlemm's canal (Shields 1989). Later development of glaucoma during early adulthood may be a result of compression of the trabecular meshwork from tension exerted by the anteriorly inserted uveal tissue (Shields 1989). The reduced normal aqueous outflow by either mechanism likely results in increased intraocular pressure believed to cause the secondary glaucoma by damaging the optic nerve head (Shields 1989). However, the glaucoma exhibited by patients is not necessarily associated with angle defects. There may therefore be another explanation for the delayed (non-congenital) development of glaucoma in patients with anterior segment dysgenesis. With the discovery that PITX2 is expressed in the adult trabecular meshwork (Figure 38A), PITX2 may have a previously unforeseen involvement in the progressive development of glaucoma in the adult eye. There is already precedent for ocular development genes that maintain a role in adult tissue. PAX6 is a key eye development gene (Fernald 1997) but is also involved in the maintenance and proliferation of corneal stem cells in adult tissues (Koroma et al. 1997), the same cells that exhibit the



developmental defect known as aniridia resulting from PAX6 mutation (Jordan et al. 1992, PAX6 mutation database: [www.hgu.mrc.ac.uk/Softdata/PAX6](http://www.hgu.mrc.ac.uk/Softdata/PAX6)).

### PITX2 Regulation of *MYOC*

In an attempt to examine the possible role of PITX2 in the adult eye, the promoter of the *Myocilin* (*MYOC*) gene was screened as a possible PITX2 target for transcriptional regulation. *MYOC*, previously known as the trabecular meshwork-inducible glucocorticoid response factor (*TIGR*) (Escribano et al. 1995), is the only gene among the seven loci (*GLC1A* to *GLC1G*) of POAG (Friedman and Walter 1999), to be characterized to date (Kubota et al. 1998, Stone et al. 1997). Mutations of *MYOC* account for ~4% of all cases of POAG (Alward et al. 1998, Stone et al. 1997). *MYOC* contains the only promoter known to be involved in ocular function that contains potential PITX2 DNA-binding sites (Figure 39), as revealed by a TargetFinder analysis (Telethon Institute of Genetics and Medicine (TIGEM)) of known promoters (conducted by post doctoral fellow Dr. Fred Berry of the Walter laboratory). Interestingly, the *MYOC* promoter also contains potential FOXC1 DNA-binding sites (Figure 39). There appears to be a conservation of PITX2 and FOXC1 DNA-binding sites among the three species of *MYOC* promoters examined (human, murine, rat) (Figure 39), suggesting that the sites may have physiological relevance. PITX2 and *MYOC* are co-expressed in the adult trabecular meshwork, but it is controversial whether FOXC1 is also co-expressed in this tissue. Some studies report expression of FOXC1 in the trabecular meshwork (Wang et al. 2001), while studies within the Walter laboratory indicate otherwise (J. Friedman, personal communication).

To examine whether wtPITX2 is able to transactivate the *MYOC* promoter from different species, HeLa cells were co-transfected with a wtPITX2 expression construct, a



βgal CMV control vector, and various pGL3 Luciferase reporter constructs (Figure 40). WtPITX2 is able to transactivate the four different *MYOC* promoter Luciferase reporter constructs above baseline levels. Transactivation by wtPITX2 ranges from 6.9x for the Human -1062/+54 *MYOC* promoter, to 18.2x for the Rat -510/+62 promoter (Figure 40A). The AR-3 Thr30Pro PITX2 homeodomain mutant was used as a control with the *MYOC* constructs. The AR-3 PITX2 mutant was unable to transactivate the *MYOC* Luciferase reporter constructs above baseline levels as expected.

Co-transfection of the *MYOC* promoter with the VAL45Leu PITX2 mutation resulted in significant increases in transactivation levels over that seen with wtPITX2 (Figure 40B). Both the Human -1062/+54 and mouse *MYOC* promoter constructs were transactivated approximately 200% better by the Val45Leu mutant, and the rat *MYOC* construct was transactivated over 300% better by Val45Leu than by wtPITX2. This further suggests the physiological relevance of the Val45Leu mutation as a gain-of-function mutant, as well as the physiological significance of the *MYOC* promoters.

The conservation of potential PITX2 and FOXC1 DNA-binding sequences in three different species of *MYOC* promoter suggests the possibility of an interaction between PITX2 and FOXC1, and co-regulation of the *MYOC* promoter. Co-transfection of wtPITX2 and wtFOXC1 results in levels of transactivation intermediate between that of independent wtPITX2 and wtFOXC1 transfections for all of the *MYOC* promoter constructs tested (Figure 40). Therefore, it appears that wtPITX2 and wtFOXC1 proteins act independently and do not interact with each other to influence transactivation of the *MYOC* promoter constructs tested, in neither a negative nor a synergistic manner.





## **Conclusions**

Electrophoretic mobility shift assays (EMSAs) confirmed that all seven PITX2 mutants tested had reduced DNA-binding ability, consistent with these alterations of the PITX2 gene being disease-causing mutations. The Val45Leu and 7aaDup (AR), Arg31His (IGD), and Arg46Trp (IH) mutant PITX2 proteins retained residual DNA binding, while the other three AR-mutant PITX2 proteins tested, Leu16Gln, Thr30Pro, and Arg53Pro, were unable to bind the CE-3 oligonucleotide at levels detectable by autoradiography (Figure 36). Transactivation analyses of the seven mutant PITX2 molecules revealed that the IH and IGD mutants had reduced transactivation capabilities, while the AR mutants (with the exception of Val45Leu) had undetectable levels of transactivation. Transactivation assays, however, revealed that the Val45Leu PITX2 was more active than wtPITX2 in transactivating an artificial reporter construct as well as the natural *MYOC* promoter. Results and possible mechanism of action are summarized in Table 5.

Based on these results, it is possible to suggest a threshold for functional PITX2 protein in the development of the anterior segment and allow for genotype-phenotype correlations to be made. In patients heterozygous for *PITX2* alleles (like Leu16Gln, Thr30Pro, and Arg53Pro) found to be inactive (by DNA-binding and transactivation assays), having only 50% of the normal amount of PITX2 protein from the remaining wildtype *PITX2* allele results in AR malformations, the severe form of anterior segment dysgenesis. It appears that additional PITX2 activity, contributed by *PITX2* alleles with some residual activity (like Arg46Trp and Arg31His), results in the milder IH or IGD phenotypes. An increase in PITX2 function to a total of over 150% of normal activity, as in the case of Val45Leu, however, also appears to result in AR malformations. On the basis of this data, it can be proposed that the variance in PITX2 activity, due to specific



**Table 5.**

Summary of clinical data, molecular data and proposed mechanism for each of the PITX2 missense mutations.

Below each mutation is the fold-reduction in DNA-binding & the retained transactivation activity.

Arg46Trp 20x 37.9%	IH 1 Family 15 iris hypoplasia 10 glaucoma 6 prominent vascular loops 4 iris processes 1 maxillary hypoplasia & dental anomalies & prominent umbilicus	<ul style="list-style-type: none"> <li>•Positively charged Arg46 occurs on the hydrophilic face of helix 3 and may be involved in contacting a sugar residue of the DNA backbone</li> <li>•Replacement with a bulky hydrophobic Tryptophan would remove that contact &amp; may interfere with stability of the protein-DNA complex</li> <li>•Would also eliminate normal repulsion between Arg31 and Arg46</li> </ul>
Arg31His 200x 12.4%	IGD 1 Family 13 iris hypoplasia + goniodysgenesis 6 glaucoma 11 maxillary hypoplasia & dental anomalies 9 prominent umbilicus 1 displaced pupil w/ corneal adhesion 1 thickened Schwalbe's line	<ul style="list-style-type: none"> <li>•Arg31 occurs on the hydrophilic face of helix2 at a critical <math>\text{PO}_4^-</math> DNA backbone contact position</li> <li>•Arg and His are both positively charged, but the shorter ring structure of His may be inappropriate for proper contact with the DNA</li> </ul>
7aaDup 500x 0%	ARS 1 Individual glaucoma iris hypoplasia narrow angles iris processes (360°) prominent Schwalbe's line maxillary hypoplasia	<ul style="list-style-type: none"> <li>•aa 6-12 are part of the proposed N-terminal arm which fits into the minor DNA groove to supplement contacts made by helix 3</li> <li>•Duplication may alter homeodomain folding or inhibit proper DNA-binding.</li> </ul>



**Table 5 Continued.**

Leu16Gln None 8.6%	ARS 1 family 2 w/ classic features	<ul style="list-style-type: none"> <li>•Leu16 is invariant</li> <li>•Substitution with a hydrophilic Gln within the hydrophobic core may disrupt the packing of helix 1 against helix 3</li> </ul>
Arg30Pro None 6.7%	ARS 1 Individual w/ classic features	<ul style="list-style-type: none"> <li>•Introduction of Pro may disrupt formation of the alpha helix</li> <li>•Thr30 occurs on the hydrophilic face of helix 3 between Arg25 and Arg31 which are required to make <math>\text{PO}_4^-</math> DNA backbone contacts</li> </ul>
Val45Leu 2-7x 228%	ARS 1 Individual iris hypoplasia displaced pupil prominent Schwalbe's line maxillary hypoplasia dental anomalies prominent umbilicus	<ul style="list-style-type: none"> <li>•Val45 is highly conserved with very few incidences of Leu45</li> <li>•Position 45 of the core experiences steric hindrance</li> <li>•Substitution of Leu with Val in the glucocorticoid receptor resulted in decreased transactivation</li> <li>•Val45Leu may increase hydrophobicity and/or helical propensity of the region thereby enhancing transactivation potential</li> </ul>
Arg53Pro None 6.9%	ARS Two unrelated individuals 1-classic features 2-iris hypoplasia displaced pupil iris tears prominent Schwalbe's line prominent Iris processes maxillary hypoplasia dental anomalies redundant umbilicus	<ul style="list-style-type: none"> <li>•Arg53 is a conserved residue responsible for two critical <math>\text{PO}_4^-</math> contacts and is surrounded by a number of DNA contact and specificity recognition points</li> <li>•Introduction of Pro may disrupt helix 3 and affect the packing of helix 3 against helix 1</li> <li>•May be part of a PITX2 NLS</li> </ul>



*PITX2* mutations, underlies the different anterior chamber anomalies classified as IH, IGD, and AR malformation (Kozlowski and Walter 2000, Priston et al. 2001). In addition, *PITX2* overactivity may be as physiologically disruptive to development of the eye as *PITX2* mutations that eliminate activity as demonstrated by the Val45Leu *PITX2* gain-of-function mutation. A dominant-negative mutation (possibly represented by Lys50Gln) that results in less than 50% normal *PITX2* may result in a more severe AR malformations and may even be associated with midline defects (Saadi et al. 2001). The differing clinical consequences due to the levels of *PITX2* function retained by different mutations of *PITX2* illustrates the tight regulation of *PITX2* activity and suggests a narrow threshold in the developmental pathways of the anterior segment.





## **Future Directions**

Future experiments may include identifying and verifying the PITX2 DNA-binding sites within the *MYOC* promoters. It might be very fruitful to test discreet fragments of the *MYOC* promoter that, based upon the above experiments, are likely to contain single PITX2 DNA-binding sites to more precisely determine the sites used by PITX2 to activate *MYOC* transcription. To confirm the use of a putative DNA-binding site, mutagenesis could be used to remove the site from the promoter with the expectation of eliminating transactivation by PITX2.

A main focus for the future will be to identify PITX2 interacting proteins. Some studies use PIT1 to demonstrate transactivational synergism with PITX2, however, PIT1 does not appear to be expressed in the eye (Figure 38B). A new trabecular meshwork library that is being developed in the Walter laboratory will be used in yeast-two hybrid assays, and possibly immuno-affinity purifications, to identify novel PITX2 interacting proteins. Proteins identified to bind PITX2 may prove to be important to either the pathways of anterior segment development or maintenance of adult trabecular meshwork.

Other researchers have used chromatin precipitation to identify promoter sequences bound by PITX2 (Hjalt et al. 2001). This technique has been successful in identifying the procollagen lysyl hydroxylase promoter from whole murine heads. The same technique could be refined using eye tissue alone, to identify additional downstream targets of PITX2.



## **APPENDIX A:**

### **Materials and Methods:**

#### **Solutions**

##### **10x PCR buffer**

200 mM TrisCl (pH 8.0)

500 mM KCl

20 mM MgCl

##### **10x TBE**

108 g TRIS Base

55 g Boric Acid

40 mL 0.5 M EDTA

~960 mL dH<sub>2</sub>O

##### **Loading dye**

47.5 mL Formamide

50 µL 10M NaOH

0.025g Bromophenol Blue

0.025 g Xylene cyanol

2.5 mL dH<sub>2</sub>O



**6% sequencing gels**

40 mL dH<sub>2</sub>O

40.5 g urea

4.5 mL 20x GTB Buffer

13 mL 40% Acrylamide/Bis-acrylamide (19:1)

850 µL 10% APS

25 µL TEMED

**20x GTB Buffer**

54 g TRIS Base

18 g Taurine

1 g Na<sub>2</sub>EDTA<sub>·2</sub>H<sub>2</sub>O

~250 mL dH<sub>2</sub>O

**LI-COR loading dye**

47.5 mL 95% Formamide

1 mL 0.5 M EDTA

0.5g Pararosanlile

1.5 mL dH<sub>2</sub>O

**Lactose Broth**

10 g NaCl

10 g Tryptone

5 g Yeast Extract

~1 L dH<sub>2</sub>O



### **LB agar plates**

1 L Lactose Broth

20 g Agar

### **TENS**

4.7 mL TE

250  $\mu$ L 10% SDS

50  $\mu$ L 10M NaOH

### **TE**

1 mL 1M TRIS (pH 7.6)

200  $\mu$ L 0.5M EDTA (pH 8.0)

100 mL dH<sub>2</sub>O

### **10x PBS (for Tissue Culture)**

60 g NaCl

1.5 g KCl

8.625 g Na<sub>2</sub>HPO<sub>4</sub>•7H<sub>2</sub>O

1.5 g KH<sub>2</sub>PO<sub>4</sub>

~ 1 L dH<sub>2</sub>O





## **Plasmid Preparation Buffers**

### **Resuspension Buffer**

50 mM TrisCl (pH 8.0)

10 mM EDTA

100 µg/mL RNase A

### **Lysis Buffer**

200 mM NaOH

1% SDS

### **Neutralization Buffer**

3.0 M potassium acetate (pH 5.5)

### **Column Equilibration Buffer**

750 mM NaCl

50 mM MOPS (pH 7.0)

15% isopropanol

0.15% Triton X-100

### **Wash Buffer**

1.0 M NaCl

50 mM MOPS (pH 7.0)

15% isopropanol



**Elution Buffer**

1.6 M NaCl

50 mM MOPS (pH 7.0)

15% isopropanol

**Immunofluorescence mounting media (Pringle et al. 1991)**

100 mg p-phenylenediamine

10 Ml PBS

90 mL glycerol

2.25  $\mu$ L 1M DAPI (4',6-diamidino-2-phenylindole dihydrochloride)

**Lysis Buffer (modified from Chalepakis et al. 1991)**

1 mL 50% Glycerol

80  $\mu$ L 0.5M HEPES

60  $\mu$ L 5M NaCl

10  $\mu$ L 0.1M DTT (dithiothreitol)

4  $\mu$ L 0.5M PMSF (phenylmethylsulfonyl fluoride)

846  $\mu$ L dH<sub>2</sub>O

**1x SDS-PAGE Electrophoresis Buffer**

1.51 g TRIS base

7.2 g Glycine

10 mL 10% SDS

490 mL dH<sub>2</sub>O



## **SDS-PAGE Western gels**

### **7% Separation Layer**

5.1 mL dH<sub>2</sub>O

2.5 mL 1.5M Tris (pH 8.8)

100 µL 10% SDS

2.35 mL 30% Acrylamide/Bis-acrylamide (37.5:1)

50 µL 10% APS

5 µL TEMED

### **3% Stacking Layer**

3.25 mL dH<sub>2</sub>O

1.25 mL 0.5M TRIS (pH 6.8)

50 µL 10% SDS

500 µL 30% Acrylamide/Bis-acrylamide (37.5:1)

25 µL 10% APS

10 µL TEMED

## **Western loading dye**

2.5 mL 4x TrisCl (pH 6.8)

4 mL 10% SDS

2 mL 2-βMercaptoethanol

0.2 g Bromophenol Blue

10 mL dH<sub>2</sub>O



### **Towbin (Western Transfer) Buffer**

3.03 g TRIS Base

14.4 g Glycine

~800 mL dH<sub>2</sub>O

200 mL Methanol

### **1x PBS (for Westerns)**

10 mL Na<sub>2</sub>HPO<sub>4</sub>/NaH<sub>2</sub>PO<sub>4</sub>

7.6 g NaCl

990 mL dH<sub>2</sub>O

### **0.05% PBS-T**

1 L 1x PBS (for Westerns)

500 µL Tween-20

### **Non-denaturing 8% PAGE gels for EMSA**

34.375 mL dH<sub>2</sub>O

1.125 10x TBE

9 mL 40% Acrylamide/Bis-acrylamide (19:1)

425 µL 10% APS

11.25 µL TEMED





### **10x Passive Lysis Buffer (Promega)**

1 L dH<sub>2</sub>O

11.5 g Na<sub>2</sub>HPO<sub>4</sub>

2 g KH<sub>2</sub>PO<sub>4</sub>

80g NaCl

2 g KCl

(pH 7.4 for 1x)



## **REFERENCES:**

- Aalfs C, Fantes J, Wenniger-Prick L, Sluijter S, Hennekam R, van Heyningen V, and Hoovers J. (1997). Tandem duplication of 11p12-p13 in a child with borderline development delay and eye abnormalities: dose effect of the PAX6 gene product? *American Journal of Medical Genetics*. **73**: 267-271.
- Alkemade P. (1969). *Dysgenesis Mesodermalis of the Iris and the Cornea: A Study of Rieger's Syndrome and Peter's Anomaly*. Van Gorcum, Assen, The Netherlands.
- Almlof T, Gustafsson J, and Wright A. (1997). Role of hydrophobic amino acid clusters in the transactivation activity of the human glucocorticoid receptor. *Molecular and Cellular Biology*. **17**(2): 934-945.
- Alward W, Semina E, Kalenak J, Heon E, Sheth B, Stone E, and Murray J. (1998). Autosomal dominant iris hypoplasia is caused by a mutation in the Rieger syndrome (RIEG/PITX2) gene. *American Journal of Ophthalmology*. **125**(1): 98-100.
- Alward W, Fingert J, Coote M, Johnson A, Lerner S, Junqua D, Durcan F, McCartney P, Mackey D, Sheffield V, and Stone E. (1998). Clinical features associated with mutations in the chromosome 1 open- angle glaucoma gene (GLC1A). *New England Journal of Medicine*. **338**(15): 1022-1027.
- Amendt B, Sutherland L, Semina E, and Russo A. (1998). The molecular basis of Rieger syndrome. Analysis of Pitx2 homeodomain protein activities. *Journal of Biological Chemistry*. **273**(32): 20066-20072.
- Anderson D. (1981). The development of the trabecular meshwork and its abnormalities in primary infantile glaucoma. *Transactions of the American Ophthalmological Society*. **79**: 458-485.



- Arakawa H, Nakamura T, Zhadanov A, Fidanza V, Yano T, Bullrich F, Shimizu M, Blechman J, Mazo A, Canaani E, and Croce C. (1998). Identification and characterization of the ARP1 gene, a target for the human acute leukemia ALL1 gene. *Proceedings of the National Academy of Sciences of the United States of America*. **95**(8): 4573-4578.
- Awan K. (1977). Peters-Rieger's syndrome. *Journal of Pediatric Ophthalmology*. **14**(2): 112-116.
- Axenfeld T. (1920). Embryotoxon corneae posterius. *Ber Deutsch Ophthalmol Ges*. **42**: 381-382.
- Banerjee-Basu S and Baxevanis A. (1999). Threading analysis of the Pitx2 homeodomain: predicted structural effects of mutations causing Rieger syndrome and iridogoniodysgenesis. *Human Mutation*. **14**(4): 312-319.
- Berg F. (1932). Erblisches jugendliches Glaukom. *Acta Ophthalmologica*. **10**: 568-587.
- Billeter M, Qian Y, Otting G, Muller M, Gehring W, and Wuthrich K. (1993). Determination of the nuclear magnetic resonance solution structure of an Antennapedia homeodomain-DNA complex. *Journal of Molecular Biology*. **234**(4): 1084-1093.
- Broughton W, Fine B, and Zimmerman L. (1981). Congenital glaucoma associated with a chromosomal defect: a histologic study. *Archives in Ophthalmology*. **99**: 481-486.
- Burglin T. (1994). *Guidebook to the Homeobox Genes*. Sambrook and Tooze, Oxford University Press, Oxford, New York.
- Burian H, Braley A, and Allen L. (1954). External and gonioscopic visibility of the ring of Schwalbe and the trabecular zone: an interpretation of the posterior corneal embryotoxon and the so-called congenital hyaline membranes on the posterior



- corneal surface. *Transactions of the American Ophthalmological Society*. **51**: 389-428.
- Campione M, Steinbeisser H, Schweickert A, Deissler K, van Bebber F, Lowe L, Nowotschin S, Viebahn C, Haffter P, Kuehn M, and Blum M. (1999). The homeobox gene *Pitx2*: mediator of asymmetric left-right signaling in vertebrate heart and gut looping. *Development*. **126**(6): 1225-1234.
- Chalepakis G, Fristch R, Fickenscher H, Deutsch U, Goulding M, and Gruss P. (1991). The molecular basis of the undulated/*Pzx-1* mutation. *Cell*. **66**: 873-884.
- Chisholm I and Chudley A. (1983). Autosomal dominant iridogoniodysgenesis with associated somatic anomalies: four-generation family with Rieger's syndrome. *British Journal of Ophthalmology*. **67**(8): 529-534.
- Dingwall C and Laskey R. (1991). Nuclear targeting sequences--a consensus? *Trends in Biochemical Sciences*. **16**(12): 478-481.
- Doward W, Perveen R, Lloyd I, Ridgway A, Wilson L, and Black G. (1999). A mutation in the *RIEG1* gene associated with Peters' anomaly. *Journal of Medical Genetics*. **36**(2): 152-155.
- Drouin J, Lamolet B, Lamonerie T, Lanctot C, and Tremblay J. (1998). The PTX family of homeodomain transcription factors during pituitary developments. *Molecular and Cellular Endocrinology*. **140**(1-2): 31-36.
- Escribano J, Ortego J, and Coca-Prados M. (1995). Isolation and characterization of cell-specific cDNA clones from a subtractive library of the ocular ciliary body of a single normal human donor: transcription and synthesis of plasma proteins. *Journal of Biochemistry (Tokyo)*. **118**(5): 921-931.
- Fernald R. (1997). The evolution of eyes. *Brain Behavior and Evolution*. **50**(4): 253-259.





- Fitch N and Kaback M. (1978). The Axenfeld syndrome and the Rieger syndrome. *Journal of Medical Genetics*. **15**: 30-34.
- Flomen R, Vatcheva R, Gorman P, Baptista P, Groet J, Barisic I, Ligutic I, and Nizetic D. (1998). Construction and analysis of a sequence-ready map in 4q25: Rieger syndrome can be caused by haploinsufficiency of RIEG, but also by chromosome breaks approximately 90 kb upstream of this gene. *Genomics*. **47**(3): 409-413.
- Fortin A, Underhill D, and Gros P. (1998). Helix 2 of the paired domain plays a key role in the regulation of DNA-binding by the Pax-3 homeodomain. *Nucleic Acids Research*. **26**(20): 4574-4581.
- Freund C, Horsford D, and McInnes R. (1996). Transcription factor genes and the developing eye: a genetic perspective. *Human Molecular Genetics*. **5**: 1471-1488.
- Friedman J and Walter M. (1999). Glaucoma genetics, present and future. *Clinical Genetics*. **55**: 71-79.
- Gage P and Camper S. (1997). Pituitary homeobox 2, a novel member of the bicoid-related family of homeobox genes, is a potential regulator of anterior structure formation. *Human Molecular Genetics*. **6**(3): 457-464.
- Gage P, Suh H, and Camper S. (1999a). Dosage requirement of Pitx2 for development of multiple organs. *Development*. **126**(20): 4643-4651.
- Gage P, Suh H, and Camper S. (1999b). The bicoid-related Pitx gene family in development. *Mammalian Genome*. **10**(2): 197-200.
- Gage P, Lindert S, and Camper S. (2001). Function of the Pitx2 homeobox gene in ocular neural crest. *Investigative Ophthalmology and Vision Science*. **42**(Suppl 4): S733.



- Gehring W, Qian Y, Billeter M, Furukubo-Tokunaga K, Schier A, Resendez-Perez D, Affolter M, Otting G, and Wuthrich K. (1994). Homeodomain-DNA recognition. *Cell*. **78**(2): 211-223.
- Gorlich D. (1997). Nuclear protein import. *Current Opinion in Cell Biology*. **9**(3): 412-419.
- Gould D, Mears A, Pearce W, and Walter M. (1997). Autosomal dominant Axenfeld-Rieger anomaly maps to 6p25. *American Journal of Human Genetics*. **61**(3): 765-768.
- Hanes S, Riddihough G, Ish-Horowicz D, and Brent R. (1994). Specific DNA recognition and intersite spacing are critical for action of the bicoid morphogen. *Molecular and Cellular Biology*. **14**(5): 3364-3375.
- Hansson H and Jerndal T. (1971). Scanning electron microscopic studies on the development of the iridocorneal angle in human eyes. *Investigative Ophthalmology*. **10**(4): 252-265.
- Héon E, Sheth B, Kalenak J, Sunden S, Streb L, Taylor C, Alward W, Sheffield V, and Stone E. (1995). Linkage of autosomal dominant iris hypoplasia to the region of the Rieger syndrome locus (4q25). *Human Molecular Genetics*. **4**(8): 1435-1439.
- Hessabi B, Ziegler P, Schmidt I, Hessabi C, and Walther R. (1999). The nuclear localization signal (NLS) of PDX-1 is part of the homeodomain and represents a novel type of NLS. *European Journal of Biochemistry*. **263**(1): 170-177.
- Hittner H, Kretzer F, Antoszyk J, Ferrell R, and Mehta R. (1982). Variable expressivity of autosomal dominant anterior segment mesenchymal dysgenesis in six generations. *American Journal of Ophthalmology*. **93**(1): 57-70.



- Hjalt T, Amendt B, and Murray J. (2001). PITX2 regulates procollagen lysyl hydroxylase (PLOD) gene expression: implications for the pathology of Rieger syndrome. *Journal Cell Biology*. **152**(3): 545-552.
- Holmstrom G, Reardon W, Baraitser M, Elston J, and Taylor D. (1991). Heterogeneity in dominant anterior segment malformations. *British Journal of Ophthalmology*. **75**(10): 591-597.
- Huang W, Zhou X, Lefebvre V, and de Crombrughe B. (2000). Phosphorylation of SOX9 by cyclic AMP-dependent protein kinase A enhances SOX9's ability to transactivate a Col2a1 chondrocyte-specific enhancer. *Molecular and Cellular Biology*. **20**(11): 149-158.
- Jakobiec F. (1982). *Ocular anatomy, embryology and teratology*. Harper & Row, Philadelphia.
- Jin Y, Hoskins R, and Horvitz H. (1994). Control of type-D GABAergic neurondifferentiation in by C. elegans UNC-30 homeodomain protein. *Nature*. **372**: 780-778.
- Johnston M, Bhakdinaronk A, and Reid Y. (1973). An expanded role of the neural crest in oral and pharyngeal development. *Symposium on Oral Sensation and Perception*. **4**: 37-52.
- Johnston M, Noden D, Hazelton R, Coulombre J, and Coulombre A. (1979). Origins of avian ocular and periocular tissues. *Experimental Eye Research*. **29**: 27-43.
- Jordan T, Hanson I, Zaletayev D, Hodgson S, Prosser J, Seawright A, Hastie N, and van Heyningen V. (1992). The human PAX6 gene is mutated in two patients with aniridia. *Nature Genetics*. **1**(5): 328-332.
- Kissinger C, Liu B, Martin-Blanco E, Kornberg T, and Pabo C. (1990). Crystal structure of an engrailed homeodomain-DNA complex at 2.8 Å resolution: a



framework for understanding homeodomain-DNA interactions. *Cell*. **63**(3): 579-590.

Koroma B, Yang J, and Sundin O. (1997). The Pax-6 homeobox gene is expressed throughout the corneal and conjunctival epithelia. *Investigative Ophthalmology and Visual Science*. **38**(1): 108-120.

Kozlowski K and Walter M. (2000). Variation in residual PITX2 activity underlies the phenotypic spectrum of anterior segment developmental disorders. *Human Molecular Genetics*. **9**(14): 2131-2139.

Kubota R, Kudoh J, Mashima Y, Asakawa S, Minoshima S, Hejtmancik J, Oguchi Y, and Shimizu N. (1998). Genomic organization of the human myocilin gene (MYOC) responsible for primary open angle glaucoma (GLC1A). *Biochemical and Biophysical Research Communications*. **242**(2): 396-400.

Kulak S, Kozlowski K, Semina E, Pearce W, and Walter M. (1998). Mutation in the RIEG1 gene in patients with iridogoniodysgenesis syndrome. *Human Molecular Genetics*. **7**(7): 1113-1117.

Kulak S. (1999). *Mutational Analysis of the Homeobox Transcription Factor PITX2*. Masters Thesis. Dept. Ophthalmology, University of Alberta, Edmonton.

Lamonerie T, Tremblay J, Lanctot C, Therrien M, Gauthier Y, and Drouin J. (1996). Ptx1, a bicoid-related homeo box transcription factor involved in transcription of the pro-opiomelanocortin gene. *Genes and Development*. **10**(10): 1284-1295.

Lehmann O, Ebenezer N, Jordan T, Fox M, Ocaka L, Payne A, Leroy B, Clark B, Hitchings R, Povey S, Khaw P, and Bhattacharya S. (2000). Chromosomal duplication involving the forkhead transcription factor gene FOXC1 causes iris hypoplasia and glaucoma. *American Journal of Human Genetics*. **67**(5): 1129-1135.





- Lin C, Kioussi C, O'Connell S, Briata P, Szeto D, Liu F, Izpisua-Belmonte J, and Rosenfeld M. (1999). Pitx2 regulates lung asymmetry, cardiac positioning and pituitary and tooth morphogenesis. *Nature*. **401**(6750): 279-282.
- Lin R, Heylbroeck C, Pitha P, and Hiscott J. (1998). Virus-dependent phosphorylation of the IRF-3 transcription factor regulates nuclear translocation, transactivation potential, and proteasome-mediated degradation. *Molecular and Cellular Biology*. **18**(5): 2986-2996.
- Lindberg C, Wunderlich M, Ratliff J, Dinsmore J, and Jacoby D. (1998). Regulated expression of the homeobox gene, rPtx2, in the developing rat. *Brain Research. Developmental Brain Research*. **110**(2): 215-226.
- Logan M, Pagan-Westphal S, Smith D, Paganessi L, and Tabin C. (1998). The transcription factor Pitx2 mediates situs-specific morphogenesis in response to left-right asymmetric signals. *Cell*. **94**(3): 307-317.
- Lu M, Pressman C, Dyer R, Johnson R, and Martin J. (1999). Function of Rieger syndrome gene in left-right asymmetry and craniofacial development. *Nature*. **401**(6750): 276-278.
- Mann E. (1964). *The development of the human eye*. Grune and Stratton Inc., New York.
- Mears A, Jordan T, Mirzayans F, Dubois S, Kume T, Parlee M, Ritch R, Koop B, Kuo W, Collins C, Marshall J, Gould D, Pearce W, Carlsson P, Enerback S, Morissette J, Bhattacharya S, Hogan B, Raymond V, and Walter M. (1998). Mutations of the forkhead/winged-helix gene, FKHL7, in patients with Axenfeld-Rieger anomaly. *American Journal of Human Genetics*. **63**(5): 1316-1328.
- Mirzayans F, Gould D, Heon E, Billingsley G, Cheung J, Mears A, and Walter M. (2000). Axenfeld-Rieger syndrome resulting from mutation of the FKHL7 gene on chromosome 6p25. *European Journal of Human Genetics*. **8**(1): 71-74.



- Moore K. (1983). *The Eye and The Ear, in Before We Are Born: Basic Embryology and Birth Defects*. W. B. Saunders Company: Philadelphia. 254-263.
- Murray J, Bennett S, Kwitek A, Small K, Schinzel A, Alward W, Weber J, Bell G, and Buetow K. (1992). Linkage of Rieger syndrome to the region of the epidermal growth factor gene on chromosome 4. *Nature Genetics*. **2**(1): 46-49.
- Nakanishi I and Brown S. (1971). The histopathology and ultrastructure of congenital, central corneal opacity (Peters' anomaly). *American Journal of Ophthalmology*. **72**(4): 801-812.
- Nishimura D, Swiderski R, Alwards L, Searby C, Patil S, Bennet S, Kanis A, Gastier J, Stone E, and Sheffield V. (1998). The forkhead transcription factor gene FKHL7 is responsible for glaucoma phenotypes which map to 6p25. *Nature Genetics*. **19**: 140-147.
- Nishimura D, Searby A, Borges J, Caran A, Betinjane E, Stone R, Susanna W, Alward W, and V S. (2000). Identification of a fourth Rieger Syndrome locus at 16q24. *American Journal of Human Genetics*. **67**(Suppl 12): A2146.
- Nishimura D, Searby C, Alwards L, Walton D, Craig J, Mackey D, Kawase K, Kanis A, Patil S, Stone E, and Sheffield V. (2001). A spectrum of FOXC1 mutations suggests gene dosage as a mechanism for developmental defects of the anterior chamber of the eye. *American Journal of Human Genetics*. **68**: 364-372.
- Nohaile M, Kern D, Wemmer D, Stedman K, and Kustu S. (1997). Structural and functional analyses of activating amino acid substitutions in the receiver domain of NtrC: evidence for an activating surface. *Journal of Molecular Biology*. **273**(1): 299-316.



- O'Neil K and DeGrado W. (1990). A thermodynamic scale for the helix-forming tendencies of the commonly occurring amino acids [published erratum appears in *Science* 1991 Aug 30;253(5023):952]. *Science*. **250**(4981): 646-651.
- Pearce W, Wyatt H, Boyd T, Ombres R, and Salter A. (1982). Autosomal dominant iridogoniodysgenesis: a genetic and clinical study. *Birth Defects*. **18**(6): 561-569.
- Pearce W, Wyatt H, Boyd T, Ombres R, and Salter A. (1983). Autosomal dominant iridogoniodysgenesis: genetic features. *Canadian Journal of Ophthalmology*. **18**(1): 7-10.
- Pearce W, Mielke B, Kulak S, and Walter M. (1999). Histopathology and molecular basis of iridogoniodysgenesis syndrome. *Ophthalmic Genetics*. **20**(2): 83-88.
- Pellegrini-Bouiller I, Manrique C, Gunz G, Grino M, Zamora A, Figarella-Branger D, Grisoli F, Jaquet P, and Enjalbert A. (1999). Expression of the members of the Ptx family of transcription factors in human pituitary adenomas. *Journal of Clinical Endocrinology and Metabolism*. **84**(6): 2212-2220.
- Perveen R, Lloyd I, Clayton-Smith J, Churchill A, van Heyningen V, Hanson I, Taylor D, McKeown C, Super M, Kerr B, Winter R, and Black G. (2000). Phenotypic variability and asymmetry of Rieger syndrome associated with PITX2 mutations. *Investigative Ophthalmology and Visual Science*. **41**(9): 2456-2460.
- Peters A. (1906). Ueber angeborene Defektbildung der Descemetischen Membran. *Klin. Mbl. Augenheilk.* **44**: 27-40 and 105-119.
- Phillips J, Del Bono E, Haines J, Pralea A, Cohen J, Greff L, and Wiggs J. (1996). A second locus for Rieger Syndrome maps to chromosome 13q14. *American Journal of Human Genetics*. **59**: 613-619.



- Piedra M, Icardo J, Albajar M, Rodriguez-Rey J, and Ros M. (1998). Pitx2 participates in the late phase of the pathway controlling left-right asymmetry. *Cell*. **94**(3): 319-324.
- Pringle J, Adams A, Drubin D, and Haarer B. (1991). Immunofluorescence methods for yeast. *Methods in Enzymology*. **194**: 565-571.
- Priston M, Kozlowski K, Gill D, Letwin K, Buys Y, Levin A, Walter M, and Heon E. (2001). Functional analyses of two newly identified PITX2 mutants reveal a novel molecular mechanism for Axenfeld-Rieger syndrome. *Human Molecular Genetics*. **10**(16): 1631-1638.
- Qian Y, Billeter M, Otting G, Muller M, Gehring W, and Wuthrich K. (1989). The structure of the Antennapedia homeodomain determined by NMR spectroscopy in solution: comparison with prokaryotic repressors. *Cell*. **59**: 573-580.
- Qian Y, Otting G, Billeter M, Muller M, Gehring W, and Wuthrich K. (1993). Nuclear magnetic resonance spectroscopy of a DNA complex with the uniformly <sup>13</sup>C-labeled Antennapedia homeodomain and structure determination of the DNA-bound homeodomain. *Journal of Molecular Biology*. **234**(4): 1070-1083.
- Ravagnani A, Gorfinkiel L, Langdon T, Diallinas G, Adjadj E, Demais S, Gorton D, Arst HJ, and Scazzocchio C. (1997). Subtle hydrophobic interactions between the seventh residue of the zinc finger loop and the first base of an HGATAR sequence determine promoter-specific recognition by the *Aspergillus nidulans* GATA factor AreA. *EMBO Journal*. **16**(13): 3974-3986.
- Ray-Gallet D and Moreau-Gachelin. (1999). Phosphorylation of the Spi-B transcription factor reduces its intrinsic stability. *FEBS Letters*. **464**(3): 164-168.
- Reese A and Ellsworth R. (1966). The anterior chamber cleavage syndrome. *Archives of Ophthalmology*. **75**(3): 307-318.





- Richards J, Brooks B, Othman M, Semina E, and Moroi S. (2001). A novel mutation in the PITX2 gene causes Rieger Syndrome. *Investigative Ophthalmology and Vision Science*. **42**(Suppl 4): S566.
- Rieger H. (1934). Verlagerung und Schitzform der Pupille mit Hypoplasie des Irisvordblattes. *Z. Augenheilk.* **84**: 98-99.
- Riordan-Eva P. (1999). *Anatomy and Embryology of the Eye*, in *General Ophthalmology*. Appleton and Lange: Stamford, Connecticut. 1-26.
- Rubel. (1913). Angeborene Hypoplasiae bzw. Aplasie des Irisvorderblattes. *Klin Monatsbl Augenheilkd.* **51**: 174.
- Ryan A, Blumberg B, Rodriguez-Esteban C, Yonei-Tamura S, Tamura K, Tsukui T, de la Pena J, Sabbagh W, Greenwald J, Choe S, Norris D, Robertson E, Evans R, Rosenfeld M, and Izpisua Belmonte J. (1998). Pitx2 determines left-right asymmetry of internal organs in vertebrates. *Nature*. **394**(6693): 545-551.
- Saadi I, Semina E, Amendt B, Harris D, Murphy K, Murray J, and Russo A. (2001). Identification of a dominant negative homeodomain mutation in Rieger syndrome. *Journal of Biological Chemistry*. **276**(25): 23034-23041.
- Saeki K, Yuo A, and Takaku F. (1999). Cell-cycle-regulated phosphorylation of cAMP response element-binding protein: identification of novel phosphorylation sites. *Biochemistry Journal*. **338**: 49-54.
- Saleem R, Banerjee-Basu S, Berry F, Baxevanis A, and Walter M. (2001). Analyses of the effects that disease-causing missense mutations have on the structure and function of the winged-helix protein FOXC1. *American Journal of Human Genetics*. **68**(3): 627-641.
- Scott M, Tamkun J, and Hartzell G. (1989). The structure and function of the homeodomain. *Biochimica et Biophysica Acta*. **989**(1): 25-48.



- Semina E, Datson N, Leysens N, Zabel B, Carey J, Bell G, Bitoun P, Lindgren C, Stevenson T, Frants R, van Ommen G, and Murray J. (1996a). Exclusion of epidermal growth factor and high-resolution physical mapping across the Rieger syndrome locus. *American Journal of Human Genetics*. **59**(6): 1288-1296.
- Semina E, Reiter R, Leysens N, Alward W, Small K, Datson N, Siegel-Bartelt J, Bierke-Nelson D, Bitoun P, Zabel B, Carey J, and Murray J. (1996b). Cloning and characterization of a novel bicoid-related homeobox transcription factor gene, RIEG, involved in Rieger syndrome. *Nature Genetics*. **14**(4): 392-399.
- Semina E, Reiter R, and Murray J. (1997). Isolation of a new homeobox gene belonging to the Pitx/Rieg family: expression during lens development and mapping to the aphakia region on mouse chromosome 19. *Human Molecular Genetics*. **6**(12): 2109-2116.
- Semina E, Ferrell R, Mintz-Hittner H, Bitoun P, Alward W, Reiter R, Funkhauser C, Daack-Hirsch S, and Murray J. (1998). A novel homeobox gene PITX3 is mutated in families with autosomal-dominant cataracts and ASMD. *Nature Genetics*. **19**(2): 167-170.
- Shields M. (1983). Axenfeld-Rieger syndrome: a theory of mechanism and distinctions from the iridocorneal endothelial syndrome. *Transactions of the American Ophthalmological Society*. **81**: 736-784.
- Shields M, Buckley E, Klintworth G, and Thresher R. (1985). Axenfeld-Rieger syndrome. A spectrum of developmental disorders. *Surveys in Ophthalmology*. **29**(6): 387-409.
- Shields M. (1989). *Axenfeld-Rieger Syndrome*, in *The Glaucomas*, Krupin T, Editor. C.V. Mosby: St. Louis. 885-896.



- Shin S, Kogerman P, Lindstrom E, Toftgard R, and Biesecker L. (1999). GLI3 mutations in human disorders mimic *Drosophila cubitus interruptus* protein functions and localization. *Proceedings of the National Academy of Sciences of the United States of America*. **96**(6): 2880-2884.
- Simeone A, Acampora D, Mallamaci A, Stornaiuolo A, D'Apice M, Nigro V, and Boncinelli E. (1993). A vertebrate gene related to orthodenticle contains a homeodomain of the bicoid class and demarcates anterior neuroectoderm in the gastrulating mouse embryo. *EMBO Journal*. **12**(7): 2735-2747.
- Smith R, Zabaleta A, Kume T, Savinova O, Kidson S, Martin J, Nishimura D, Alward W, Hogan B, and John S. (2000). Haploinsufficiency of the transcription factors FOXC1 and FOXC2 results in aberrant ocular development. *Human Molecular Genetics*. **9**(7): 1021-1032.
- Stone E, Fingert J, Alward W, Nguyen T, Polansky J, Sunden S, Nishimura D, Clark A, Nystuen A, Nichols B, Mackey D, Ritch R, Kalenak J, Craven E, and Sheffield V. (1997). Identification of a gene that causes primary open angle glaucoma. *Science*. **275**(5300): 668-670.
- Swan K. (1981). Developmental glaucomas in juveniles. *Perspectives in Ophthalmology*. **5**: 21-25.
- Szeto D, Ryan A, O'Connell S, and Rosenfeld M. (1996). P-OTX: a PIT-1-interacting homeodomain factor expressed during anterior pituitary gland development. *Proceedings of the National Academy of Sciences of the United States of America*. **93**(15): 7706-7710.
- Tawara A and Inomata H. (1981). Developmental immaturity of the trabecular meshwork in congenital glaucoma. *American Journal of Ophthalmology*. **92**: 508-525.



- Tremblay J, Lanctot C, and Drouin J. (1998). The pan-pituitary activator of transcription, Ptx1 (Pituitary Homeobox 1), acts in synergy with SF-1 and Pit1 and is an upstream regulator of the Lim-homeodomain gene Lim3/Lhx3. *Molecular Endocrinology*. **12**(3): 428-441.
- Tremblay J, Marcil A, Gauthier Y, and Drouin J. (1999). Ptx1 regulates SF-1 activity by an interaction that mimics the role of the ligand-binding domain. *EMBO Journal*. **18**(12): 3431-3441.
- Tripathi R. (1974). *The eye*. Academic Press, New York.
- van Burskirk E. (1981). Clinical implications of iridocorneal angle development. *Ophthalmology*. **88**: 361-367.
- Walter M, Mirzayans F, Mears A, Hickey K, and Pearce W. (1996). Autosomal-dominant iridogoniodysgenesis and Axenfeld-Rieger syndrome are genetically distinct. *Ophthalmology*. **103**(11): 1907-1915.
- Wang W, McNatt L, Shepard A, Jacobson N, Nishimura D, Stone E, Sheffield V, and Clark A. (2001). Optimal procedure for extracting RNA from human ocular tissues and expression profiling of the congenital glaucoma gene FOXC1 using quantitative RT-PCR. *Molecular Vision*. **17**(7): 89-94.
- Waring G, Rodriques M, and Laibson P. (1975). Anterior chamber cleavage syndromes: a stepladder classification. *Surveys in Ophthalmology*. **20**: 3-27.
- Weatherill J and Hart C. (1969). Familial hypoplasia of the iris stroma associated with glaucoma. *British Journal of Ophthalmology*. **53**: 433-438.
- Wilson D, Sheng G, Lecuit T, Dostatni N, and Desplan C. (1993). Cooperative dimerization of paired class homeo domains on DNA. *Genes and Development*. **7**(11): 2120-2134.





- Wilson D, Sheng G, Jun S, and Desplan C. (1996). Conservation and diversification in homeodomain-DNA interactions: a comparative genetic analysis. *Proceedings of the National Academy of Sciences of the United States of America*. **93**(14): 6886-6891.
- Wulle K. (1972). Electron microscopy of the fetal development of the corneal endothelium and Descemet's membrane of the human eye. *Investigative Ophthalmology*. **11**: 897-904.
- Wyatt H, Pearce W, Boyd T, Ombres R, and Salter A. (1983). Autosomal dominant iridogoniodysgenesis: glaucoma management. *Canadian Journal of Ophthalmology*. **18**(1): 11-14.



Letter of permission from Dr. Sulik regarding use of the eye embryology  
electro-micrographs.

**Subject: embryo images**

**Date:** Thu, 14 Jun 2001 22:31:32 -0600

**From:** Kathy Kozlowski <kayk1@powersurfr.com>

**To:** [etg@med.unc.edu](mailto:etg@med.unc.edu)

Good day,

I am currently writing my master's thesis entitled:

"Anterior segment abnormalities and the PITX2 transcription  
factor:

Molecular analyses of PITX2 homeodomain mutations with  
genotype-phenotype correlations"

with an introductory chapter on development of the  
eye/anterior segment.

I would greatly appreciate permission to reproduce the  
fantastic micrographs displayed on your website if possible.

Thank you very much,

--

Kathy Kozlowski

**Subject: embryo images**

**Date:** Mon, 18 Jun 2001 09:37:50 -0400

**From:** "K.K.Sulik" <[mouse@med.unc.edu](mailto:mouse@med.unc.edu)>

**To:** <[kk1@ualberta.ca](mailto:kk1@ualberta.ca)>

Hello,

You are welcome to use the eye images for your dissertation.

Best wishes,

Kathy Sulik











University of Alberta Library



0 1620 1493 8367

**B45564**